

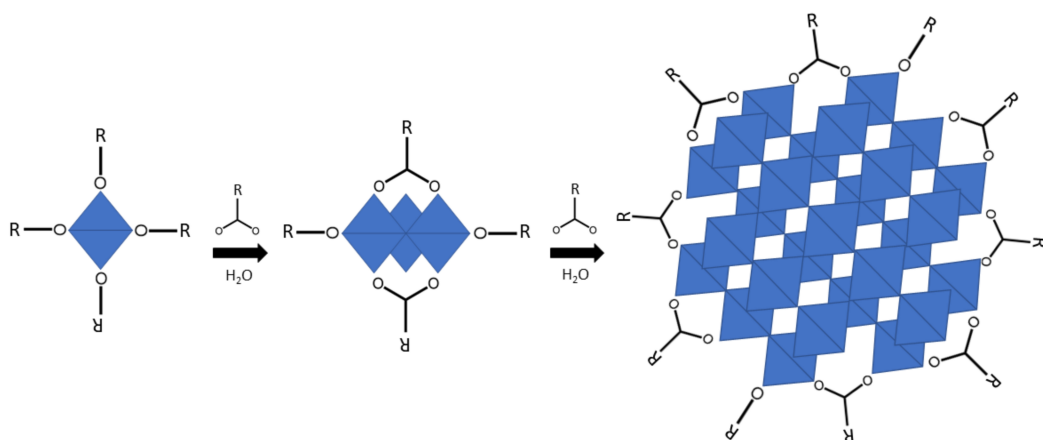


DOCTORAL THESIS NO. 2020:56  
FACULTY OF NATURAL RESOURCES AND AGRICULTURAL SCIENCES

# Hybrid Nano Titania

## Molecular Formation Mechanisms and Applications in Nanotechnology

FREDRIC G. SVENSSON



# Hybrid Nano Titania

## Molecular Formation Mechanisms and Applications in Nanotechnology

Fredric G. Svensson

*Faculty of Natural Resources and Agricultural Sciences*

*Department of Molecular Sciences*

*Uppsala*

Doctoral thesis  
Swedish University of Agricultural Sciences  
Uppsala 2020

Acta Universitatis Agriculturae Sueciae

2020:56

Cover: Simplified illustration of the Micelles Templated by Self-Assembly of Ligands (MTSAL) mechanism, starting from mononuclear precursors and transforming them via oligonuclear oxo-complexes into oxide particles.

ISSN 1652-6880

ISBN (print version) 978-91-7760-630-7

ISBN (electronic version) 978-91-7760-631-4

© 2020 Fredric Svensson, Uppsala

Print: SLU Service/Repro, Uppsala 2020

# Hybrid Nano Titania. Molecular Formation Mechanisms and Applications in Nanotechnology.

## Abstract

Nanomaterials are defined as materials with one dimension smaller than 100 nm. At this size, exotic properties start to emerge, making them interesting for a wide range of applications including catalysis, electronics, theranostics, and “smart materials”. Particularly engineered metal oxide nanoparticles have found advanced applications in medical therapy and catalysis. Because of the small size and required homogeneity of these materials, bottom-up synthesis starting from molecular precursors is often the preferred way of production. The present work was initiated with the main purpose to bring insight in the whole chain in materials design and application – from precursor chemistry in the synthesis to physical chemical and biological characteristics of the resulting nanomaterials. It is thus an interdisciplinary project, covering the fields of both chemistry and biology. The chemical part presents synthesis, self-assembly, and chemical characterization of titania nanopowders, hollow titania spheres, and nanotitania-nanocellulose hybrid materials. The biological part primarily evaluates titania-nanocellulose hybrid materials for drug delivery applications using *in vitro* bacterial cultures and immunological (coagulation-related) responses in human whole blood. Not unexpectedly, titania-nanocellulose hybrids generally induced strong coagulation via the contact activation system.

An extensive part of the thesis is dedicated to the solution behavior, stability, and transformation of heteroleptic titanium oxo-alkoxides into nanotitania, using a variety of characterization techniques. The observations support the MTSAL mechanism for formation of metal oxide nanoparticles. No hydrolytic stability, however, from ligand-modification of titanium (oxo-) alkoxides could be observed.

*Keywords:* Titania, Nanocellulose, Nanomaterials, Hybrid materials, Biomaterials, Drug delivery, Coordination chemistry, MTSAL, Photocatalysis.

*Author's address:* Fredric Svensson, SLU, Department of Molecular Sciences, P.O. Box 7015, 750 07 Uppsala, Sweden.

E-mail: [fredric.svensson@slu.se](mailto:fredric.svensson@slu.se)

*Education isn't something you can finish.*

Isaac Asimov

# Contents

<b>List of publications</b> .....	8
<b>List of tables</b> .....	11
<b>List of figures</b> .....	12
<b>Abbreviations</b> .....	14
<b>1. Introduction</b> .....	17
1.1. Background .....	17
1.1. Titanium dioxide .....	18
1.1.1. Increasing the catalytic activity of titania.....	20
1.1.1.1. Sensitizers.....	21
1.1.1.2. Doping of titania.....	22
1.2.2. Solution chemistry of titanium coordination complexes.....	23
1.2.3. Heteroleptic titanium oxo-alkoxide complexes as models for surface interactions and precursors for metal oxide nanoparticles ...	25
1.2.4. Bimetallic oxides of titanium .....	25
1.2.5. Synthesis of titania nanoparticles .....	26
1.2.5.1 The sol-gel process.....	26
1.2.5.2. The solvo/hydrothermal process.....	29
1.3. Self-assembly .....	30
1.4. Nanotechnology.....	30
1.4.1. Nanocellulose .....	31
1.4.2. Nanotitania–nanocellulose hybrid materials for medical applications.....	31
1.4.3. Nanomaterials safety .....	32
1.5. Characterization techniques .....	33
1.5.0. The physical basis .....	33
1.5.1. X-ray crystallography.....	34
1.5.2. Nuclear magnetic resonance spectrometry .....	37
1.5.3. Scanning electron microscopy.....	41
1.5.4. Transmission electron microscopy.....	43

1.5.5. Energy-dispersive X-ray spectrometry .....	44
1.5.6. Atomic force microscopy .....	45
1.5.7. Infrared spectrometry .....	46
1.5.8. Raman spectroscopy .....	47
1.6. Objectives of this thesis .....	49
<b>2. Methods .....</b>	<b>51</b>
2.0. General information .....	51
2.1. Syntheses of compounds and materials .....	51
2.1.1. Syntheses of modified titanium (oxo-) alkoxide complexes ..	51
2.1.2. Synthesis of rare-earth modified titania nanopowders .....	53
2.1.3. Self-assembly of titania nanoshells .....	53
2.1.4. Syntheses of nanotitania-nanocellulose hybrid materials .....	53
2.2. Chemical analysis and characterization .....	54
2.2.1. Stability of modified titanium (oxo-) alkoxide complexes .....	54
2.2.1.1. Hydrolytic stability .....	54
2.2.1.2. Solution stability of selected modified titanium complexes .....	54
2.3. Photocatalysis .....	55
2.4. Drug release from CNC_TiO <sub>2</sub> _TR and hydrolyzed complex 1a .....	55
2.4.1. Hydrolyzed complex 1a .....	55
2.4.2. CNC_TiO <sub>2</sub> _TR .....	56
2.5. Immunological studies of the nanocellulose-nanotitania hybrid materials .....	56
2.5.1. Human whole blood chamber model .....	56
2.5.2. ELISA analyses of immunological markers .....	57
<b>3. Results and Discussion .....</b>	<b>59</b>
3.1. Synthesis of modified titanium (oxo-) alkoxide complexes .....	59
3.1.1. Structural comments .....	59
3.1.2. Characterization of REE-modified titania nanopowders .....	64
3.1.4. Characterization of self-assembly of titania nanoshells .....	71
3.1.5. Characterization of nanotitania-nanocellulose hybrid materials .....	74
3.2. Hydrolytic stability and solution behavior of modified titanium oxo-alkoxide complexes .....	75
3.2.1. Hydrolytic stability of ligand-modified complexes .....	76
3.2.2. Complex oxide structures from hydrolysis of precursors .....	79
3.2.3. Solution stability of selected modified titanium complexes .....	81

3.3. Photocatalytic properties of REE-modified titania.....	83
3.3.1. Photoluminescence.....	85
3.4. Drug release from CNC_TiO <sub>2</sub> _TR and hydrolyzed complex 1a....	86
3.4.1. Drug release from hydrolyzed complex 1a .....	86
3.4.2. Drug release from CNC_TiO <sub>2</sub> composites .....	87
3.5. Immunological studies of the nanocellulose-nanotitania hybrid materials .....	89
3.5.1. Human whole blood chamber model.....	89
3.5.2. Thrombin-antithrombin ELISA.....	90
3.5.3. C3a ELISA .....	91
3.5.4. sC5b-9 ELISA .....	91
3.5.5. C1-inhibitor complex with FXI and FXII .....	92
3.6. What are the nanosafety risks associated with this work?.....	94
<b>4. Conclusions and outlook .....</b>	<b>95</b>
<b>5. References .....</b>	<b>97</b>
<b>Popular science summary .....</b>	<b>113</b>
<b>Populärvetenskaplig sammanfattning.....</b>	<b>114</b>
<b>Acknowledgements.....</b>	<b>115</b>

# List of publications

This thesis is based on the work contained in the following papers, referred to by Roman numerals in the text:

- I **Fredric G. Svensson**, Gulaim A. Seisenbaeva, and Vadim G. Kessler\*. Mixed-Ligand Titanium “Oxo Clusters”: Structural Insights into the Formation and Binding of Organic Molecules and Transformation into Oxide Nanostructures on Hydrolysis and Thermolysis. *European Journal of Inorganic Chemistry* (2017) 4117–4122.
- II Olga L. Evdokimova, **Fredric G. Svensson**, Alexander V. Agafonov, Sebastian Håkansson, Gulaim A. Seisenbaeva, and Vadim G. Kessler\*. Hybrid Drug Delivery Patches Based on Spherical Cellulose Nanocrystals and Colloid Titania – Synthesis and Antibacterial Properties. *Nanomaterials* (2018) 8, 228–245.
- III **Fredric G. Svensson\*** and Vadim G. Kessler. Solid-State Structure and Solution Behavior of Two Titanium Oxo-Alkoxide Complexes with Phenylphosphonate Ligands. *Polyhedron* (2020) 178, 114276.
- IV **Fredric G. Svensson**, Geoffrey Daniel, Cheuk-Wai Tai, Gulaim A. Seisenbaeva, and Vadim G. Kessler\*. Titanium Phosphonate Oxo-Alkoxide “Clusters”: Solution Stability and Facile Hydrolytic Transformation into Nanotitania. *RSC Advances* (2020) 10, 6873–6883.
- V **Fredric G. Svensson**, Karin Fromell, Vivek Anad Manivel, Gulaim A. Seisenbaeva, Vadim G. Kessler\*, Bo Nilsson, and Kristina Nilsson-Ekdahl\*. Haemocompatibility of Nanotitania-Nanocellulose Hybrid Materials. *Manuscript in Preparation*.
- VI **Fredric G. Svensson**, Gulaim A. Seisenbaeva, Nicholas A. Kotov, and Vadim G. Kessler\*. Self-Assembly of Asymmetrically Functionalized Titania Nanoparticles into Nanoshells. *In Revision*.
- VII **Fredric G. Svensson**, Bogdan Cojocaru, Zhen Qui, Vasile Parvulescu, Tomas Edvinsson, Gulaim A. Seisenbaeva, Carmen Tiseanu\*, and Vadim G. Kessler\*. Rare-Earth Modified Titania Nanoparticles: Synthesis and Photochemical Properties. *Manuscript in Preparation*.

Papers I-IV are reproduced with the permission of the publishers.

\* Corresponding author.

### **Publications outside the scope of the thesis**

1. Suresh Ganji, **Fredric G. Svensson**, and C. Rikard Unelius\*. Asymmetric Synthesis of Oxygenated Monoterpenes of Importance for Bark Beetle Ecology. *Revision Submitted*.
2. **Fredric G. Svensson\*** and Vadim G. Kessler. Interaction Between Dopamine and the  $[\text{HPW}_{12}\text{O}_{40}]^{2-}$  Keggin Ion – an X-ray and NMR Study. *Journal of Molecular Structure* (2021) 1226, 129343.
3. **Fredric G. Svensson\***. Synthesis and Crystal Structures of  $[\text{Al}(\text{H}_2\text{O})_6]\text{SO}_4\text{NO}_3 \cdot 2\text{H}_2\text{O}$  and  $[\text{Al}(\text{H}_2\text{O})_6]\text{SO}_4\text{Cl} \cdot \text{H}_2\text{O}$ . *In Revision*.

The contribution of F.G.S. to the papers included in this thesis was as follows:

**Paper I** Synthesized the compound. Performed SEM-EDS, PXRD, and the microbiological experiment. Wrote major part of the manuscript.

**Paper II** Synthesized the molecular structure and assisted solving the structure and performed the microbiological studies. Wrote a minor part of the manuscript

**Paper III** Performed all syntheses, solved the structures and performed the SEM-EDS analyses. Recorded and analyzed the NMR data. Wrote major part of the manuscript.

**Paper IV** Synthesized all compounds. Participated in solving the structures of the compounds. Performed the SEM-EDS analyses, performed part of NMR data collection and analyzed the data. Performed the hydrolysis studies. Wrote major part the manuscript.

**Paper V** Synthesized the hybrid materials. Performed the SEM-EDS analyses and the blood incubation experiment. Carried out the C3a, sC5b-9, and TAT ELISAs. Participated in preparation of the manuscript.

**Paper VI** Developed the self-assembly process based on discussions with the co-authors. Performed drug release studies and part of SEM imaging. Wrote major part of the manuscript.

**Paper VII** Synthesized the REE-modified titania nanopowders and performed most of the SEM-EDS analyses. Collected and analyzed part of the powder X-ray data. Collected and analyzed the FTIR data. Synthesized and solved the crystal structure of the molecular compound. Compiled and assisted in interpretation of the data from the collaborators. Wrote major part of the manuscript.

## List of tables

Table 1. Measured inhibitory zones on *E. coli* and *S. aureus* after incubation with the CNC\_TiO<sub>2</sub> composites.

## List of figures

- Figure 1.* Structure fragments of anatase and rutile.
- Figure 2.* Simplified illustration of an organic sensitizer attached to a TiO<sub>2</sub> NP.
- Figure 3.* Overview of the sol-gel process.
- Figure 4.* MTSAL formation.
- Figure 5.* A steel autoclave with a Teflon container for hydro/solvothermal synthesis.
- Figure 6.* X-ray diffraction in crystalline and amorphous materials.
- Figure 7.* Diffraction patterns from a single crystal and a nanocrystalline powder.
- Figure 8.* Simplified scheme of the excitation process in NMR.
- Figure 9.* The free induction decay (FID) signal.
- Figure 10.* Transformation of the FID signal.
- Figure 11.* Scheme of the approximate areas of some important carbon NMR shifts in ppm.
- Figure 12.* Simplified principle of a SEM instrument.
- Figure 13.* Simplified principle of a TEM instrument.
- Figure 14.* Principle of EDS.
- Figure 15.* Simplified principle of AFM.
- Figure 16.* Different types of scattering in Raman spectrometry between energy states.
- Figure 17.* Incubation cell for blood experiment.
- Figure 18.* Molecular structures of compounds **1a** and **1b**.
- Figure 19.* Core-structures of compounds **1a** and **1b**.
- Figure 20.* Molecular structure of **1c**.
- Figure 21.* Metal-oxo core-structures of the titanium oxo-alkoxide phosphonates from **paper IV**.
- Figure 22.* Molecular structure of compound **1e**.
- Figure 23.* PXRD patterns of the REE-modified titania powders at different annealing temperatures.
- Figure 24.* SEM micrographs of the TiO<sub>2</sub>-REE powders used for catalysis.
- Figure 25.* Elemental mapping of REE-modified titania for the different dopants.

*Figure 26.* Raman spectra for europium and samarium modified titania.  
*Figure 27.* FTIR-spectra of powders used for photocatalysis.  
*Figure 28.* FTIR spectra of amorphous Ti-Eu<sub>5</sub> and TiSm<sub>5</sub> powders and reference titania.  
*Figure 29.* SEM micrographs of self-assembled titania nanoshells.  
*Figure 30.* Elemental mapping of the titania nanoshells, showing presence of titanium, oxygen, and phosphorous.  
*Figure 31.* AFM micrographs of titania nanoshells.  
*Figure 32.* Photographs of the different nanotitania-nanocellulose materials.  
*Figure 33.* SEM micrographs of the different nanotitania-nanocellulose materials.  
*Figure 34.* SEM and TEM micrographs of compound **1a**.  
*Figure 35.* AFM of hydrolyzed compound **1a**.  
*Figure 36.* TEM and AFM micrographs of compound **1d** and compound **6d**.  
*Figure 37.* HRTEM micrograph of **1e** submerged in water.  
*Figure 38.* Hydrolyzed “complex **7d**” under different conditions.  
*Figure 39.* <sup>31</sup>P NMR spectra of two titanium oxo-alkoxide phosphonates with different solution stability.  
*Figure 40.* DOSY NMR spectra of compound **1c** and the reaction mixture of **2c**.  
*Figure 41.* <sup>31</sup>P NMR spectra over different temperatures for compound **5d**.  
*Figure 42.* Photocatalytic degradation of trimethylphenol using titania modified with Eu and Sm under different wavelengths.  
*Figure 43.* Inhibitory effect of triclosan released from filter paper.  
*Figure 44.* Inhibition zones of antibacterial activity against *E.coli* and *S. aureus*.  
*Figure 45.* Blood chambers after incubation of the control, control material, and the three different hybrid materials.  
*Figure 46.* Concentrations of platelets, TAT, C1In-FXI, and C1In-FXII  
*Figure 47.* Relative concentrations of C3a and sC5b-9 in the different treatments.

# Abbreviations

acac	Acetylacetonate
AFM	Atomic Force Microscopy
ALD	Atomic Layer Deposition
BC	Bacterial Cellulose
BSE	Back-Scattered Electron
Captigel	Colloidal titania nanoparticles
CB	Conduction Band
CNC	Cellulose Nanocrystals
CNF	Cellulose Nanofibrills
Cp	Cyclopentadienyl
DOSY	Diffusion Ordered Spectrometry
DPA	<i>n</i> -Dodecylphosphonic Acid
EDS	X-ray Energy Dispersive Spectroscopy
EELS	Electron Energy Loss Spectrometry
ELISA	Enzyme-Linked Immunosorbent Assay
EM	Eletromagnetic
ESR	Electron Spin Resonance
EXAFS	Extended X-ray Absorption Fine Structure
FID	Free Induction Decay
FT	Fourier-Transform
FTIR	Fourier-Transform Infrared Spectroscopy
G6P	Glucose-6-phosphate
HPLC	High-Performance Liquid Chromatography
MIC	Minimal Inhibitory Concentration
MOCVD	Metal-Organic Chemical Vapor Deposition
MRI	Magnetic Resonance Imaging
MTSAL	Micelles Templated By Self-Assembly By Ligands
NP	Nanoparticle
PEG	Polyethylene Glycol
PL	Photoluminescence
POM	Polyoxometalate
PXRD	Powder X-Ray Diffraction
QLED	Quantum Dot Light Emitting Diode

REE	Rare-Earth Element
RF	Radio Frequency
RM	Reaction Mixture
ROS	Reactive Oxygen Species
RT	Room Temperature
SAXS	Small Angle X-ray Scattering
SE	Secondary Electron
SEM	Scanning Electron Microscope
tBPA	<i>tert</i> -Butylphosphonic Acid
TEM	Transmission Electron Microscope
TGA	Thermogravimetric Analysis
TiBALDH	Ammonium oxo-lactato titanate (Erroneous custom formulation Titanium Bis-Ammonium Lactato Di-Hydroxide)
TMP	Trimethylphenol
UV	Ultraviolet
VB	Valence Band
vis	Visible Light
XAS	X-ray Absorption Spectrometry
XRD	X-Ray Diffraction
XPS	X-Ray Photoelectron Spectroscopy



# 1. Introduction

## 1.1. Background

Nanomaterials with novel properties are expected to be the basis for next generation technologies in the areas of catalysis, electronics, computing, energy, and medicine (Chakraborty et al., 2011; Shulaker et al., 2017; Khanal et al., 2019; Bhardwaj & Kaushik, 2017). The nature of nanomaterials differs from that of their bulk counterparts in ways of, for instance, higher available surface area, higher surface energies because of larger surface-to-area ratio, crystal facettes, grain boundaries, more noticeable contribution of quantum effects due to the small particle size, modification of surface electronic structure, and due to crystal defects usually not present in the bulk form (Bruce et al., 2010). Nanoparticles are a common form of manufactured nanomaterials and usually are represented by pure metals (e.g. Pd, Ag), metal oxides (e.g. TiO<sub>2</sub>, ZnO), or chalcogenides (e.g. CdSe, MoSe<sub>2</sub>). The industrial production of nanoparticles typically relies on top-down processes where smaller particles are produced from bigger particles. This allows for production of large quantities but homogeneity in both size and shape tend to be low. Better control over both size and shape is often achieved by bottom-up processes, where the starting materials are molecular precursors. However, a drawback of the latter one is smaller production volumes. Popular bottom-up syntheses includes the sol-gel process and the solvothermal process. Other, more complicated processes, are the metalorganic chemical vapor deposition (MOCVD, which utilizes pyrolysis of gaseous metalorganics of high purity to form thin crystalline films) and atomic layer deposition (ALD, which uses sequential deposition of different gaseous precursors to form complex layered materials). Decomposition of

metal-organics can yield both simple and complex oxides (Rao & Kanishka, 2015). Good control over the syntheses is prerequisite to obtain homogenous materials. The prepared nanoparticles can be employed in a variety of applications including: nanoabsorbents (Polido et al., 2015; Gao et al., 2004), immobilization of enzymes (Pogorilyi et al., 2017; Miller et al., 2019), self-assembled structures (Deng et al., 2017; Andala et al., 2012; Boles et al., 2016), fillers, drug delivery, catalysis, and organic-inorganic hybrids (Rozes & Sanchez, 2011; Cargnello et al., 2014). Among nanoparticles based on transition metal oxides, the titanium dioxide (titania/TiO<sub>2</sub>) nanoparticles are, undoubtedly, the most well studied material (Cargnello et al., 2014). The interest primarily stems from its photocatalytic properties (e.g. H<sub>2</sub> production from water and formation of ROS) and (until recently) considered biological inertness for applications in medicine, cosmetics, and food. Despite intense research on nanomaterials, many safety aspects still are not clear and concerns regarding environmental and health issues from novel nanomaterials have emerged (Boyes et al., 2017). Nevertheless, nanomaterials are expected to bring new powerful diagnostic and therapeutic possibilities, including combined diagnostics and treatments, popularly called “theranostics” (Bhardwaj & Kaushik, 2017; Kelkar & Reineke, 2011). The intention with this thesis is to contribute to the development of molecular<sup>1</sup> nanotechnology based on titanium dioxide with particular emphasis on medical applications and photocatalysis.

## 1.1. Titanium dioxide

Oxide minerals are the major constituents of the Earth’s crust; silicon-, aluminum-, and iron oxides being their most abundant representatives. A less abundant fraction consists of titanium oxides, such as anatase, rutile, and brookite (different forms [polymorphs] of titania, TiO<sub>2</sub>), ilmenite (TiFeO<sub>3</sub>) and ulvospinel (Fe<sub>2</sub>TiO<sub>4</sub>) (Greenwood & Earnshaw, 1997). The main industrial application of titania is as white pigment in paints, but it also finds use in self-cleaning windows and photocatalysts (Cargnello et al., 2014; Nakata & Fujishima, 2012). Most commercially important today are two crystal phases of titania; rutile and anatase, Figure 1. Rutile is the thermodynamically stable phase in bulk form while anatase is the

---

<sup>1</sup>*Molecular nanotechnology* refers in this text to nanomaterials produced from molecular precursors. Different definitions for this term exist, see e.g. Boström (2016).

thermodynamically stable phase below ~14 nm, due to reversal of surface energies at this size (Gribb & Banfield, 1997). Rutile, with two shared edges, as compared to anatase with four shared edges, is more stable according to Pauling's third rule (Essington, 2015). The crystallization of amorphous titania to anatase is strongly dependent on the conditions (acidic, basic, contaminants, wet, or dry, etc.), but can occur at relatively low temperatures starting from 250°C-300°C (Yanagisawa & Ovenstone, 1999) and anatase crystallites were reported to form at room temperature (Seisenbaeva et al., 2013). Enzymatic and peptide-assisted synthesis of amorphous and nanocrystalline titania have been reported (Katagiri et al., 2009; Tong et al., 2014), although this is likely not a true enzymatic reaction but rather an interaction between precursors and the peptide chains. At temperatures about 500°C anatase undergoes irreversible phase-transition forming rutile (Cargnello et al., 2014), although the transition temperature can be increased if dopants are added (cf. section 1.1.1.2.). As phase-transformation from anatase to rutile is initiated from the surface (Zhang & Banfield, 2005), also surface morphology, e.g. ligand functionalization, has been demonstrated to have an impact on phase-transitions (Machon et al., 2010; Machon et al., 2011).

In the early 1970's Honda and Fujishima discovered the ability of titania to photocatalytically decompose water (Honda & Fujishima, 1972). This spurred intensive research in applications of titania nanoparticles for photocatalytic decomposition of organic pollutants and for hydrogen gas production (Nakata & Fujishima, 2012).

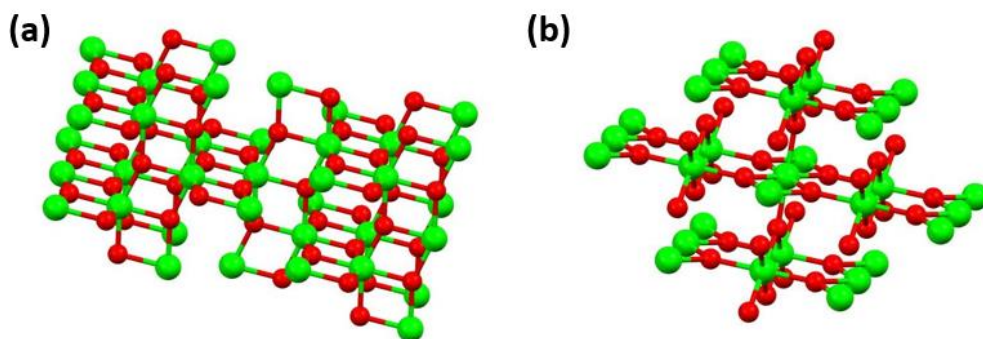


*Figure 1.* Structure fragments of (a) anatase and (b) rutile, two different crystal phases of titania. Green is titanium and red is oxygen.

Unfortunately, in terms of efficiency, the band gaps of titania (~3.0 eV and ~3.2 eV for rutile and anatase, respectively) are wide and require electromagnetic radiation (EM) in the ultraviolet (UV) range for promoting an electron to the conduction band (Cargnello et al., 2014). Anatase is considered as a more efficient photocatalyst compared to rutile despite its wider bandgap. This has been explained by slower recombination rates of electron–holes and higher density of localized states in anatase (Youkun et al., 2011; Maity et al., 2018). Catalytic reactions on nanoparticles occur at the particle surface and, evidently, surface properties, such as crystallographic faces, oxygen vacancies, metal-oxide interfaces, and dopants are critical. The (0 0 1) face of anatase titanium dioxide has high surface energy (because of coordinatively unsaturated titanium atoms) and is the catalytically most active face but also tends to be reduced in area because of this (Cargnello et al., 2014). Yang et al., (2008) produced anatase titania with close to 50 area% of the (0 0 1) face via solvothermal synthesis using acidified aqueous  $\text{TiF}_4$  solution. When titanium atoms in (0 0 1) plane were terminated with fluorine, their surface energy became lower than the otherwise more stable (1 0 1) face. The same strategy was employed by Fang and co-workers (2017) to synthesize titania with high percentage of  $\text{Ti}^{3+}$  ions and (1 0 1)–(0 0 1) junctions which were favorable for photoreduction. It showed increased photoreduction of  $\text{CO}_2$ , with product selectivity towards  $\text{CH}_4$ , compared to unmodified titania. Ignatchenko and co-workers (2006) investigated surface adsorption of water to titania (anatase) surfaces. They found a molecular adsorption on the (1 0 1) face, while a dissociative adsorption on the (1 0 0) face. In another study Bikondoa and co-workers (2006) found a dissociative adsorption of water on the rutile (1 1 0) face. Hydroxide groups on the titania surface were found to stabilize adsorbed water via hydrogen bonding.

### 1.1.1. Increasing the catalytic activity of titania

The constraint of UV-radiation to photoexcite electrons in titania has resulted in several strategies to utilize radiation in the visible range. This includes the use of *sensitizers* and *dopants*, as discussed in the sections below.

### 1.1.1.1. Sensitizers

Organic sensitizers (visible light absorbing molecules) have been attached to the titania surface via functional groups (Figure 2.), including carboxylates, phosphates and phosphonates (Miller et al., 2019; Willkomm et al., 2016). The photoexcited electron from the sensitizers valence band (VB) is then transferred to the conduction band (CB) of titania where it is available for a reduction reaction (which requires the CB of the sensitizer to possess lower energy than for  $\text{TiO}_2$ ). This methodology has been applied together with immobilized reductases, i.e. *formate dehydrogenase* and *carbon monoxide dehydrogenase I*, to assist reduction of carbonates into formate and carbon monoxide, respectively (Miller et al., 2019; Woolerton et al., 2010). This does, however, require the addition of an electron donor to reduce the oxidized sensitizer. Lin and co-workers (2014) coated titania nanotubes used as photoanode in a dye-sensitized solar cell (DSSC) with a wide band gap semiconductor ( $\text{Y}_2\text{O}_3$ ). Electrons could tunnel through the yttria layer but were prevented from flowing back and recombine with the hole in the sensitizer, considerably increasing the efficiency.

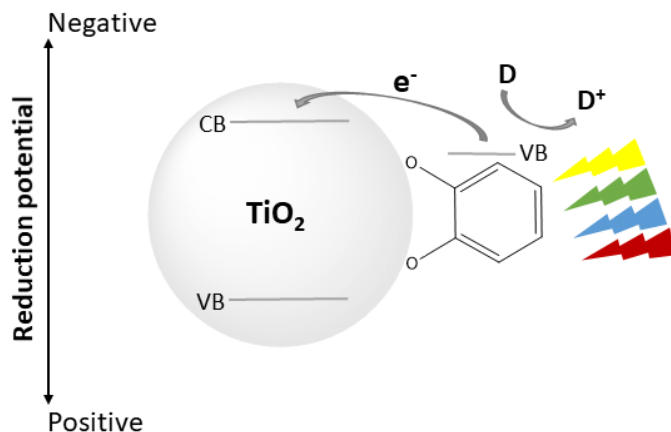


Figure 2. Simplified illustration of an organic sensitizer attached to a  $\text{TiO}_2$  NP. An electron is excited by absorption of visible light and is transferred from the valence band (VB) from the sensitizer to the conduction band (CB) of titania. An electron donor (D) is oxidized to reduce the sensitizer. The electron in the  $\text{TiO}_2$  CB can then be used for reduction by transfer to a band of more positive reduction potential.

Analogously, Nattestad et al., (2010) developed a DSSC with a perylenemonoimid group as light harvester coupled to a triphenylamine donor connected via oligothiophene linker. The longer linker, the lower recombination rate. The authors explained this by improved electron-hole separation. Recent work by Peng and co-workers (Peng et al., 2018) revealed that functionalizing TiO<sub>2</sub> NPs with acetylene derivatives (M-O-C≡C-) drastically increased charge-transfer between the sensitizer and TiO<sub>2</sub> due to formation of interfacial states because of delocalization from  $\pi$ -bonds in the ligand.

Inorganic compounds may serve as sensitizers as well (Cao et al., 2011). A compound with a narrow band gap (e.g. Bi<sub>2</sub>O<sub>3</sub>, CdS) is then used. Excited electrons from the inorganic sensitizers are transferred into the CB of titania.

The electron transfer between two semiconductor crystals is called *heterojunction charge transfer*. The reaction is driven by a potential difference over the interface (Cao et al., 2011). A benefit of this system is that the heterojunction retards electron-hole recombination, allowing the electron to “escape”. The advantage of inorganic sensitizers can be lower cost and less leakage but they can suffer from photo-corrosion (Willkomm et al., 2016). However, similar crystallinity, close contact, and properly placed conduction bands are required for electron transfer between two semiconductors. The inorganic dopants can be attached by different approaches, for example, Robel et al., (2006) used organic linkers to connect CdSe to TiO<sub>2</sub> nanoparticles. The CdSe particles efficiently transferred photoexcited electrons to the titania. Nguyen and co-workers (2019) deposited CdS nanoparticles on titania nanofibers. The CdS efficiently transferred photoexcited electrons to titania, significantly increasing water-splitting compared to unmodified titania.

### 1.1.1.2. Doping of titania

Titanium or oxygen ions can be substituted in the titania lattice by other elements, which is called doping. These elements can be either anions, e.g. N or F (Asahi et al., 2001; Chen et al., 2016; Dwyer et al., 2019), or cations, e.g. d-block and f-block (Colmenares et al., 2006; Weber et al., 2012). This has several beneficial effects on the catalytic properties; first, the band gap can be decreased, and result in a red shift in EM absorption (Stengl et al., 2011) which is explained by introduction of intermediate energy levels between the VB and CB of titania (Weber et al., 2012). Second, disruption in the lattice structure by inclusion of heteroelements aggravates the

coalescence of primary nanocrystals and therefore gives smaller particles which results in larger active surface area. However, formation of dopant oxide phases (particularly at higher concentrations) on pure titania nanoparticles can also prevent coalescence (Yurtsever & Ciftcioglu, 2017). These oxide phases may in smaller amounts act as inorganic sensitizers (Weber et al., 2012). The substituting element should have an ionic radius similar to the element it replaces, i.e. titanium or oxygen.

Third, the structural reorganization of the anatase phase to the rutile phase is hindered by dopants, which then will require higher temperatures for phase-transition (Burns et al., 2004). This allows for higher annealing temperatures that gives better crystallinity. Higher crystallinity facilitates the electron transfer through the crystal, which is of particular interest in photocatalysis. Intriguingly, small amounts of dopants can alter the electronic structure at the catalyst surface affecting adsorption of reagents and stabilization of reaction intermediates (Abbasi et al., 2017). Likewise different faces have different electronic structures which explains varying reactivity and selectivity. Oxygen vacancies can be introduced via doping with cations to balance charges (Schottky-Wagner type defect). The oxygen vacancies may either promote or decrease catalytic activity of the material and can act as a recombination center. The vacancy sites have been identified as active sites for carbon dioxide reductions in, for example,  $\text{In}_2\text{O}_3$  (Wang et al., 2020) and for dissociative water adsorption on some  $\text{TiO}_2$  faces (Bikondoa et al., 2006).

### **1.2.2. Solution chemistry of titanium coordination complexes**

Titanium has a rich coordination chemistry in solution, particularly for anhydrous organic solvents, but recently even progress in aqueous titanium coordination compounds has been reported, particularly from the groups of Nyman (2017 & 2019) and Wang (2016 & 2018). Common commercially available titanium(IV) compounds include titanium(IV) ethoxide and titanium(IV) isopropoxide, titanium(IV) tetrachloride, and titanium ammonium oxo-lactato-titanate (TiBALDH). In solution, titanium alkoxides (with ethoxide, isopropoxide, *n*-propoxide etc. side chains) tend to form oligomers to achieve octahedral coordination of the titanium centers. However, alkoxides with bulkier sidechains, such as *tert*-butyls, tend to remain monomeric in solution (for steric reasons).

In particular titanium(IV) ethoxide and titanium(IV) isopropoxide have been used as precursors to synthesize an enormous diversity of titanium

coordination compounds (Kessler, 2003; Schubert, 2005; Rozes & Sanchez, 2011). The titanium ions in these complexes tend to be octahedrally coordinated and have especially good affinity for oxygen ligands, where carboxylates, phosphonates, phenolates, and  $\beta$ -diketonates are common (Czakler et al., 2015; Chen et al., 2013; Davidson et al., 2006; Kessler et al., 2006).

The formation of a complex is an equilibrium reaction where the thermodynamically most stable species form. At occasions, several stable compounds may form in the same time, including metastable (kinetically stable) compounds, but not the most thermodynamically stable. Thus, introducing a new ligand to a system can shift the equilibrium to favor a new product via ligand exchange (Lawrence, 2010). The concurrent hydrolysis of titanium alkoxides during reaction with ligands tends to form a limited set of ordered titanium-oxo cores, e.g.  $Ti_3O$ ,  $Ti_7O_4$ ,  $Ti_8O_6$ ,  $Ti_{11}O_{13}$ , and  $Ti_{16}O_{16}$  (Rozes & Sanchez, 2011). The basic structure that forms is the  $Ti_3O$  fragment that is common, for example, in titanium alkoxy phosphonates.

Importantly, no hydroxo ( $-OH-$ ) groups are revealed, as they are extremely reactive and, most importantly, unstable thermodynamically because of the strong polarizing effect of  $Ti(IV)$  cations.

The kinetic chemical reactivity increases for oxo-alkoxides compared to metal alkoxides (Turova, 2002). Bridging alkoxides were reported to have a higher reactivity compared to terminal ones, due to higher basicity that facilitates attacks from protic solvents/ligands (Beichel et al., 2004). Several stable aqueous titanium species exist, including mononuclear titanium carboxylates,  $TiL_3$  (where L can be citrate, oxalate and lactate) and the oligonuclear titanium ammonium oxo-lactato-titanate  $[Ti_4O_4(OCOCHOCH_3)_8]^{8-}$  and oxo-oxalato titanate. Mixed peroxo-carboxylate complexes are formed when the peroxo-ligand coordinate via both oxygen atoms, resulting in 7-coordinated titanium centers, compared to the otherwise usually 6-coordinated titanium (Kessler, 2013). An amount of complexes containing the cyclopentadienyl (Cp) ligand.  $TiCp_2Cl_2$  may be the most common precursor compound of this class. It has been used as precursor for bimetallic (Ca, Mn, Sr) complexes with ligand exchange of a Cp ligand for 2-methoxymethanol (Sobota, et al., 2009).

### 1.2.3. Heteroleptic titanium oxo-alkoxide complexes as models for surface interactions and precursors for metal oxide nanoparticles

The formation of titania nanoparticles from titanium(IV) alkoxides proceeds via titanium oxo-alkoxide intermediates (Turova et al., 1994; Kessler et al., 2006; Cheng, et al., 2017). The oxo-alkoxide intermediates grow further to form nanoparticles. At a certain size the species will become unstable in solution and will form a separate phase (precipitate). Before phase-separation occurs, an equilibrium between molecular precursors, intermediates and nanoparticles exists (Seisenbaeva et al., 2013). As the oxo-alkoxide complexes are intermediates (and their structure can be solved by X-ray diffraction of crystallized complexes), they are useful models for interactions between ligands bonded to titania nanoparticle surfaces. Modification with ligands or polymers is also used to control porosity and structure of titania from hydrolyzed precursors (Zhang et al., 2012).

### 1.2.4. Bimetallic oxides of titanium

Titania (in its different polymorphs) is not the only important oxide of this element – titanium may be combined with many other metals to form technologically important bimetallic oxides. Examples include, but are not limited to, the spinel ( $\text{TiM}_2\text{O}_4$ ,  $\text{M}^{\text{II}}$ ), perovskite ( $\text{TiMO}_3$ ,  $\text{M}^{\text{II}}$ ), and pyrochlore ( $\text{Ti}_2\text{M}_2\text{O}_7$ ,  $\text{M}^{\text{III}}$ ) phases. They have, for instance, piezoelectric, superconductivity, magnetic, ion conducting, catalytic activities, and potential application in nuclear waste storage (Farmer et al., 2014; Bramwell & Gingras, 2001; Maeda, 2014; Yang et al., 2016). It is rather common to synthesize mixed oxides via fine mixing of the individual oxides (or carbonates) and subsequently anneal them (solid-state reaction). This can, however, result in phase impurities. Instead hydrolysis or thermolysis of single-source precursors may be used to obtain a purer product (Eslava et al., 2010; Lu et al., 2020). Parola and co-workers (1997) synthesized a number of bimetallic titanium-bismuth complexes. Hydrolysis of these yielded bimetallic oxides which phases were dependent on the annealing temperature. However, to synthesize a desired complex with the proper stoichiometry can at times be very challenging (Lu et al., 2020) and depending on factors such as ionic radius and charge, a bimetallic complex may decompose into an oxide phase of another stoichiometry than desired, despite existent M-O-M' bonds in the complex (Kessler, 2009).

### 1.2.5. Synthesis of titania nanoparticles

A plethora of methods for synthesizing titania nanoparticles exists (Cargnello et al., 2014). Two of the most common, and relevant for the present work, are the *solution-gelation* (sol-gel) process and *solvo/hydrothermal process*. These methods start from molecular precursors (e.g. metal alkoxides, chlorides, or carboxylates), with or without additives, from which nanoparticles form via simultaneous hydrolysis-condensation reactions with metal-oxo species as intermediates.

#### 1.2.5.1 The sol-gel process

The sol-gel process (Figure 3) starts from a molecular precursor solution that evolves to form colloidal particles (*sol*) through simultaneous hydrolysis-condensation reactions (Kessler, 2009). The particles will eventually aggregate and form a network in the solution (*gel*). Evaporating the solvent will leave an amorphous product powder. When dried, it is called a *xerogel*.

If a supercritical drying of the gel is applied, an *aerogel* is obtained. The aerogels are among the lightest materials known to exist. The sol can also be dispersed onto a substrate to obtain thin films or coatings. It is possible to obtain extremely high surface areas of the dried gels, but these typically shrink if a heat-treatment is applied (Loryuenyong et al., 2012; Zhang et al., 2012). The crystallinity of sol-gel derived metal oxides is generally poor and a heat-treatment is commonly needed to obtain good crystallinity. Additives (e.g. organic ligands) can control shape, size, and porosity of the obtained powder (Cargnello et al., 2014; Ding et al., 2011; Goutailler et al., 2003; Rahal, 2008). In one of the studies it was revealed that addition of hydrochloric acid favors rutile while nitric acid favors anatase (Andersson et al., 2002).

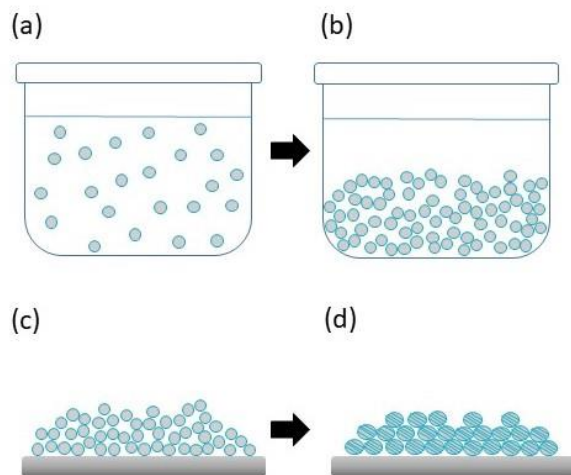


*Figure 3.* Overview of the sol-gel process. Starting from a colloidal precursor solution (a), a gel eventually evolves (b). Drying of the gel results in a porous, amorphous powder (c). During annealing crystallinity improves but porosity decreases and particle size typically increases (d).

Much of the fundamental studies of sol-gel chemistry were elucidated from studies on silicon alkoxides (e.g. see Hench & West, 1990) and then directly transferred to metal alkoxides (e.g. see Livage et al., 1989). Silicon, however, is a semimetal while titanium is a transition metal implying differences in reactivity. The growth mechanism of silicon alkoxides is hydrolysis of Si-OR groups in silicon alkoxides to Si-OH groups that subsequently condense to Si-O-Si (+H<sub>2</sub>O). The same mechanism was proposed for the growth of titania from Ti(OR)<sub>4</sub> and TiX<sub>4</sub> (where X is a halogen). For convenience, titanium alkoxides are often written as Ti(OR)<sub>4</sub>, while they tend to be oligomeric in solution, e.g. (Ti(OEt)<sub>4</sub>)<sub>n</sub>, except those with bulky side-chains, such as *tert*-butyl ligands.

Modification of titanium(IV) alkoxides with chelating (e.g. carboxylates and  $\beta$ -diketonates) was supposed to kinetically decrease the reactivity of titanium alkoxides, and even prevent hydrolysis (Rozes & Sanchez, 2011; Lomoschitz et al., 2010; Chatry et al., 1994; Hubert-Pfalzgraf, 1992; Mahata et al., 2015). Detailed experimental studies of reactivity in metal precursors, including those of Ti(IV) by Kessler and co-workers (2006) have

demonstrated that modification (e.g. chelation) does not decrease reactivity of titanium alkoxides. On the contrary, it increases kinetic reactivity and does not protect against hydrolysis. The chelating ligands can, however, stabilize the formed particles in solution and prevent precipitation. This creates an impression of delayed gelation that gave rise to the misconception about retarded reactivity.

Kessler (2009) proposed a different growth model; the formation of titania (metal oxides in general) nanoparticles goes via formation of oligonuclear oxo-species in one simultaneous hydrolysis-condensation step, i.e. a hierarchical growth. This results in so-called *micelles templated by self-assembly of ligands* (“MTSAL”), Figure 4, consisting of highly ordered metal-oxygen cores with the particle surface stabilized by organic ligands (Kessler et al., 2006). The size of the MTSALs themselves are dictated by, for instance, solution stability and the activation energy needed to incorporate additional metal ions as they grow (Kessler, 2009). This model is supported by observations by Kanaev and co-workers (2017) who studied the hydrolysis of titanium(IV) isopropoxide in different solvents. It was found that nanosized “clusters” formed rather instantaneously after mixture of the precursor and solvent-water mixture.

Further, the growth appeared to be solvent-dependent. Similarly, Nyman and co-workers (2019) studied the dissolution of  $\text{TiOSO}_4$  in water by small-angle X-ray scattering (SAXS) and extended X-ray absorption fine structure (EXAFS). They observed an immediate formation of  $\text{Ti}_8$  complexes upon dissolution that evolved into bigger complexes over time and eventually precipitated as larger particles.

Synthesizing mixed-metal alkoxides is an attractive way of producing mixed-metal oxides. These species can be crystallized, separated and hydrolyzed/thermolyzed to obtain complex oxides. Formation of  $\text{M}^n\text{-O-M}$  bonds may follow from oxo-alkoxide to the oxide phase on condition of thermodynamic stability of the latter (Turova et al., 1994). Obviously, the crystallized solid-state species may not be representative in solution and careful characterization is required (cf. **paper III** and **paper IV**).

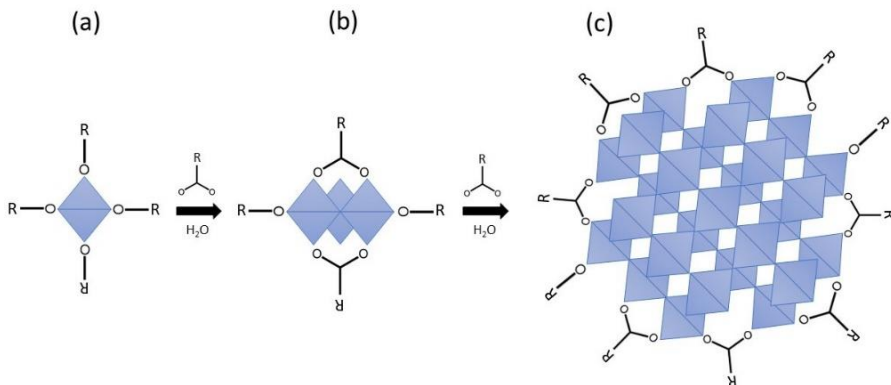


*Figure 4.* MTSAL formation. Titanium(IV) alkoxide monomers (a) hydrolyze and condense into oligonuclear species (b). These oligonuclear species then grow, becoming MTSALs, stabilized in solution by surface bound ligands (c).

### 1.2.5.2. The solvo/hydrothermal process

The solvo- or hydrothermal process (using organic or aqueous solvents, respectively) is performed at elevated temperature and pressure, often resulting in better crystallinity compared to the sol-gel process. Anatase and rutile NPs of good crystallinity were obtained at 120°C by hydrothermal treatment (Andersson et al., 2002). Sometimes an annealing step is anyhow necessary to further improve crystallinity. The RM is placed in a Teflon container which in turn is sealed in an "autoclave" (sometimes called "steel bomb"), see Figure 5, and heated. The morphology of the powder can be controlled by adding organic polymers (Zhang et al., 2012). These methods are also useful to crystallize certain compounds.



*Figure 5.* A steel autoclave with a Teflon container for hydro/solvothermal synthesis.

### 1.3. Self-assembly

Self-assembly is the spontaneous process where small building blocks (e.g. molecules or nanoparticles) spontaneously organize themselves into larger, more complex structures, commonly interacting via van der Waals and/or hydrogen bonding, without any external forces directing the process (Boles, 2016). These building blocks are usually anisotropic and high homogeneity in size and shape is required (Glotzer et al., 2004). Spherical nanoparticles can be made anisotropic by uneven surface functionalization, e.g. via partial masking or from the interface between two immiscible solvents. Self-assembly is an attractive method for production of complex structures in advanced materials.

### 1.4. Nanotechnology

Nanotechnology deals with the production and modification of nano-sized ( $1 \text{ nm} = 10^{-9} \text{ m}$ ) materials. By convention, a nanomaterial has at least one dimension that is smaller than 100 nm. Examples of nanotechnology in everyday-life includes titania nanoparticles as UV-dispersers in sun screens, quantum dots in the displays in QLED TVs, silver nanoparticles in “antibacterial fabrics”, and nanoparticles as contrast in magnetic resonance imaging (MRI). Nanotechnology is also present in agriculture, with applications in, for instance, more efficient fertilizing and pest control (Prasad et al., 2017). Intriguingly, Nature itself is the master of nanomaterials, having evolved ingenious functional nanostructures that includes the waxy nanopatterns on Lotus plant leaves that results in ultrahydrophobicity, the patterning on crustaceans which inhibits algae growth, and the intricate patterning of butterfly wings which are responsible for their beautiful colors, to mention a few examples.

More than a few interesting applications have been developed within the area of bionanotechnology. Bacteria was encapsulated using a titania sol and release them with good viability by applying organic, chelating ligands to dissolve the shell (Kessler et al., 2008). The latter work was extended to human immune cells which could be encapsulated with titania NPs and still retain high viability and biological function (Youn et al., 2017). Ink-jet printed, paper-based, biosensors containing enzymes or aptamers with potential use in diagnostics have been developed by Brennan’s group (Wang et al. 2014; Hui et al., 2017). Functionalization of nanoparticles with enzymes has received some attention during the last years (Wu et al., 2011;

Woolerton et al., 2010). Benefits of this include greater structural stability (e.g. heat-resistance), improved resilience to heavy metal poisoning, higher reusability (e.g. magnetic nanoparticles), and “boosting” of activity in some reactions by co-attachment of light-harvesting dyes to provide electrons (Miller et al., 2019; Woolerton et al., 2010).

Hybrid materials consist of two different components, often one organic and one inorganic, on the nanoscale. By mixing two components with different properties, it is possible to get synergistic effects not present in the individual parts (Rozes & Sanchez, 2011; Lionel et al., 2010).

Carbohydrates, in particular cellulose – the most abundant biopolymer on the Earth – are popular components in hybrid materials (Klemm et al., 2005; Patel et al., 2019). The nanosized form of cellulose, nanocellulose, is an especially attractive component in hybrids (Oun et al., 2019). For instance, its hydrophobicity and hydrophilicity can be controlled by chemical modification (Shimizu et al., 2014) and by functionalization, inorganic nanoparticles can be attached (Galkina et al., 2015). Alginate, another carbohydrate, derived from brown algae has also received some attention for use in hybrid materials recently (Leroux et al., 2020; Lovatel et al., 2015).

#### **1.4.1. Nanocellulose**

Several types of nanocellulose exist, namely cellulose nanocrystals (CNC), cellulose nanofibrils (CNF), and bacterial cellulose (BC) (Abitbol et al., 2016). The CNC are rather small, highly crystalline particles of 20-40 nm in size. The CNF are fibrous and have a diameter of 10-40 nm while they can be over one micrometer long. CNC and CNF are produced from plant sources. BC, on the other hand, are produced by certain bacteria, e.g. *Gluconacetobacter xylinum*. Unlike CNC and CNF, BC is obtained as a neat product without any wood constituents (Abitbol et al., 2016). Nanocellulose has found potential use in a vast number of applications ranging from packaging material (Herrera et al., 2017) to wound-dressings (Czaja et al., 2006; Hakkarainen et al., 2016) and audio-membranes (Galland et al., 2013).

#### **1.4.2. Nanotitania–nanocellulose hybrid materials for medical applications**

Nanomaterials are emerging as promising tools for treatment and diagnosis (Bhardwaj & Kaushik, 2017). A thin layer of titania on implants has shown to improve regrowth, due to affinity of the phospholipid phosphate groups to titania (Le et al., 2014). Schütz and co-workers (2012)

studied the synthesis of CNF-TiO<sub>2</sub> hybrids and found that properties like transparency, hardness, and Young's modulus was dependent on the homogeneity of hybrids. Smaller additions of titania improved both hardness and Young's modulus of the hybrid films but at certain amounts of titania they sharply decreased.

Nanocellulose has proved to be promising in new wound-dressings, providing beneficial healing environment, and possibly promoting healing of tissues by templating effect (Abitbol et al., 2016). Unfortunately, nanocellulose does not have any antibacterial effect so there is a risk of infection. Different solutions have been applied, for instance introduction of antibiotics to the films (Volova et al., 2018) and addition of silver nanoparticles (Diez et al., 2011). Free drugs, however, in nanocellulose may lead to dangerous burst-releases and require frequent changes of the dressing. It is possible to embed drug carriers, e.g. titania nanoparticles, which surface has good affinity for many functional groups. Adsorption of drugs via carboxylic, phenolic, phosphonic groups etc. results in a delayed release of drugs from the nanocellulose-nanotitania hybrids compared to drugs loaded in pure nanocellulose (Galkina et al., 2015; Evdokimova et al., 2018).

### **1.4.3. Nanomaterials safety**

Concerns regarding the safety of engineered nanomaterials have been raised (Nel et al., 2006; Boyes et al., 2017). The possible uptake of nanoparticles and their toxicity to organisms are of particular concern (Fadeel, 2019; Kranjc & Drobne, 2019). Part of the risk with nanomaterials is that they are of the same size range as components in the cellular signaling pathways and the “molecular factories” which allows for interference. Properties like crystalline phase, size, composition, and surface energies have been proposed to be critical factors contributing to the toxicity (Boyes et al., 2017). One example is asbestos, a silicate mineral. Asbestos is carcinogenic, not because of chemical toxicity but as a result of its fibrous structure which causes physical cell damage. Recent studies have demonstrated that nanomaterials can enter cells and affect gene expressions (Chen et al., 2017; Xun et al., 2017; Gliga et al., 2017). For example, Cooper & Spitzer (2015) found that sub-lethal levels of Ag nanoparticles accumulate in rat tissues and result in negative effects on neural cell development. Crosera and co-workers (2015) investigated uptake of TiO<sub>2</sub> NPs on epidermal cells and found that the particles did not cross the skin barrier.

Cytotoxicity of TiO<sub>2</sub> NPs towards HeLa cells was observed, but only at very high concentrations. In contact with blood, on the other hand, TiO<sub>2</sub> nanoparticles have been found to induce blood coagulation at very low concentrations (Ekstrand-Hammarström, 2015). This effect was exploited by applying a spray of colloidal TiO<sub>2</sub> NPs on rats with burn wounds. The result was an improved wound-healing with decreased fibrosis (scar formation) (Seisenbaeva et al., 2017). According to several studies, cytotoxicity of a nanomaterial may differ dramatically; it can be apparently harmless for one cell type while being highly toxic for another.

Toxicity may also differ for a compound dependent on its crystalline phase. Sayes et al., (2006) investigated cytotoxicity of anatase and rutile titania. They found that the overall toxicities for both phases were low, but that anatase was about 100 times more toxic compared to rutile. The reason for this was believed to be the better production of ROS from anatase.

## **1.5. Characterization techniques**

A variety of different analytical instruments with different working principles have been used to characterize the compounds and materials synthesized in this thesis. Basic theory principles for the most important instruments are briefly described below, as well as which kind of information that can be obtained from them. References to more elaborate theoretical descriptions are provided in the end of each section. The reader acquainted with chemical analysis may jump ahead to the Materials and Methods section.

### **1.5.0. The physical basis**

Our current understanding of the atomic nucleus is based on the quantum mechanical model. It introduces a number of properties not explained by the classical mechanics, namely *quantization*, *wave-particle duality*, *the uncertainty principle*, and *quantum entanglement*, where the two former ones are fundamental in chemical analysis. The spectrometric methods in analytical chemistry are based on the interaction between electromagnetic radiation and matter (often the electrons).

Electrons populate discrete energy levels around to the atomic core and cannot exist between these discrete energy levels, i.e. they are *quantized*. To promote an electron to a higher energy level the exact difference in energy must be added to the electron (by electromagnetic radiation, for instance) and if an electron transit from a higher energy level to a lower the energy difference between the higher and lower level must be emitted. If the transition involves electromagnetic radiation in the range of 400 nm to 750 nm, we will perceive this as colors. The *wave-particle duality* states that an electron can behave both as a particle and as a wave. This it is the basis of electron microscopy where the extremely small wavelength of high-energy electrons is used to view objects below the nanometer scale. The detected signals in spectrometric analyses are forms of electromagnetic radiation.

Older instruments used to scan wavelength-by-wavelength and overlay spectrum, which was time consuming, especially when many scans were necessary. Newer instruments (e.g. IR and NMR) scan the entire spectrum simultaneously and produce an interferogram, containing a periodic function that is the sum of all detected signals. The components, i.e. the individual functions, of the interferogram are extracted by a mathematical procedure called *Fourier Transformation* (FT) (Williams & Fleming, 1995; Lennerstad & Jogr eus, 2013).

### 1.5.1. X-ray crystallography

X-rays ( $\lambda < 10$  nm) passing through a material will interact with the material's electrons (Figure 6). The heavier the element (i.e. more electrons) the more interaction between X-rays and the atom. Hence, hydrogen is difficult to detect while heavier element such as tungsten diffracts very well.

If the material's atoms are ordered regularly, i.e. being crystalline, the X-rays will be diffracted regularly giving rise to a diffraction pattern (Figure 6). By combining diffraction intensities, diffraction angles, and distances from the detector, the structure of the compound can be mathematically modelled by a computer program (with user input), also called "solving the structure". The strongest diffraction occurs when Bragg's law is satisfied:

$$2d \sin \theta = n\lambda$$

Here,  $\theta$  is the scattering angle,  $d$  is the interplanar spacing,  $\lambda$  is the wavelength, and  $n$  is an integer. The X-rays are elastically scattered by lattice planes in the crystal (Figure 6). The “ $\alpha$ ” wave in Figure 6a is deflected by the second lattice plan, which means it travels a longer distance than the “ $\beta$ ” wave does. If the path length difference is an integer ( $n$ ) of  $2d \sin \theta$ , the two waves will be in phase, resulting in constructive interference, and diffraction spots are observed. If the path length difference is not an integer of  $2d \sin \theta$ , the waves will be out of phase and mostly cancel out and no diffraction spots will be observed. For crystalline nanopowders the crystallites will be randomly oriented and give rise to a ring pattern instead of individual diffraction spots, Figure 7.

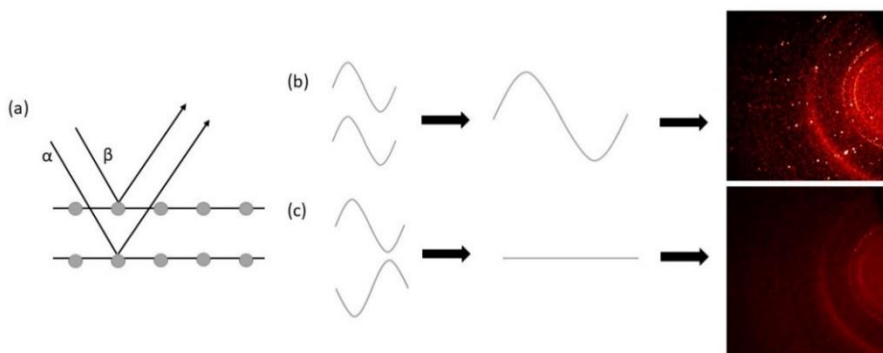


*Figure 6.* X-ray diffraction in crystalline and amorphous materials. (a) Incident X-rays are being scattered by different lattice planes and the outgoing waves will interfere. When the waves are in phase, constructive interference occurs and the amplitudes add on as in (b) and diffraction spots are observed. (c) In an amorphous sample, the atoms are randomly distributed and scattered X-rays will mostly cancel out, thus no diffraction pattern is observed.

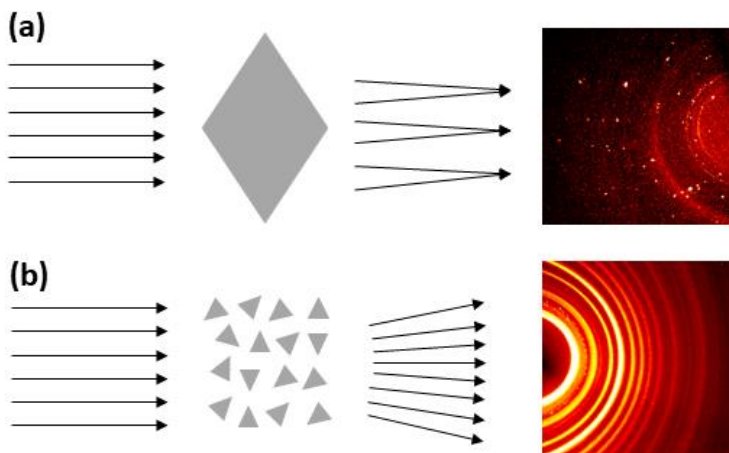


*Figure 7.* Diffraction patterns from a single crystal and a nanocrystalline powder. (a) For a single crystal, a diffraction pattern with discrete spots is obtained due to the regular diffraction. (b) As the nanocrystallites in (b) are randomly oriented as ring pattern is obtained. The black arrows indicate directions of X-ray photons.

To obtain structural information from amorphous/short range ordered materials, synchrotron based X-ray absorption spectrometry (XAS) techniques, such as extended X-ray absorption fine structure (EXAFS) are useful. The structure of both organic and inorganic compounds, as well as more complicated biomolecules such as enzymes, are routinely solved with X-ray techniques. It is a corner-stone in structure determination, particularly in inorganic chemistry, but also in organic chemistry together with  $^{13}\text{C}/^1\text{H}/^{31}\text{P}/^{15}\text{N}$  NMR, mass spectrometry, and IR spectrometry. To obtain diffraction data for a compound, single crystals of sufficient quality must be grown which can be very challenging. When the crystals are air and/or moisture and/or temperature sensitive (or all at once!), cooling to about  $-70^\circ\text{C}$  by liquid nitrogen is very useful. Data collection at low temperatures in general improves data quality by reducing thermal movements of atoms that otherwise may contribute to disorder in the structural model.

Powder X-ray diffraction (PXRD) is used to determine crystalline phases for inorganic materials (but can also be done by high-resolution TEM and Raman spectrometry). As the crystallites are oriented randomly in a sample, ring patterns from the summation of individual reflections, rather than

discrete diffraction spots as in the case of a single crystal, will be obtained. By applying the Scherrer equation, an average crystallite size in the sample can be calculated:

$$r = \frac{K\lambda}{\beta \cos \theta}$$

Where  $r$  is the *average* crystallite size,  $K$  is a shape constant (0.9 for spherical particles),  $\lambda$  is the X-ray wavelength (0.71073 Å for MoK $\alpha$ ),  $\beta$  is full width at half maximum (FWHM), and  $\theta$  is the Bragg angle. From the peak intensities, peak positions, and peak shapes in a powder diffractogram, a vast amount of information (e.g. unit cell parameters, porosity, defects) can be extracted via Rietveld refinement. It is possible to solve the 3D structure of a crystalline powder. This requires the construction of a structural model to fit the experimental data against, thus good chemical knowledge of the sample in addition to high-quality PXRD data are required for Rietveld refinement. Deeper theory about X-ray diffraction and crystallography is found in Hammond (2001) and Zou et al., (2011). A nicely written introduction about XAS (including EXAFS) is available in the thesis by Jalilehvand (2000).

### 1.5.2. Nuclear magnetic resonance spectrometry

Nuclear magnetic resonance (NMR) spectrometry is based on the interaction of electromagnetic radiation of rather long wavelengths (radio waves) with certain atomic nuclei. Atoms with an odd atomic number have an intrinsic nuclear magnetic moment and can be considered as a magnet. Examples are the  $^1\text{H}$ ,  $^{13}\text{C}$ , and  $^{31}\text{P}$  nuclei. In the presence of an external magnetic field, these nuclei will align either parallel or anti-parallel to the external magnetic field (Figure 8). An excess of the nuclei will be aligned parallel with the field and smaller number of nuclei are aligned anti-parallel. This ratio is described by the Boltzmann distribution, which is a probability distribution describing the likelihood of a system being in a particular state, depending on the temperature:

$$\frac{N_h}{N_l} = \exp\left(\frac{\Delta E}{kT}\right)$$

Where  $N_l$  and  $N_h$  are numbers of nuclei in low and high energy states, respectively,  $\Delta E$  is the difference in energy between the states,  $k$  is the Boltzmann constant, and  $T$  is the temperature. A radio frequency pulse can be absorbed by a nuclei if the RF matches the frequency of its precessing movement, and then “flip” from low to high energy state (Figure 8).

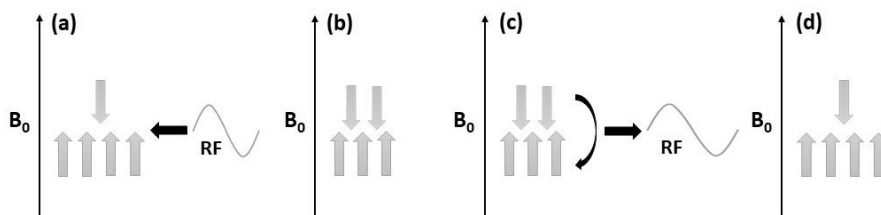


*Figure 8.* Simplified scheme of the excitation process in NMR. The arrow indicate direction of the external magnetic field ( $B_0$ ). (a) A nucleus (grey arrows) in the low energy state absorbs a RF pulse and is excited to the high energy state, i.e. anti-parallel to  $B_0$  (b). (c) The relaxation process induces an electric current in the detector coil which is recorded and the RF energy is re-emitted during the relaxation (see main text and *Figure 9* for more detailed explanation). (d) The system has returned to its equilibrium state. In reality, the distribution ratio  $N_h/N_l$  is in the order of ca. 1 to  $10^5$ .

The energy required to “flip” a nucleus is dependent on its chemical and electronic environment, i.e. its neighboring atoms. A high density of electrons around a nucleus will screen it from the applied magnetic field and requires higher energies for resonance and vice versa. For instance, an oxygen atom bonded to a carbon atom will withdraw electron density from the carbon atom due to its higher electronegativity and therefore lower energies are required for resonance. When bonded to hydrogen, which has similar electronegativity to carbon, more electron density will remain close to carbon and higher energies are needed for resonance. Regardless of the specific molecule, a nucleus with a certain bonding environment will always absorb in a narrow, specified region (Figure 11), thus NMR is one of the most powerful tools for structural determination. The NMR spectrum is a diagram of the absorption intensity as a function of the applied RF *frequency*.

As the resonant frequency is dependent on the field strength of the spectrometer's magnet, the x-axis is instead calibrated to display the system independent *part per million* (ppm) scale. The actual signal detected in the NMR spectrometer is called free induction decay (FID). When the RF pulse is applied, alignment of the nuclei is flipped  $90^\circ$  relative to the z direction, i.e. to the xy-plane. When it spins in the xy-plane, the magnetic field will induce a current in the detection coils which is the detected signal. As the nuclei are returning to their equilibrium state (aligned to z-axis), the amplitude of the signal decreases (Figure 9). The recorded FID is converted via FT to a frequency-domain spectra (Figure 10b).

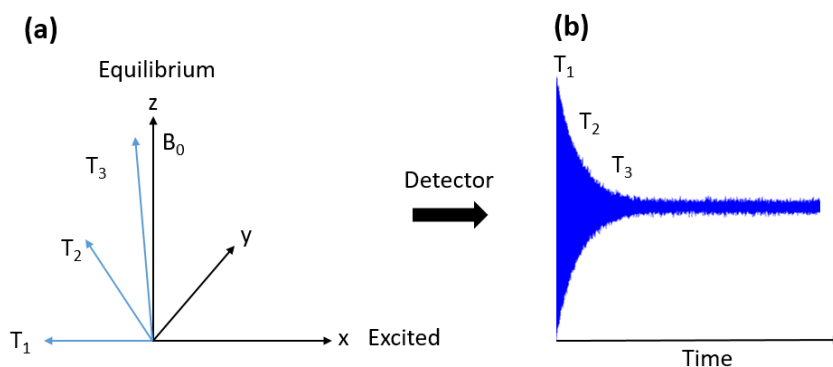


*Figure 9.* The free induction decay (FID) signal. When excited with a  $90^\circ$  RF pulse, the nuclei precess along the yx-plane. This induces a current in the detector coil which then is recorded. As it relaxes, the nuclei returns to its equilibrium state by a spiral precessing around the z-axis (i.e. the direction of the external magnetic field,  $B_0$ ). As the nuclei approaches its equilibrium state (aligned to the z-axis), the FID signal becomes weaker.  $T_1$ ,  $T_2$ , and  $T_3$  indicates in (a) different precessing positions at different times and their approximate FID responses in (b).

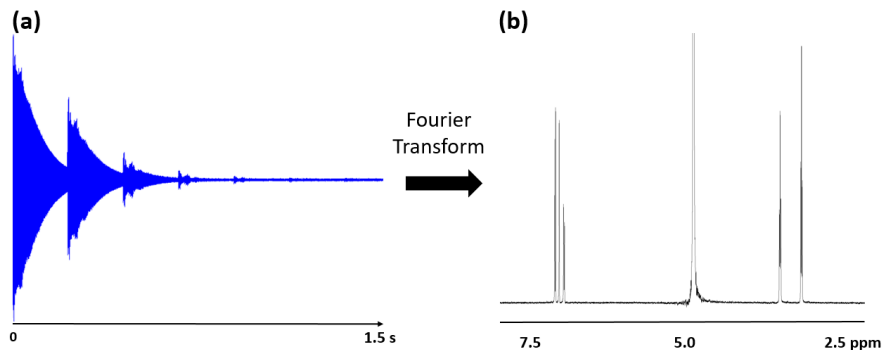


Figure 10. Transformation of the FID signal. The FID signal (in time domain) from a  $^1\text{H}$  NMR experiment is shown to the left and is the sum of all detected signals. The individual functions of the FID are extracted by Fourier Transformation to display a spectrum in the frequency domain (right).

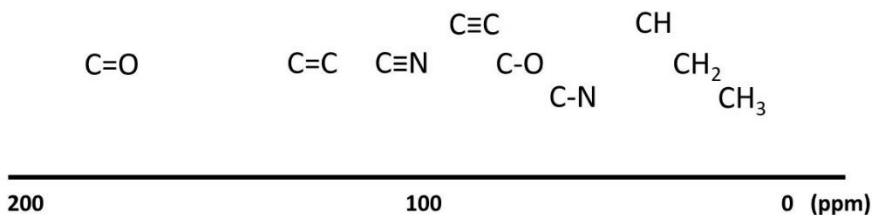


Figure 11. Scheme of the approximate areas of some important carbon NMR shifts in ppm.

The same principle applies for  $^1\text{H}$  NMR, but it covers a lower and more narrower frequency region, equal to about 0-10 ppm. However, for the proton NMR an additional phenomenon called *spin-spin splitting* is present.

Coupling between spins of a proton nuclei located on a nearby atom give rise to a total amount of signals equal to  $N+1$ , where  $N$  is the number of neighboring protons. For instance, the molecule  $\text{Cl}-\text{CH}_3$  would have one single proton signal (all three H are equivalent). However, the molecule  $\text{Cl}-\text{CH}_2-\text{CH}_3$  have two different kinds of protons and will result in two sets of proton signals. Due to spin-spin splitting, they will be represented by one

triplet (for  $-\text{CH}_3$ ) and one quartet (for  $-\text{CH}_2-$ ). Thus, this is very helpful in structure determination, particularly in combination with 2D NMR methods (e.g. COSY and HSQC). The theory behind NMR is intricately complex, although good introduction texts include McMurry (2007), Holler et al., (2008), and Williams & Fleming (1995).

### 1.5.3. Scanning electron microscopy

The size of the objects we can see is limited by the wavelengths of visible light, which lies in the range of 400 nm to 750 nm. At best, optical microscopy can visualize objects down to about 200 nm. According to the particle-wave duality, the electron can be seen as both a wave and a particle. When it moves, the electron has a wavelength (*de Broglie wavelength*) determined by its kinetic energy according to:

$$\lambda = \frac{h}{\sqrt{2m_0E \left(1 + \frac{E}{2m_0c^2}\right)}}$$

where  $\lambda$  is the wavelength of the electron,  $E$  is the electron speed,  $m_0$  is the electron mass,  $c$  is the speed of light, and  $h$  is Planck's constant. The higher the speed (i.e. kinetic energy), the smaller the wavelength. It is possible to reach wavelengths below 1 Å by replacing visible light with high energy electrons, enabling visualization of the smallest nanoscale objects. Scanning electron microscopy (SEM) is based on a highly focused, coherent beam of electrons being electromagnetically directed toward a sample surface.

Examples of acceleration voltages can be about 5-15 keV. The electron beam is typically emitted by a tungsten filament and accelerated via an anode. Electromagnetic coils (condenser lenses) are used to focus the beam and apertures sort out electrons with deviating paths. Pairs of deflection coils move the electron beam in the x and y directions so that the sample surface is scanned in a raster fashion. A simplified scheme of a SEM instrument is illustrated in Figure 12.

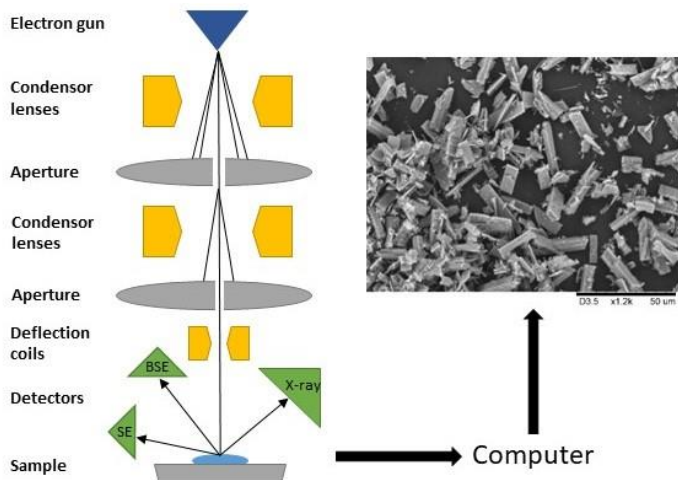


*Figure 12.* Simplified principle of a SEM instrument. The electron beam is emitted from the electron gun and focused to a narrow beam by electromagnetic lenses and apertures. The deflection coils moves the beam to scan the sample surface and detectors register either, secondary electrons, back-scattered electrons and X-rays (for elemental analysis).

Back-scattered electrons (BSE) or secondary electrons (SE) are collected by different detectors. The instrument computer convert the detector signals into a digital image. The BSE originates from the electron beam and the SE are ejected from the sample atoms. SE are emitted from electrons near the surface from impact by the electron beam and provides information of the surface morphology, providing a pseudo-3D image. BSE originates deeper from the sample and can give rough information about differences in chemical composition in a sample seen as differences in contrast (but not chemical identity, which can be done by couple the SEM (and TEM) to an EDS system (cf. section 1.5.5.)). The SEMs used for the work in this thesis are of the environmental type. While being comparatively small, easy to handle, operating at lower vacuum, and do not require nitrogen cooling, they do not reach the same magnification and resolution as the conventional SEM models. More information about SEM is found in Egerton (2006).

#### 1.5.4. Transmission electron microscopy

Transmission electron microscopy (TEM), contrary to SEM, detects electrons that pass *through* the sample, rather than being deflected. This obviously requires much thinner samples and higher accelerating voltages, typically 100 keV to 300 keV. The detector, a charge-coupled device (CCD) detector, is situated under the sample. Even more sets of electromagnetic lenses and apertures are required and the electron source is now typically a LaB<sub>6</sub> single crystal or a field emission gun. Contrary to the raster scan of SEM, the whole image is projected simultaneously by using condenser lenses above the sample to spread the electron beam. A 2D image of the sample as seen in Figure 13 is projected. TEM is indispensable for investigation and characterization of small nanoscale objects, such as nanoparticles. Resolutions below 1 Å can be achieved. Crystalline samples will diffract the electron beam orderly and produce rows of regularly ordered row of “dots” which represent atoms (Figure 13). The distance between these rows are characteristic for different chemical compounds in different crystal phases and thus serves as an identifier.

TEM is routinely coupled with techniques for chemical identification such as EDS (cf. below) or electron energy loss spectrometry (EELS). A more recent application of TEM includes electron crystallography where the crystal structures of nanoscale particles can be solved. This is achieved by collecting diffraction patterns from different angles and then combining them. Electron crystallography is a viable option when the crystals are too small for single crystal XRD. An outstanding textbook covering nearly all aspects of TEM in exquisite detail has been written by William & Carter (2009). A good introduction to electron crystallography is available by Zou et al., (2011).

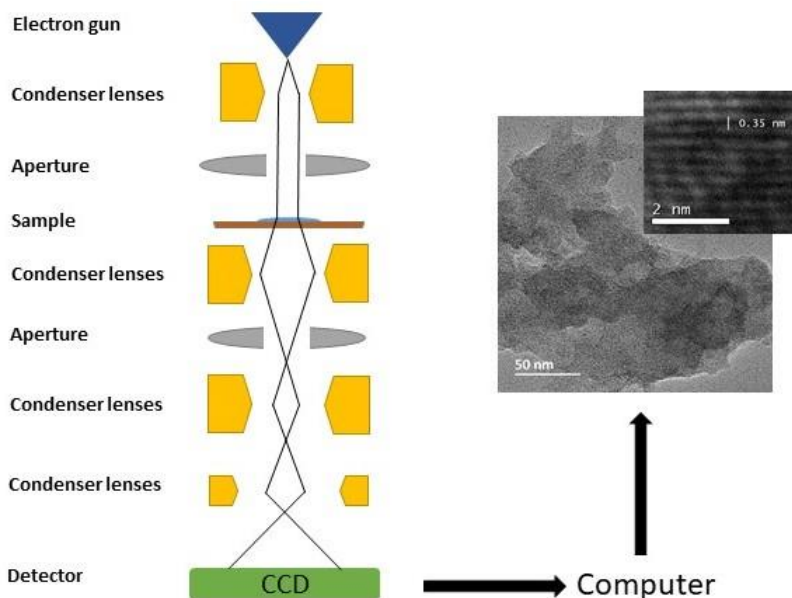


*Figure 13.* Simplified principle of a TEM instrument. The electron beam is spread by condenser lenses to cover an area of the sample. After passing the sample, a series of apertures and condenser lenses are used to form an image that is registered by a CCD camera. The inset shows a HRTEM micrograph of anatase TiO<sub>2</sub>.

### 1.5.5. Energy-dispersive X-ray spectrometry

If an electron with sufficiently high energy collides with an atom's core electrons, it may cause ejection of a core electron from the atom with formation of an electron vacancy. This vacancy is unstable and an electron from a higher energy level will de-excite to fill the vacancy. The energy difference between the two energy levels will be emitted in form of X-rays (Figure 14). The energy of the emitted X-rays are characteristic for each element (with a few overlaps, such as Bi and S) and are routinely used for elemental analysis. It is possible to analyze a very small area ("spot analysis") and map a "larger" area in both SEM and TEM. The theory of EDS is covered in detail by Egerton (2006).

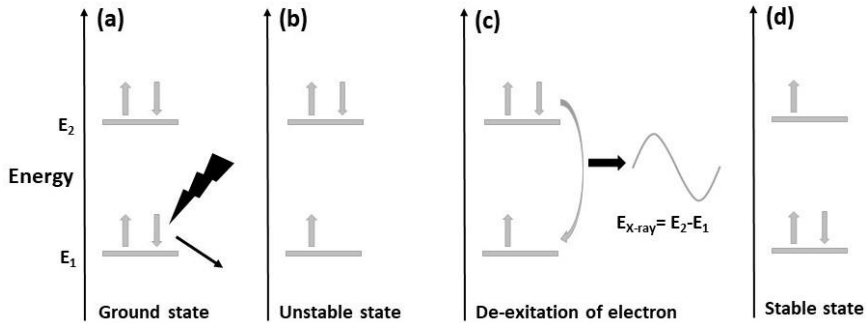


*Figure 14.* Principle of EDS. In (a) a core-electron is knocked out by the impact from a high-energy electron leaving a vacancy (b). An electron from a higher energy level will lose energy (equal to the energy difference between the two levels  $E_2$  and  $E_1$ ) and take the place of the ejected electron to result in a new, stable state. This energy is emitted in the form of X-rays, characteristic for each element. The grey arrows represent electrons of different spin states.

### 1.5.6. Atomic force microscopy

Atomic force microscopy (AFM), in contrast to the spectrometric and electron microscopy methods, is based on electrostatic or direct physical interaction between the sample surface and a probe (Figure 15). The surface probe consists of an extremely thin tip on a cantilever, down to a few nanometer, that “senses” the surface. Like SEM, AFM performs a raster scan over the surface. A pseudo color image where the color hue is dependent on the sample height is created by the system. The higher surface structures, the lighter the image. AFM is a high-resolution technique and can reach magnifications and resolutions good enough to see details down to a few nanometers. AFM can be operated in either *contact mode* or *non-contact mode*. In the contact mode, the tip is dragged over the sample surface while the change in height is detected, commonly by deflection of a reflected laser beam on the cantilever (Figure 15). The contact mode is suitable for hard samples, such as metal (oxide) nanoparticles and metal/mineral surfaces, but can cause damage to softer samples such as gels and biological samples.

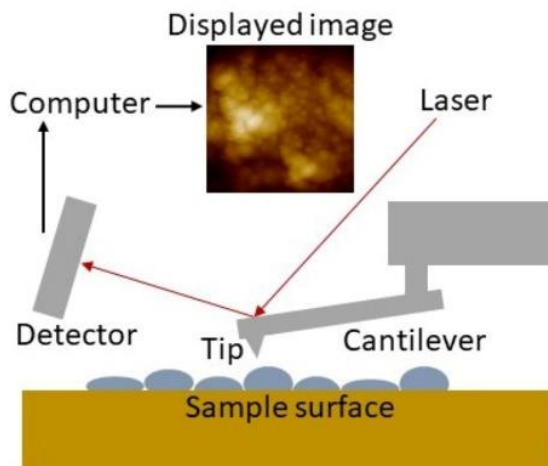


*Figure 15.* Simplified principle of AFM. A surface probe with an extremely thin tip scans the sample surface (either by contact or non-contact mode). The movements of the probe changes the reflection of a laser beam. The changes of the laser beam is translated into image of the surface.

In the non-contact mode, the cantilever is set to resonate close to its resonance frequency, which leads to a constant oscillation amplitude. This oscillation is usually achieved by a piezoelectric component. When the tip approaches the surface, interactions (van der Waals, electrostatic, etc.) causes changes in the oscillation. A feedback system adjusts the height of the cantilever based on changes in the oscillation and creates a surface image from this. Less surface damage is done by the tapping mode compared to the contact mode. A good overview of the AFM technique is given by Haugstad (2012).

### 1.5.7. Infrared spectrometry

Infrared spectrometry (IR) is an absorption spectrometry technique based on the absorption of specific energies of certain chemical bonds in the infrared region. Commonly the mid-infrared region is used,  $4000\text{--}400\text{ cm}^{-1}$  (equivalent to wavelengths between  $2.5\text{--}25\text{ }\mu\text{m}$ ). This energy is not sufficient to excite electrons but instead causes vibrations that temporarily changes

bond lengths and bond angles. Collectively with Raman spectrometry, IR is referred to as *vibration spectrometry*. A dipole moment, permanent or temporary, is required. Compounds such as O<sub>2</sub> and N<sub>2</sub> are thus not IR active.

The FTIR spectrum provides valuable information about functional groups in a molecule. FTIR is commonly used together with mass spectrometry and NMR to determine the structure of organic compounds, but also to confirm, for instance, structures of coordination compounds and organometallic compounds as determined by single crystal X-ray diffraction, as in this work. Organic compounds and inorganic powders are typically milled in anhydrous KBr and pressed to transparent discs that are analyzed.

Samples sensitive to hydrolysis, such as metal (oxo-) alkoxide crystals can be milled in paraffin oil and placed between to KBr slides to avoid decomposition during data collection. Liquid samples are possible to analyze. However, when the sample contains water, signals from the analyte can be masked due to the broad signals of water. The region between 1500 – 4000 cm<sup>-1</sup> contains very specific absorptions representing organic functional groups while the region 400 – 1500 cm<sup>-1</sup> (sometimes referred to as “fingerprint region”) contains a more complex pattern that can be used for compound identification by comparing with a database of known spectra.

Many bands corresponding to inorganic bonds (e.g. Ti–O, Ti–O–Ti, P–O) are found in the 400 – 1000 cm<sup>-1</sup> region. More in-depth theory about infrared spectrometry can be found in Simonsen (2003), Holler et al., (2008), and Williams & Fleming (1995).

### **1.5.8. Raman spectroscopy**

The sample surface is radiated with a laser and a detector records the scattered radiation (Figure 16). The technique builds on the interaction between the electric field of the laser and the electron density of the sample molecule. The more polarizable the sample molecule, the higher the signal intensity. In Raman a bond can absorb radiation and be excited from a vibrational state to a so-called virtual energy state (an intermediate step in a quantum mechanically forbidden transition). Most bonds will return to their initial vibrational level and emit the same amount of energy as they absorbed, which is called Rayleigh scattering (elastic scattering). However, some of the excited bonds will return from the virtual state down to a higher (Stokes) or a lower (Anti-Stokes) vibrational level than before, i.e. inelastic scattering

(Figure 16), although these are very few compared to the elastically scattered ones.

The scattering is dependent on the structural arrangement (chemical bonds and symmetry) of atoms and Raman spectrometry is useful in identification of crystalline phases (to separate anatase from rutile, for instance). Via Raman microscopy, very small sample areas, such as individual particles, can be analyzed. More Raman theory is available in Holler et al., (2008) and Nakamoto (1997).

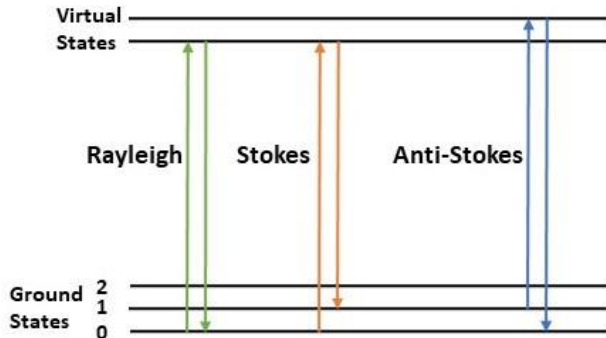


*Figure 16.* Different types of scattering in Raman spectrometry between energy states. Radiation which is elastically scattered is called Rayleigh scattering. Inelastic, radiation of lower energy is called Stokes scattering and radiation of higher energy is called Anti-Stokes scattering.

## 1.6. Objectives of this thesis

The work within this thesis is highly interdisciplinary, consisting of both a chemical part and a biological part. The overall objective was to develop new titania-based nanomaterials from molecular precursors for applications in photocatalysis and medicine. **Paper I** and **paper II** reports two coordination complexes between the drug triclosan and titanium. The hydrolytic stability of the complex in **paper I** was thoroughly investigated.

A drug delivery system based on nanocellulose with titania nanoparticles as drug carriers for triclosan was developed in **paper II**. **Paper III** and **paper IV** investigates a series of new titanium (oxo-) alkoxide complexes with different phosphonate ligands. Ligand-titanium interaction, hydrolytic stability, solution stability, and their applicability as molecular precursors for surface-modified hybrid oxide materials was investigated.

With the encouraging results from the nanocellulose-nanotitania drug delivery system in **paper II**, **manuscript V** was dedicated to investigate the haemocompatibility of the CNF-TiO<sub>2</sub> materials by *in vitro* exposure to human whole blood. In **manuscript VI** hollow titania spheres was developed by ligand-driven (phosphonate and phosphate) self-assembly as possible candidates for encapsulation. Rare-earth element (REE) modified titania nanopowders were synthesized by a solvothermal method in **manuscript VII**. The photochemical properties of the powders were investigated. A bimetallic titanium-yttrium alkoxide was synthesized, to our knowledge the first Ti-REE complex without any oxo-bridges or organic heteroligands.



## 2. Methods

### 2.0. General information

All synthetic and microbiological work were performed at SLU, Uppsala, Department of Molecular Sciences. Detailed synthetic and analytic information are available in the respective papers. Anhydrous solvents were always used for syntheses with titanium alkoxides if not otherwise stated. Analyses and characterization of materials and compounds were made at several locations:

**SLU (Uppsala):** Single crystal and powder XRD, SEM-EDS, AFM, FTIR, TGA, NMR, and part of TEM. **Uppsala University**, Rudbeck Laboratory, Department of Immunology, Genetics and Pathology: Blood incubation with nanocellulose-nanotitania films, platelet counting, ELISA analyses. **Uppsala University**, Department of Materials Science and Engineering: X-ray photoelectron spectrometry (XPS). **Stockholm University**, Department of Materials and Environmental Chemistry: TEM imaging. **National Institute for Laser, Plasma & Radiation Physics, (Romania):** Raman spectrometry, photoluminescence, and photocatalysis. For statistics the R program for statistical computing was used (R Core Team, 2019).

### 2.1. Syntheses of compounds and materials

#### 2.1.1. Syntheses of modified titanium (oxo-) alkoxide complexes

A number of heteroleptic titanium (oxo-) alkoxide complexes were synthesized throughout this work for studies of ligand interaction, hydrolytic stability, and as molecular precursors for complex oxide materials. Their syntheses are briefly described here.

$[\text{Ti}_4(\mu_3\text{-O})_2(\mu_2\text{OEt})_2(\text{C}_9\text{H}_{16}\text{O}_3)_2(\text{C}_8\text{H}_{12}\text{O}_3)_2(\text{C}_{12}\text{H}_6\text{Cl}_3\text{O}_2)_2 \cdot 4\text{C}_3\text{H}_6\text{O}]$ , **1a**, Triclosan (0.46 mmol, 0.3 eq.) was dissolved in acetone and titanium(IV) ethoxide (1.43 mmol) was added. The RM was stored at  $-18^\circ\text{C}$ .

$[\text{Ti}_5(\mu_3\text{-O})_2(\mu_2\text{-OEt})_5(\mu\text{-OEt})_8(\text{C}_9\text{H}_{16}\text{O}_3)(\text{C}_{12}\text{H}_6\text{Cl}_3\text{O}_2)]$ , **1b**, Triclosan (0.071 mmol, 0.3 eq.) was dissolved in acetone and titanium(IV) ethoxide (0.24 mmol) was added. The RM was stored at  $-18^\circ\text{C}$ .

[Ti<sub>6</sub>(μ<sub>3</sub>-O)<sub>2</sub>(μ-OEt)<sub>6</sub>(μ<sub>2</sub>-OEt)<sub>6</sub>(μ<sub>3</sub>-PPA)<sub>4</sub>] $\cdot$ 0.5C<sub>7</sub>H<sub>8</sub>, **1c**, Phenylphosphonic acid (1.0 mmol, 2 eq.) was dissolved in a 1 mL 1:4 toluene: ethanol mixture and titanium(IV) ethoxide (0.50 mmol) was added. The RM was heated in an autoclave at 85°C for 48 h.

[Ti<sub>5</sub>(μ<sub>3</sub>-O)(μ<sub>2</sub>-O)(μ-HOEt)<sub>2</sub>(μ-OEt)<sub>3</sub>(μ<sub>2</sub>-OEt)(μ<sub>3</sub>-tBPA)<sub>3</sub>(μ<sub>3</sub>-HtBPA)(μ<sub>2</sub>-tBPA)<sub>2</sub>(μ<sub>2</sub>-HtBPA)] $\cdot$ 3EtOH, **1d**, *Tert*-butylphosphonic acid (0.48 mmol, 2 eq.) was dissolved in 0.3 mL toluene + 4 mL ethanol and titanium(IV) ethoxide (0.24 mmol) added. The RM was refluxed for 2 hours and then concentrated and stored at -18°C.

[Ti<sub>4</sub>(μ<sub>4</sub>-O)(μ-OEt)<sub>5</sub>(μ<sub>2</sub>-OEt)<sub>7</sub>(μ<sub>3</sub>-tBPA)], **2d**, *Tert*-butylphosphonic acid (0.48 mmol, 2 eq.) was dissolved in 0.3 mL toluene + 4 mL ethanol and titanium(IV) ethoxide (0.24 mmol) added. The RM was refluxed 2 hours and then concentrated and stored at -18°C.

[Ti<sub>4</sub>(μ<sub>2</sub>-O)<sub>2</sub>(μ-OEt)<sub>2</sub>(μ-HOEt)<sub>2</sub>(μ<sub>2</sub>-tPBA)<sub>2</sub>(μ<sub>2</sub>-HtPBA)<sub>6</sub>] $\cdot$ 4EtOH, **3d**, and [Ti<sub>4</sub>(μ<sub>2</sub>-O)<sub>2</sub>(μ-OEt)<sub>2</sub>(μ-HOEt)<sub>2</sub>(μ<sub>2</sub>-tPBA)<sub>2</sub>(μ<sub>2</sub>-HtPBA)<sub>6</sub>] $\cdot$ 2EtOH, **4d**, *Tert*-butylphosphonic acid (0.95 mmol) was dissolved in 0.4 mL toluene plus 4 mL ethanol and titanium(IV) ethoxide (0.24 mmol) was added. The RM was refluxed for 2 hours and then concentrated and stored at -18°C.

[Ti<sub>6</sub>(μ<sub>2</sub>-O)(μ<sub>3</sub>-O)<sub>2</sub>(μ<sub>2</sub>-OEt)<sub>5</sub>(μ-OEt)<sub>6</sub>(tBPA)<sub>3</sub>(HtBPA)], **5d**, *Tert*-butylphosphonic acid (0.48 mmol, 2 eq.) was dissolved in 0.3 mL toluene plus 4 mL ethanol and titanium(IV) ethoxide (0.24 mmol) added. The RM was refluxed 2 for hours and then concentrated and stored at -18°C.

[Ti<sub>4</sub>(μ<sup>-i</sup>OPr)<sub>4</sub>(acac)<sub>4</sub>(tBPA)<sub>4</sub>], **6d**, *Tert*-butylphosphonic acid (0.85 mmol) was dissolved in 5 mL acetone and Ti(acac)<sub>2</sub>iOPr<sub>2</sub> (0.20 mmol) was added. The RM was refluxed for 3 hours and then concentrated and stored at -18°C.

[Ti<sub>5</sub>(μ<sub>4</sub>-O)(μ<sub>2</sub>-O)<sub>3</sub>(μ<sub>2</sub>-OEt)<sub>4</sub>(μ-OEt)<sub>6</sub>(μ-HOEt)(μ<sub>3</sub>-tBPA)]<sub>2</sub>, **7d**, *Tert*-butylphosphonic acid (0.24 mmol) was dissolved in 0.3 mL toluene plus 3 mL ethanol and titanium(IV) ethoxide (0.24 eq.) was added. The RM was refluxed for 0.5 h and stored at 4°C.

Ti<sub>2</sub>Y(NO<sub>3</sub>)<sub>2</sub>(<sup>i</sup>OPr)<sub>9</sub>, **1e**. To titanium(IV) isopropoxide in toluene, 0.15 eq. yttrium(III) nitrate hexahydrate was added. The RM was solvothermally treated at 85°C for 44 hours and cooled down to room temperature.

### **2.1.2. Synthesis of rare-earth modified titania nanopowders**

Rare-earth element (REE) modified titania nanopowders were synthesized by solvothermal processing. Titanium(IV) ethoxide was added to REE nitrates (Y, Eu, and Sm) dissolved in anhydrous ethanol. The REEs were added in two different concentrations; 2.5 mol% and 5 mol% with respect to titanium. Clear, dark-brown solutions were obtained after reaction.

These were dried at ambient conditions yielding amorphous, brown to orange-brown powders. The powders were carefully grinded to fine powders in an agate mortar. Finally, the powders were annealed in air between 400°C and 800°C (with 100°C increments) in ceramic crucibles. Ramping from RT to the final temperature was one hour, this temperature was held for 2 hours. The powders were subsequently cooled naturally to RT in the furnace. The different powders are hereafter referred to as Ti-REEx-t, where REE is Y, Sm, or Eu, and x is either 2.5 or 5 mol%, and t is the annealing temperature. Characterization of the powders includes PXRD, SEM-EDS, FTIR, Raman, XPS, and UV-Vis.

### **2.1.3. Self-assembly of titania nanoshells**

Typically, ca. 2 mg hydrothermally synthesized titania were sonicated in toluene containing 0.5 mg/mL *n*-dodecylphosphonic acid for 1 hour. Following, under vigorous magnetic stirring, 1 mL 0.1 w% alginate and 2 mL 0.5 mg/L glucose-6-phosphate (both as aqueous solutions) were simultaneously added. Stirring was continued for 2 hours.

### **2.1.4. Syntheses of nanotitania-nanocellulose hybrid materials**

Cellulose nanofibrills (ca. 0.5 w%) aqueous suspension, with addition of 2 mL 1 w% polyethylene glycol, was heated to 70°C under magnetic stirring. At 70°C, the appropriate amount of titania (hydrothermally synthesized, Captigel, or TiBALDH) was added. The suspensions were stirred for 2 hours at 70°C and then transferred into Petri dishes and kept in an oven at ca. 40°C until dry.

## 2.2. Chemical analysis and characterization

### 2.2.1. Stability of modified titanium (oxo-) alkoxide complexes

#### 2.2.1.1. Hydrolytic stability

It was of interest to investigate whether addition of different organic ligands (phenoxide,  $\beta$ -diketonate, phosphonate) could stabilize oligonuclear titanium-oxo cores in aqueous solution. Titanium oxo-alkoxide single crystals of complexes with phenoxide (**1a**), phosphonate (**1d**), phosphonate plus  $\beta$ -diketonate (**6d**) ligands, and one bimetallic complex ( $\text{Ti}_2\text{Y}$ , **1e**) were submerged into  $\text{dH}_2\text{O}$  and the resulting products were analyzed by electron microscopy and AFM. For a selected titanium oxo-alkoxide complex (**5d**) with phosphonate ligands the hydrolysis was followed by  $^{31}\text{P}$  NMR.

Phosphorous NMR was considered a good tool due to the high abundance of the NMR-active  $^{31}\text{P}$  isotope (ca. 100 %) and cleaner spectrum compared to  $^1\text{H}$  NMR. During hydrolysis of the titanium alkoxy-phosphonate complex the phosphonate ligands are expected to be mostly retained on the surface of the emerging particles. Therefore, all or most P signals should diminish in intensity and/or shift position if the compound hydrolyzed and precipitated.

It was demonstrated earlier that hydrolysis of modified titanium alkoxides under controlled conditions afforded oxide phases with complex morphology and porosity (Seisenbaeva et al., 2010a; Seisenbaeva et al., 2010b). Therefore, the obtained morphology under different hydrolysis conditions was of interest. Selected complex **7d**, being the most pre-hydrolyzed compound ( $\text{O}/\text{Ti} = 0.8$ ) of the titanium alkoxy-phosphonates, was hydrolyzed under two different conditions in attempts to obtain oxide phases with complex morphologies. The conditions used were a near-boiling Pickering suspension of CNF, and water-acetone mixtures with different v% acetone at room temperature.

#### 2.2.1.2. Solution stability of selected modified titanium complexes

In the application of molecular precursors, the structure might be essential for the function, e.g. in the coupling of inorganic metal oxo-cores containing ligands with terminal functional groups for use as linkers in organic-inorganic hybrid materials (Rozes & Sanchez, 2011) or for the production of

bimetallic oxides such as BaTiO<sub>3</sub> of a particular stoichiometry. As the crystallized form may or may not be the dominant form in solution, investigation of a complex solution behavior is important. In this work (**papers III and IV**) <sup>31</sup>P NMR was employed to investigate solution stability of titanium oxo-alkoxide complexes with phosphonate ligands in anhydrous CDCl<sub>3</sub> or acetone-d<sub>6</sub>. Diffusion ordered spectroscopy (DOSY) was used to confirm stability of compounds **1c** and **2c**. DOSY was additionally applied in an attempt to distinguish different species in the reaction mixture of **2c** which revealed a complex <sup>31</sup>P NMR spectrum.

### **2.3. Photocatalysis**

The Sm- and Eu-modified titania nanopowders were evaluated for their photocatalytic properties. For this, 30 mg of each catalyst were added to a 5 mL solution of 5 mM trimethylphenol (TMP). To achieve an adsorption-desorption equilibrium the suspension were stirred for 15 minutes in dark. Three different wavelengths were used; 445-465 nm, 510-530 nm, and a wide range visible lamp. Degradation of TMP was measured by HPLC-UV/vis. The photocatalytic studies were performed by collaborators in the National Institute for Laser, Plasma & Radiation Physics, (Romania).

## **2.4. Drug release from CNC\_TiO<sub>2</sub>\_TR and hydrolyzed complex 1a**

### **2.4.1. Hydrolyzed complex 1a**

As mentioned above, nanocellulose dressings have demonstrated potential for wound healing but they have the disadvantage of not being inherently antibacterial. To overcome this, drug carriers in form of titania nanoparticles were attached to the nanocellulose and subsequently loaded with an antibacterial agent (triclosan) (**paper II**). Patches of nanocellulose-nanotitania-triclosan (CNC\_TiO<sub>2</sub>\_TR) containing the minimal inhibitory

concentration (MIC) of triclosan was incubated with agar cultivations of *Escherichia coli* (CCUG24T) and *Staphylococcus aureus* (CCUG1800T) at 37°C in darkness. Inhibitory zones were measured after 18 hours.

#### **2.4.2. CNC\_TiO<sub>2</sub>\_TR**

A certain amount of **1a** single crystals was dissolved in ethanol to equal the minimal inhibitory concentration (MIC) of triclosan for *Staphylococcus aureus* (CCUG1800T) (**paper I**). Filter paper pieces (1 cm<sup>2</sup>) were soaked by the solution and the ethanol was evaporated. Filter paper pieces (1 cm<sup>2</sup>) with MIC concentration of triclosan was used as control. During hydrolysis of the complexes, the oxo-cores will coalesce to nanoparticles decorated with the organic ligands. *S. aureus* was grown on agar plates together with filter papers and the inhibitory zone measured after 18 hours at 37°C in darkness.

### **2.5. Immunological studies of the nanocellulose-nanotitania hybrid materials**

The immunological studies and cell cultivations were performed at the Rudbeck Laboratory, Department of Immunology, Genetics and Pathology, Uppsala University.

#### **2.5.1. Human whole blood chamber model**

Human whole blood where exposed to pieces of the nanotitania-nanocellulose hybrids and the control material (CNF\_PEG) for 1 hour at 37°C under rotation in special incubation cells (Figure 17). Immediately after incubation, platelets were counted using a Sysmex XP-300 Hematology Analyzer (Sysmex Corp.). The blood samples were centrifuged at 4°C and the supernatant (plasma) was separated and stored at -80°C until further analyses.

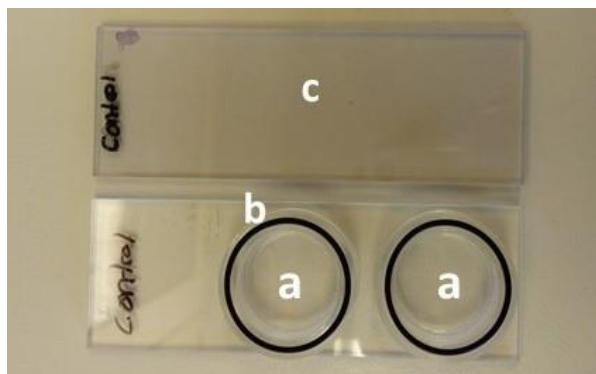


*Figure 17.* Incubation cell for blood experiment. The cell has two chambers (a), rubber tightening (b), and a lid (c). The purple spot on the lid indicates successful heparinization.

### **2.5.2. ELISA analyses of immunological markers**

To get deeper insight into the immunological responses induced by the control material (CNF\_PEG) and the three hybrid materials (CNF\_PEG\_TiO<sub>2</sub>, CNF\_PEG\_Captigel, and CNF\_PEG\_TiBALDH), a number of protein markers for complement activation, contact activation, and coagulation were quantified by enzyme-linked immunoassays (ELISA).

The proteins analyzed were thrombin-antithrombin (TAT) complex, C3a, sC5b-9, C1-inhibitor-Factor XII-complex, and C1-inhibitor-Factor XI-complex. The functions of these are briefly described in Results and Discussion (section 3.5.) in context with the results. More details are available in **manuscript V**.



## 3. Results and Discussion

### 3.1. Synthesis of modified titanium (oxo-) alkoxide complexes

A number of different titanium (oxo-) alkoxide complexes have been synthesized. Complexes **1a** and **1b** (**paper I** and **paper II**) contain triclosan as ligand and were synthesized as model for triclosan-titanium interactions.

A series of phosphonate ligand modified complexes (**1c**, **1d** through **7d**, **paper III** and **paper IV**) were synthesized as models for phosphonate-titania ligand interactions for phosphonate-containing drugs and ligands used in self-assembly processes (**manuscript VI**). Finally, a bimetallic titanium-yttrium alkoxide complex, without oxo-bridges, (**1e**, **manuscript VII**) was synthesized as an intermediate/potential single source precursor for yttrium-doped titania.

#### 3.1.1. Structural comments

Two different complexes were obtained when reacting triclosan with titanium(IV) ethoxide in acetone. The first complex (**1a**) has a  $Ti_4O_2$  core and two triclosan ligands and the second complex (**1b**) has a  $Ti_5O_2$  core with one triclosan ligand (Figure 18). **1a** and **1b** share the same principle core-structure with four titanium octahedra connected via edge sharing. In **1b**, an additional titanium atom is attached, sharing edges with two other octahedra (Figure 19). These fragments are structurally related to the packing of Ti and O in anatase. In both complexes condensation products of acetone, catalyzed by the titanium-oxo core (Meerwein-Ponndorf-Verley reduction), were present as coordinating ligands. The condensation of solvent acetone by a titanium oxo-core, with subsequent coordination of the condensation product, has been reported previously by Barkley and co-workers (1997).

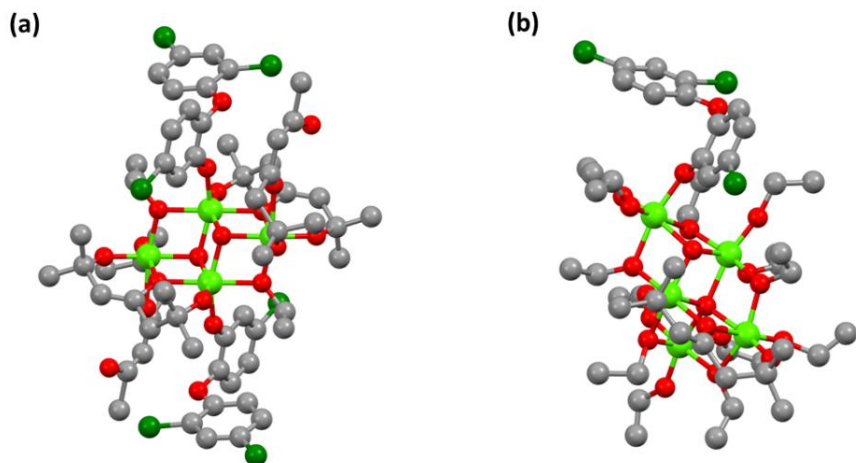


Figure 18. Molecular structures of compounds **1a** (a) and **1b** (b). Hydrogen atoms and solvating molecules have been omitted for clarity. Light green is titanium, grey is carbon, red is oxygen, and dark green is chlorine.

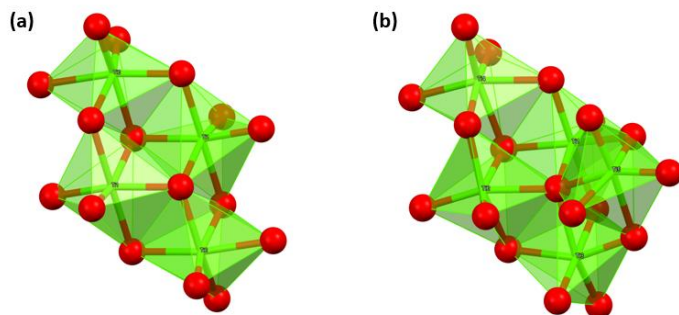


Figure 19. Core-structures of compound **1a** (a) and **1b** (b). Green octahedra are titanium and red is oxygen.

The reaction between *tert*-butylphosphonic acid and titanium(IV) ethoxide or titanium(IV) diisopropoxide *bis*(acetylacetonate) (**paper IV**) and between titanium(IV) isopropoxide and phenylphosphonic acid (**paper III**) resulted in a series of phosphonate-modified titanium (oxo-) alkoxides.

Structurally, they can be divided into two groups, one with compact oxo-cores and one with more open oxo-cores. Compounds **1c**, **1d**, **3d**, **4d**, and **5d** are all based on  $Ti_2O$  and/or  $Ti_3O$  fragments connected via phosphonate groups, forming open oxo-cores (Figure 20 & Figure 21). This arrangement appears to be very a common structure for titanium alkoxide complexes with

phosphonate ligands (Hayami et al., 2018; Czakler et al. 2014; Czakler et al., 2015) in the view of generally respected energetic stability of Ti-O-P bonds. The compounds thus formed can be considered as titanium oxo-phosphonates.

However, complexes with one phosphonate ligand (Seisenbaeva et al., 2015; Chen et al., 2015), or the large "clusters" reported by Coppens' group (2013) which are examples of MTSALs stabilized by phosphonate ligands on their surfaces, display a more compact core structure. Generally, all structures have either edge or corner sharing, or both. The exception is complex **6d**, where the four titanium octahedra are completely separated from contact with each other by bridging tBPA ligands.

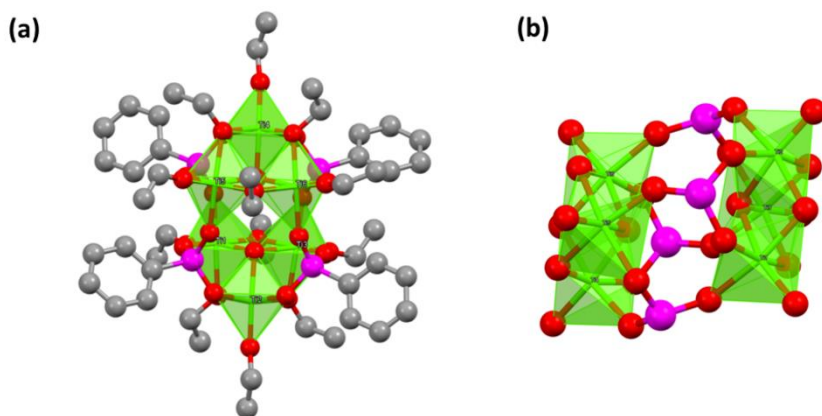


*Figure 20.* Molecular structure of **1c**. (a) Hydrogen atoms and the solvating toluene molecule have been removed for clarity. (b) The core-structure of **1c** in a different orientation. Green octahedra are titanium, magenta is phosphorous, and red is oxygen.

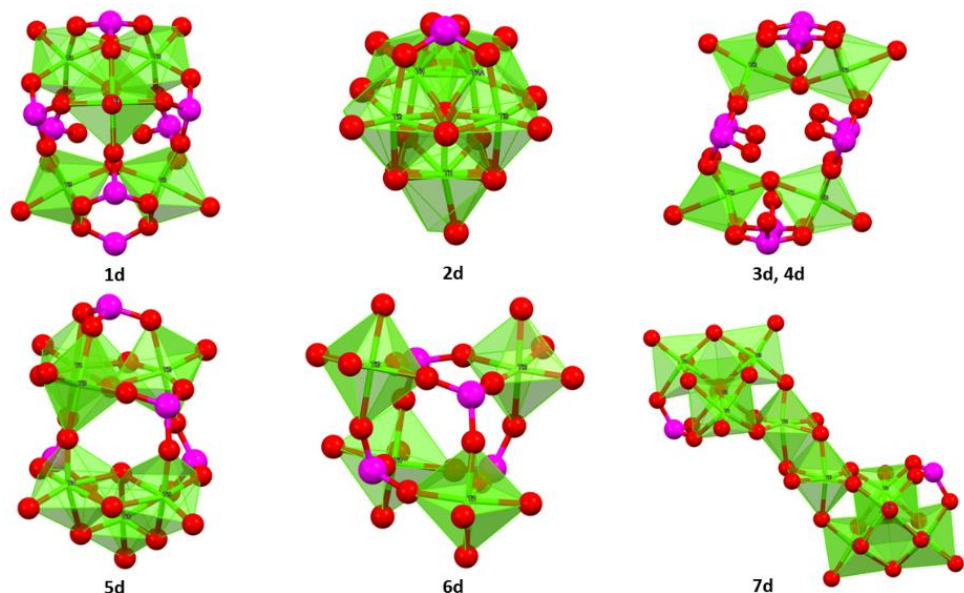
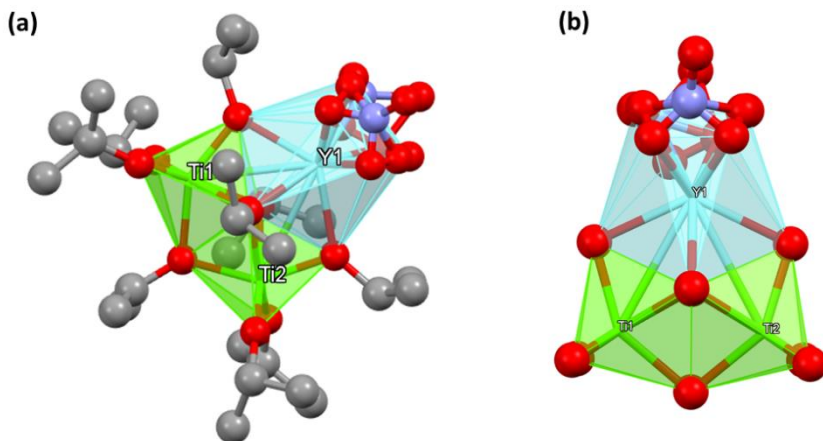


Figure 21. Metal-oxo core-structures of the titanium oxo-alkoxide phosphonates from **paper IV** in polyhedral representation. Green octahedra are titanium, magenta is phosphorous, and red is oxygen.

In comparison, titanium (oxo-) alkoxide complexes with chelating ligands, such as carboxylates, catechols, and  $\beta$ -diketonates, tend to have a more compact, ordered core-structure (Czakler et al., 2012; Stenuo et al., 1999; Werndrup & Kessler, 2001). Wright and Eslava have reported a series of bimetallic (Co, Fe, Cr, Mo, Cu) titanium oxo-alkoxides without chelating or bridging hetero-ligands (Eslava et al., 2010; Eslava et al., 2010; Eslava et al., 2011). They generally obtained cage-like structures with formulas such as  $[\text{Ti}_4\text{O}(\text{OEt})_{15}(\text{MCl})]$  (where  $\text{M} = \text{Co}, \text{Zn}, \text{Fe}, \text{Cu}$ ) and  $[\text{Ti}_7\text{O}_5(\text{OEt})_{19}(\text{CoCl})]$  resembling the types of core-structures obtained in this work.

The majority of mixed titanium-lanthanide alkoxide complexes reported to date consists of larger metal oxo-cores (e.g.  $\text{M}_z\text{Ti}_x(\text{O})_n$ ) where chelating ligands (often carboxylic acids) act as linkers between titanium and the lanthanide (Ln) (Artner et al., 2014; Li et al., 2018; Zhao et al., 2019). Work by Schubert and co-workers (2014) found a dependence of the ionic radius of the lanthanide on the type of complex formed, where the smaller ions

formed a  $\text{Ln}_2\text{Ti}_4\text{O}_4$ -type complex while the larger ions formed a  $\text{Ln}_2\text{Ti}_6\text{O}_6$ -type complex. Both complexes contained methacrylic acid as a linker between Ln and Ti. The  $\text{Ti}_2\text{Y}(\text{iOPr})_9(\text{NO}_3)_2$  complex (**1e**) (Figure 22) is unique in the sense that the titanium and yttrium atoms are linked exclusively via  $\mu_2$ -iOPr ligands, and that it does not contain any oxo-bridges or organic heteroligands. The  $\text{Ti}_2\text{Y}$ -oxo core resembles the halide structure of titanium and is isostructural with  $[\text{Ti}_3\text{Br}_{13}]$  and  $[\text{Ti}_3\text{Cl}_{13}]$  (Meyer et al., 2009). **1e** is highly moisture sensitive and readily hydrolyzes outside a protected environment. The yttrium atom in **1e** is octa-coordinated by six  $\mu_2$ -iOPr ligands and two chelating nitrate groups. The metal oxo-core differs from the above structures as there is only face sharing between the polyhedra in **1e**.



*Figure 22.* (a) Molecular structure of compound **1e**. (b) Oxo-core of **1e**. Green is titanium, turquoise is yttrium, purple is nitrogen, red is oxygen, and grey is carbon. Hydrogen atoms have been removed for clarity. The two nitrate groups on the yttrium ion were heavily disordered. Figure from **manuscript VII**.

The yttrium polyhedron shares one face with each titanium atom and the two titanium atoms share one face with each other. According to Pauling's third rule, the stability of a coordination compound decreases if edge-sharing, and particularly face-sharing is present. In edge- and face-sharing the cations are closer to each other compared to corner-sharing and the electrostatic repulsion increases, resulting in instability (Essington, 2015).

Compound **1e** formed by solvothermal reaction between 0.10 eq. to 0.35 eq.  $\text{Y}(\text{NO}_3)_3 \cdot 6\text{H}_2\text{O}$  and  $\text{Ti}(\text{iOPr})_4$ . When using 0.4 eq.  $\text{Y}(\text{NO}_3)_3$  a white

precipitate of amorphous titania with ca. 15 w% yttrium after washing was obtained. Recording of a  $^{15}\text{N}$  NMR spectrum for **1e** was attempted but because of the isotope's low natural abundance (ca. 0.4 %) a satisfactory spectrum could not be obtained.

### 3.1.2. Characterization of REE-modified titania nanopowders

Rare-earth elements (REE) are key components in many advanced electronic devices due to their special magnetic, optical, and electronic properties which originates from their shielded  $f$ -orbitals. An introduction about occurrence, processing, applications, and concerns of REEs is available in the thesis by Polido-Legaria (2018). During the last two decades, doping of titania with REEs has been a popular method to red-shift the EM absorption into the visible region, thereby facilitating photocatalysis.

Here, titania was modified by addition of REE-nitrates in different concentration using a solvothermal method. The annealed powders were characterized by a variety of methods and finally evaluated for photocatalysis in narrow and broad visible ranges.

PXRD patterns were recorded for all annealing temperatures, Figure 23. In accordance with the literature, addition of “dopants” generally increase crystal phase-transition temperatures. For the titania samples with the addition of 2.5 mol% REE, annealing at 400°C was not enough to obtain crystalline anatase, instead 500°C was required. These particles were stable up to 700°C before transformation into rutile became evident. A systematic substitution of  $\text{Ti}^{4+}$  for REE ions in the titania lattice is not expected because of the large difference in ionic radii. Instead, surface bound REE and deposition of REE-oxides, and possibly REE titanates, are hypothesized to be responsible for the increased crystallization and phase-transition temperatures observed. The phase-transition from anatase to rutile is initiated from the crystallite surface. Thus, if Ti-O-REE bonds are present on the surface, the transition could be impeded since the larger REE ions will not easily be integrated into the titania lattice. It is also possible (but would require further studies) that deposited rare-earth oxides and rare-earth titanates could provide stabilization by decreasing surface energy or provide steric hindrance against phase-transformation. This would be a topic for an interesting, potential future study.

The 5 mol% REE-modified samples required even higher annealing temperatures, 600°C, to obtain fully crystalline anatase. Note at this temperature pristine anatase is undergoing phase transformation to rutile (Arroyo et al., 2002). However, the Y-doped sample became fully crystalline at 500°C. The reason for this difference in crystallization temperature might be explained by the differences in ionic radii between  $Y^{3+}$  (104 Å) and the larger  $Eu^{3+}$  (109.8 Å) and  $Sm^{3+}$  (108.7 Å) (Shannon, 1976). Ti-O-REE where REE is  $Eu^{3+}$  or  $Sm^{3+}$  might provide better blocking/stabilization against phase-transition and particle growth compared to  $Y^{3+}$ . At annealing on 700°C traces of the rutile begin to appear for both the 2.5 mol% and the 5 mol% modified at 700°C. This became more evident at 800°C when the (1 0 1) reflection of rutile appears for Ti-Y2.5, Ti-Y5, Ti-Eu5, and Ti-Sm2.5.

Between annealing temperatures 500°C and 800°C no obvious signs of secondary phases (such as  $TiREEO_3$ ,  $REE_2O_3$ , or  $Ti_2REE_2O_7$ ) for either dopant concentration are visible from the X-ray pattern. However, formation of  $Ti_2REE_2O_7$  has been reported to start above 800°C and this phase may not be very prominent below this temperature (Mrazek et al., 2014; Mrazek et al., 2015). The detection of secondary phases in small amounts can be difficult by PXRD and they could be present below the limit of detection. Even though the REE ions may not enter the  $Ti^{4+}$  positions, they could take an interstitial position that would increase oxygen vacancies and thereby lattice defects. This could lead to delayed phase transformation, and possibly also to the observed delayed amorphous-to-anatase transformation (Arroyo et al., 2002).

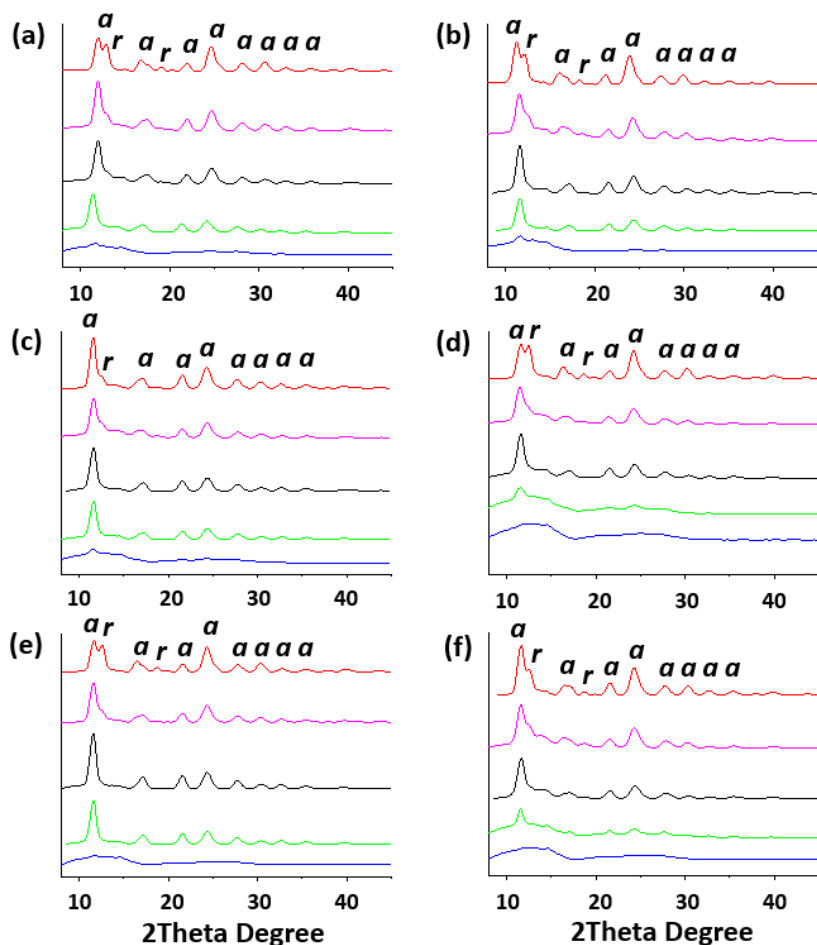
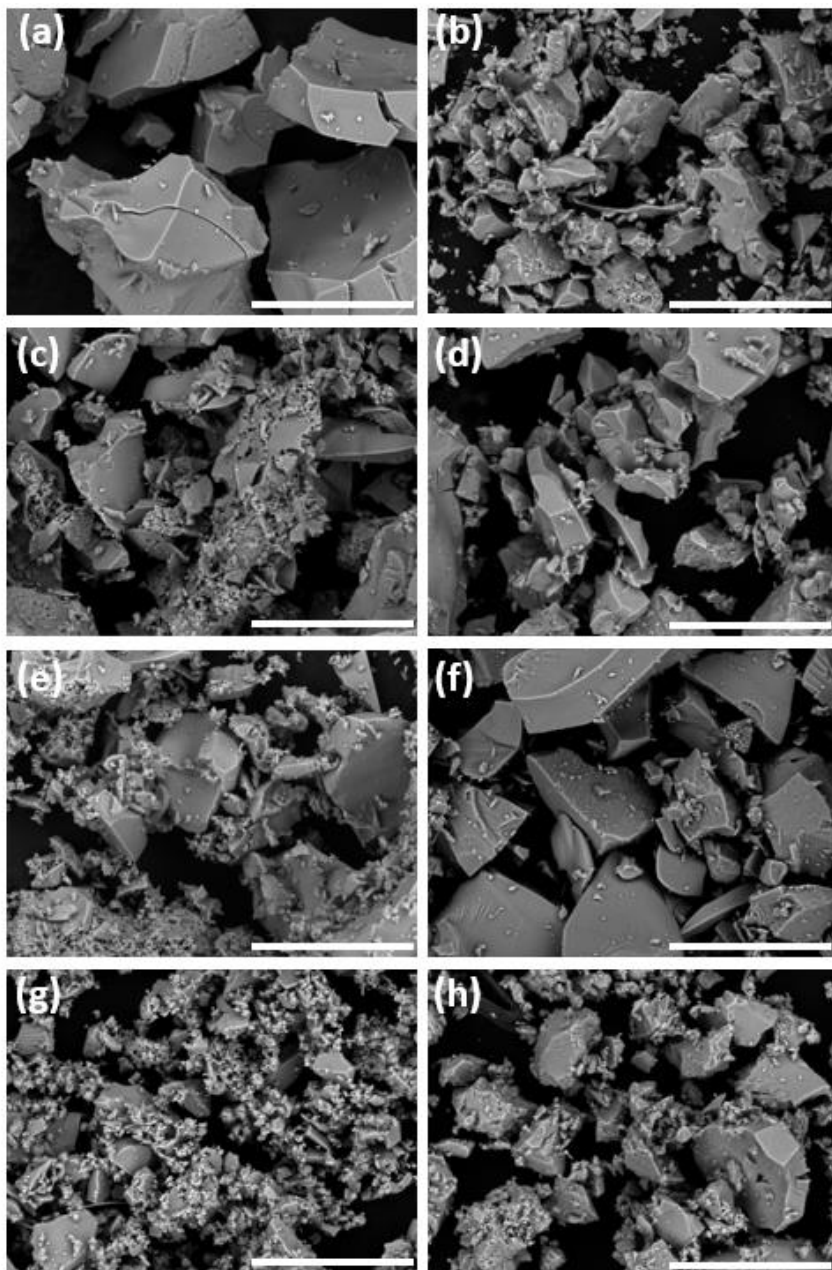


Figure 23. PXRD patterns of the REE-modified titania powders at different annealing temperatures. (a) Ti-Y2.5, (b) Ti-Y5, (c) Ti-Eu2.5, (d) Ti-Eu5, (e) Ti-Sm2.5, and (f) Ti-Sm5. Red, magenta, black, green, and blue represents annealing temperatures (top to bottom) 800°C, 700°C, 600°C, 500°C, and 400°C, respectively. Peaks labeled “a” and “r” belong to the anatase and rutile phases, respectively. Figure from **manuscript VII**.

SEM imaging of the powders indicate that the powders mostly consist of rather big aggregates mixed with smaller particles (Figure 24). The EDS mapping of 2.5 mol% doped samples in Figure 25 indicates a homogenous distribution of the REEs in the samples.



*Figure 24.* SEM micrographs of the  $\text{TiO}_2$ -REE powders used for catalysis. (a) Ti-Eu2.5-500, (b) Ti-Sm2.5-500, (c) Ti-Eu2.5-600, (d) Ti-Sm2.5-600, (e) Ti-Eu5-600, (f) Ti-Sm5-600, (g) Ti-Eu5-700, (h) Ti-Sm5-700. Scale bars represent 50  $\mu\text{m}$ . Figure from **manuscript VII**.

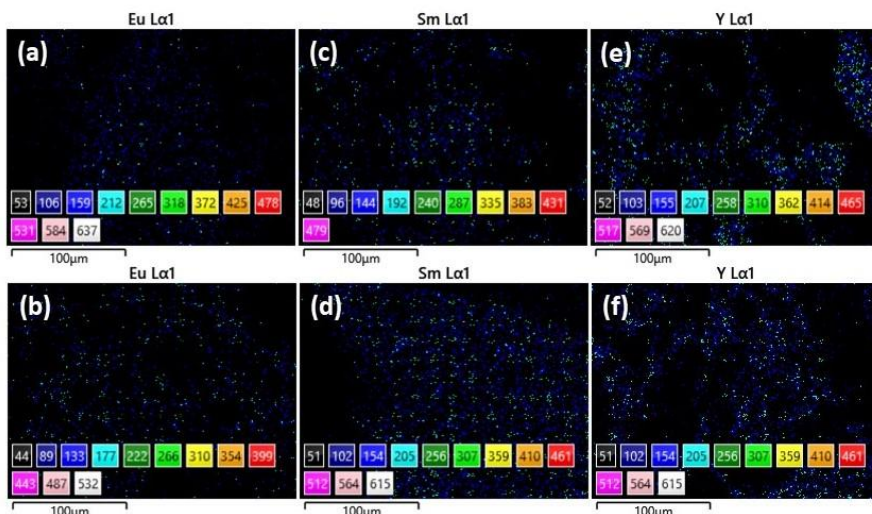


Figure 25. Elemental mapping of titania nanopowders modified with Eu and Sm. (a) Ti-Eu2.5-500, (b) Ti-Eu2.5-600, (c) Ti-Sm2.5-500, (d) Ti-Sm2.5-600, (e) Ti-Y2.5-500, (f) Ti-Y2.5-600. Figure from **manuscript VII**.

Ti-O-REE bonds in titania have reported based on FTIR-analyses of REE “doped” titania (Sibu et al., 2002). This could potentially come, for instance, from  $Ti_2REE_2O_7$ ,  $TiREEO_3$ , or possible REEs bond to terminal titanium ions (Cruz et al., 2011). A number of publications report the syntheses of “REE-doped titania” and the authors concluded that the REE formed  $REE_2O_3$  (and other oxides), rather than that REE was incorporated into the titania lattice (Rozman et al., 2019; Zhou et al., 2013;) or that the REEs possibly occupied interstitial positions (Dhanalakshmi et al., 2017). In other studies, it was claimed that REE ions ( $Gd^{3+}$  and  $Ce^{3+}$ ) indeed entered the titania lattice in  $Ti^{4+}$  positions (Toloman et al., 2017). The latter conclusion was based on electron spin resonance (ESR) and Raman spectrometry together with reduced primary particle sizes. Due to the large ionic radii of  $Gd^{3+}$  and  $Ce^{3+}$  (107.8 ppm and 115 ppm, respectively), it is doubtful that they can enter the titania lattice in the Ti-position. In another study, Reszczyńska and co-workers (2015) reported doping of titania with  $Er^{3+}$  and  $Yb^{3+}$  based on photoluminescence data. The most likely position of the REE-dopants are either a fine dispersion over the  $TiO_2$  surfaces in form of REE oxides or surface bound REE (Ti-O-REE) (Choi et al., 2010).

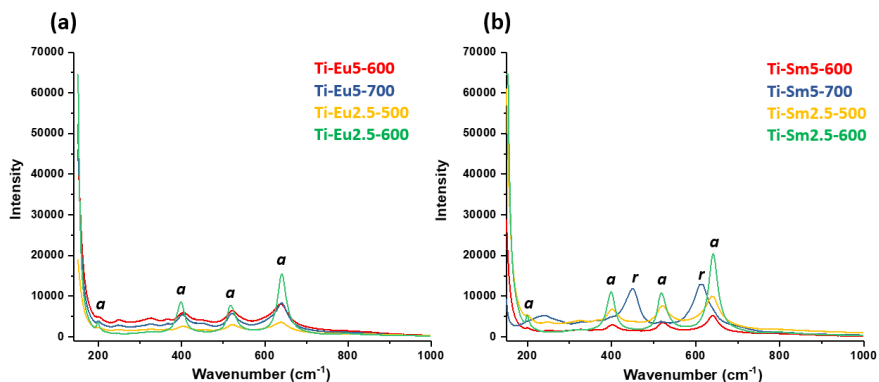


Figure 26. Raman spectra for europium (a) and samarium (b) modified titania at 488 nm excitation wavelength. *a* = anatase and *r* = rutile. Figure from **manuscript VII**.

The modified powders were investigated by Raman spectrometry, Figure 26. The spectra for the Eu-modified powders are very similar, displaying four vibration modes: 199  $\text{cm}^{-1}$  ( $E_g$ ), 401 ( $A_{1g}$ ), 520  $\text{cm}^{-1}$  ( $B_{1g}$ ), and 643  $\text{cm}^{-1}$  ( $E_g$ ), all assigned to anatase (Qian et al., 2005). Three of the Sm-modified titania nanopowders display the same anatase vibrations, except Ti-Sm5-700 which shows vibration modes belonging to the rutile phase (Qian et al., 2005): 449  $\text{cm}^{-1}$  ( $E_g$ ) and 617  $\text{cm}^{-1}$  ( $A_{1g}$ ). The PXRD spectra of Ti-Sm5-700 (Figure 23f) indicate this sample to mainly consist of the anatase phase. It is possible the Raman spectrum was collected in an area with higher rutile content than representative for the whole sample.

FITR spectra of powders used for photocatalysis indicate that they are essentially free from organic compounds. Minor intensity signal centered around 1615  $\text{cm}^{-1}$  may be assigned to bending of Ti-OH-bonds on the surface. Its intensity appears to diminish with increased annealing temperature. For the amorphous powders the nitrate signal is clearly visible at 1384  $\text{cm}^{-1}$  (Figure 28). It is apparent from Figure 27 that nitrate is removed during annealing. The amorphous powders also contains higher amount of the bending OH-signal at 1615  $\text{cm}^{-1}$ , as well as Ti-OH bonds stretching in the 3100-3500  $\text{cm}^{-1}$  region.

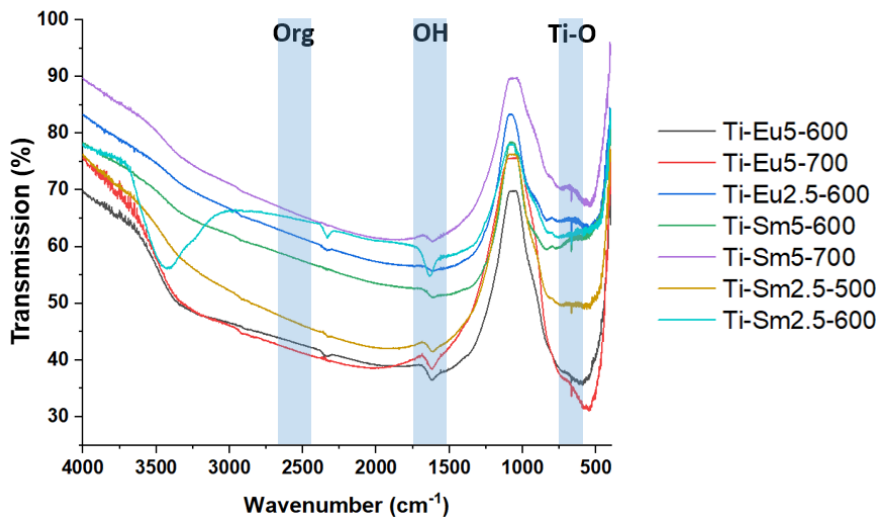


Figure 27. FTIR-spectra of the annealed titania nanopowders used for photocatalysis. Interpretation of signals are indicated.

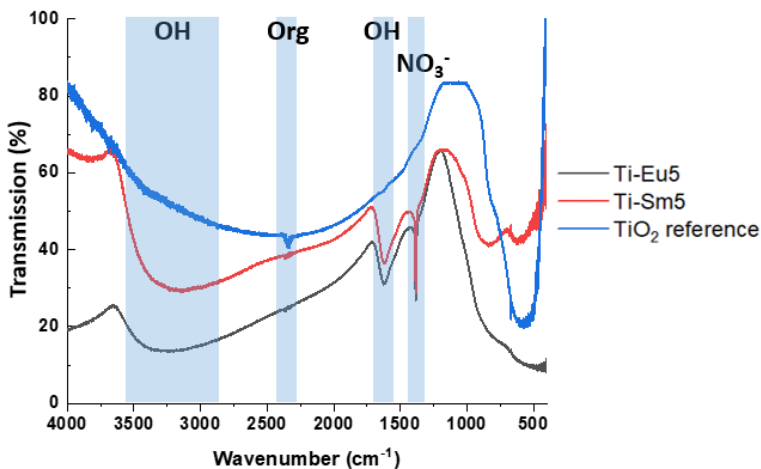


Figure 28. FTIR spectra of amorphous Ti-Eu5 and TiSm5 powders and reference titania. Interpretation of signals are indicated.

### 3.1.4. Characterization of self-assembly of titania nanoshells

In the first attempts to produce self-assembled nanoshells (hollow spheres), titania nanopowders were added directly to a vigorously stirred mixture of 0.5 mg/mL DPA in toluene + 0.5 mg/mL G6P + 0.1 w% alginate.

This did not work. Sonication in pure toluene or water also lead to fast re-aggregation of the dispersions. Instead, sonication in toluene with the hydrophobic ligand (DPA) resulted in stabilization of the smaller particles.

Under vigorous stirring, the hydrophilic ligand (G6P) and alginate were added simultaneously. Following stirring for two hours followed by settling of the system, the titania nanoshells were obtained.

The stirring resulted in a water-toluene emulsion. Nanoparticles are known for their ability to migrate to phase-boundaries and acting as stabilizers, i.e. Pickering stabilizers. In the interface, the particles will be exposed to DPA from the toluene phase and G6P from the water phase, resulting in particles with hemispheres of opposite polarity. Hydrogen bonding between alginate and G6P is hypothesized to increase stability, as no spheres were obtained without the presence of alginate, or at very low alginate concentrations. The sizes of the obtained titania nanoshells are fairly homogenous, commonly between 500 nm to 3  $\mu\text{m}$ . As seen in Figure 29 some spheres are always broken and the extent of broken nanoshells vary by batch.

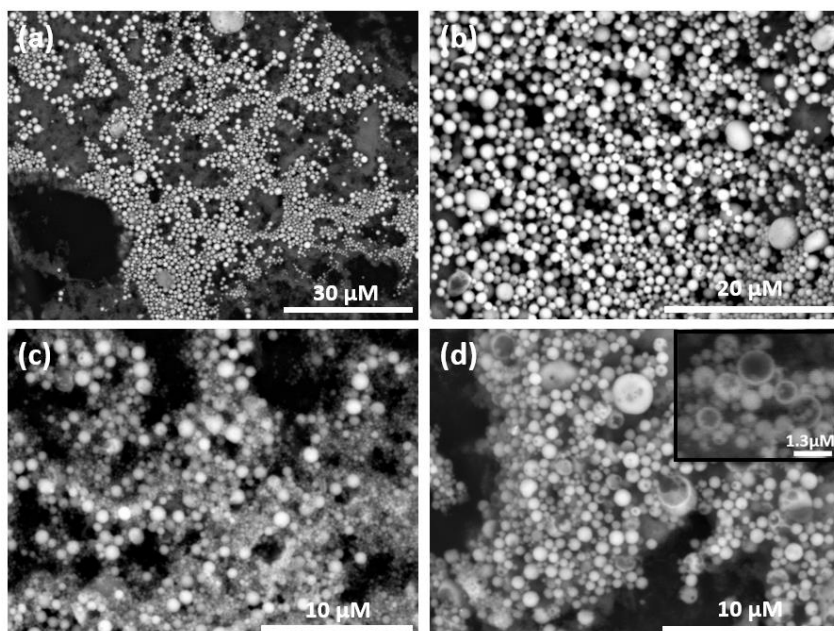


*Figure 29.* SEM micrographs of self-assembled titania nanoshells. (a) Lower magnification micrograph of nanoshells dispersed over a matrix. (b) Micrograph of titania nanoshells of rather narrow size distribution. Average diameter calculated from 40 random nanoshells was ca. 1  $\mu\text{m}$  (standard deviation (SD) 760 nm). (c) An example of nanoshells with higher size distribution. (d) Micrograph with several broken nanoshells. Average diameter calculated from 40 random nanoshells was ca. 680 nm (SD = 410 nm). The inset in (d) shows several incomplete nanoshells at 9000X magnification. Figure from **manuscript VI**.

The nanoshells were analyzed by elemental mapping. It is seen from Figure 30 that the spheres consist of titania. However, not all material will self-assemble and is instead dispersed on the carbon tape, resulting in signals around the spheres, particularly for phosphorous. The higher concentration of phosphorus on the nanoshells according to EDS mapping, together with no observed formation of nanoshells in the absence of the organic ligands, suggests that ligands are essential for the self-assembly process. To obtain better information about the surface, the nanoshells were imaged by AFM. Figure 31 shows the AFM micrographs of several nanoshells, including magnified surface on one nanoshell, clearly displaying that it consists of smaller aggregates.

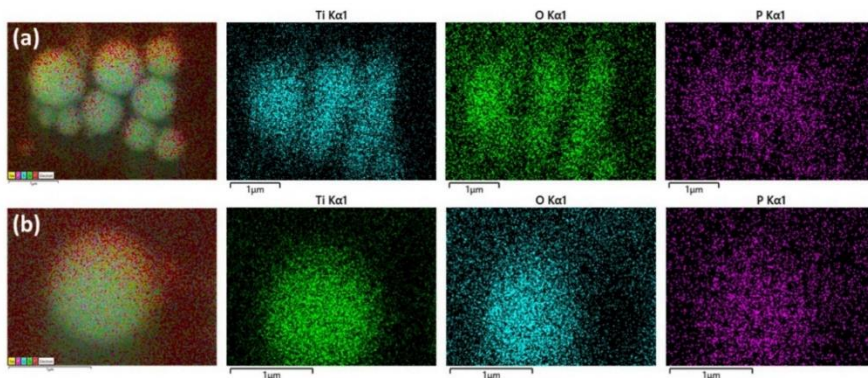


Figure 30. Elemental mapping of the titania nanoshells, showing presence of titanium, oxygen, and phosphorous. Analysis of (a) an aggregate of self-assembled spheres and (b) an individual sphere. Figure from **manuscript VI**.

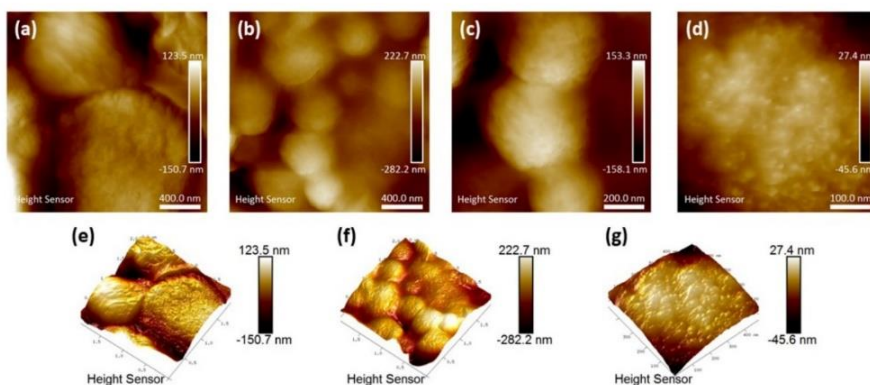


Figure 31. AFM micrographs of titania nanoshells. (a) Micrographs of a few larger nanoshells. (b) An aggregate of smaller nanoshells average diameter is 420 nm (SD = 80 nm). (c) Magnified micrograph of three small nanoshells average diameter is 416 nm (SD = 55 nm). (d) Magnified micrograph of the surface of a nanoshell. Nanoshell topography is shown in e, and f, and a 3D image of a surface in g. Figure from **manuscript VI**.

### 3.1.5. Characterization of nanotitania-nanocellulose hybrid materials

Three different nanotitania-nanocellulose hybrid materials were synthesized, using titania from three different sources. In addition, with one control material (CNF\_PEG) without titania was synthesized. The different titania used were; pre-synthesized titania (ca. 10 nm), 3 nm colloidal anatase nanoparticles, and one *in situ* formed titania from the aqueous TiBALDH precursor. The materials were stabilized by small amounts of PEG to avoid wrinkling during drying. Rather strong and flexible materials were obtained (Figure 32). It is apparent from SEM micrographs (and by visual inspection) that the titania source is important for the homogeneity. The pre-synthesized titania nanopowder, even though sonicated in solution before addition, tended to form aggregates in the material.

On the other hand, the colloidal titania and *in situ* formed titania from TiBALDH produced very homogenous materials as can be seen by the SEM micrographs (Figure 33). It is noted though that the TiBALDH containing hybrids have a rougher surface compared to the Captigel containing hybrids.

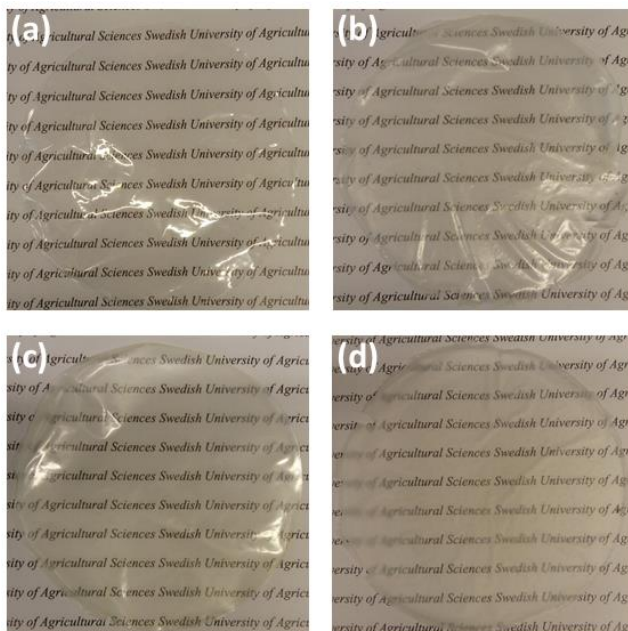
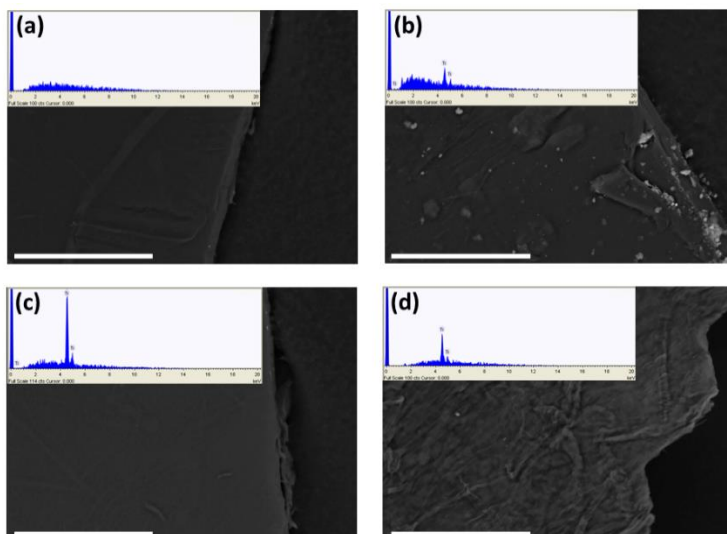


Figure 32. Photographs of the control material CNF\_PEG (a), and the three different hybrid materials CNF\_PEG\_TiO<sub>2</sub> (b), CNF\_PEG\_Captigel (c), and CNF\_PEG\_TiBALDH (d). Figure from **manuscript V**.



*Figure 33.* SEM micrographs of the control material CNF\_PEG (a), and the three different hybrid materials CNF\_PEG\_TiO<sub>2</sub> (b), CNF\_PEG\_Captigel (c), and CNF\_PEG\_TiBALDH (d). EDS insets in b, c, and d indicate presence of titanium. The scale bars represent 50  $\mu\text{m}$ . Figure from **manuscript V**.

Immersing the materials in water resulted in swelling to thin gels. They retained their structure in water for at least one week, although the mechanical strength obviously decreased. This is promising properties from the wound-dressing point of view.

### **3.2. Hydrolytic stability and solution behavior of modified titanium oxo-alkoxide complexes**

Modified titanium oxo-alkoxide complexes are of interests for several applications including single-source precursors, homogenous catalysis, and components in organic-inorganic hybrid materials. As previously mentioned the solid-state structure of a complex may not be retained in upon dissolution or may vary dependent on solvent (e.g. non-coordinating vs. coordinating).

Another concern is the use of titanium oxo-alkoxides “stabilized” by chelating ligands in aqueous systems for homogenous catalysis. Several complexes synthesized within this work were characterized for their solution stability and thoroughly characterized for hydrolytic stability.

### 3.2.1. Hydrolytic stability of ligand-modified complexes

Selected modified titanium complexes were submerged in water and analyzed with microscopic techniques (SEM, HRTEM, HRAFM) and NMR to verify whether certain ligands (phenoxide, phosphonate, and phosphonate + acetylacetonate, **1a**, **1d**, and **6d**, respectively) imposed any hydrolytic stability. Also **1e**, the bimetallic titanium-yttrium complex, was treated with water and investigated by HRTEM. In the case when modified titanium alkoxide complexes are used, for instance, as precursors for hybrid materials or as single source precursors for complex metal oxides, their integrity in solution is critical. The solution stability of titanium alkoxide phosphonates in **paper III** and **paper IV** were probed by a combination of NMR techniques, i.e.  $^1\text{H}$ ,  $^{13}\text{C}$ ,  $^{31}\text{P}$ , and  $^1\text{H}$  DOSY NMR. Water-treatment of **1a** (phenoxide ligands) with water resulted in hydrolysis of the complex. Dried precipitates of **1a** were analyzed by SEM, HRTEM, and AFM. The SEM micrograph in Figure 34b shows pieces of precipitates are distinct from non-water treated **1a** (Figure 34a). The precipitate had an appearance quite similar to hydrothermally synthesized titania. High-resolution microscopy by AFM of precipitates revealed rather homogenous nanoparticles of about 20 nm in size (Figure 35). Measurements of lattice fringe distance (0.35 nm) of particles from HRTEM micrographs (Figure 34d) concluded the particles were titania in the anatase phase. This strongly suggest that the phenoxide ligands did not stabilize compound **1a** against hydrolysis.

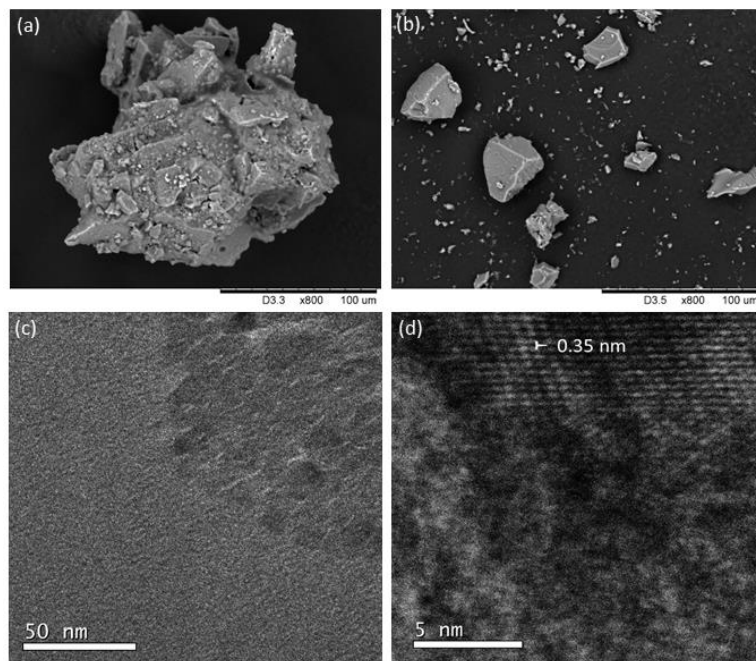


*Figure 34.* SEM and TEM micrographs of compound **1a**. SEM micrographs of (a) non-hydrolyzed crystal of **1a** and hydrolyzed crystal of **1a** (b). TEM micrographs of hydrolyzed **1a** showing secondary particles (c) and lattice fringes of an anatase particle (d). Figure reproduced from **paper I** with permission from the publisher.

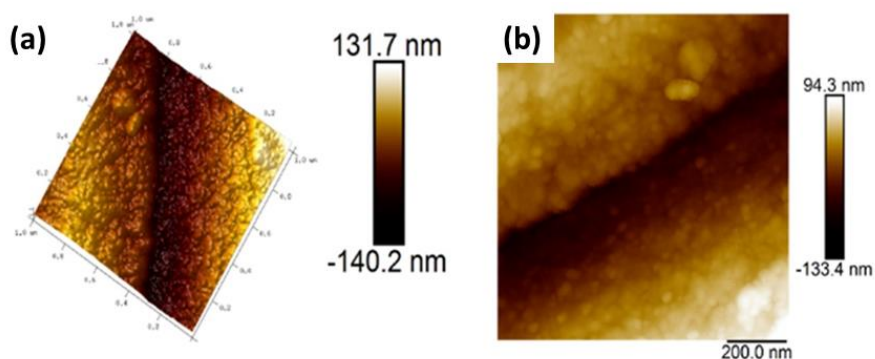


*Figure 35.* AFM of hydrolyzed compound **1a**. 3D image (a) and 2D image (b) of the same area. Figure reproduced from **paper I** with permission from the publisher.

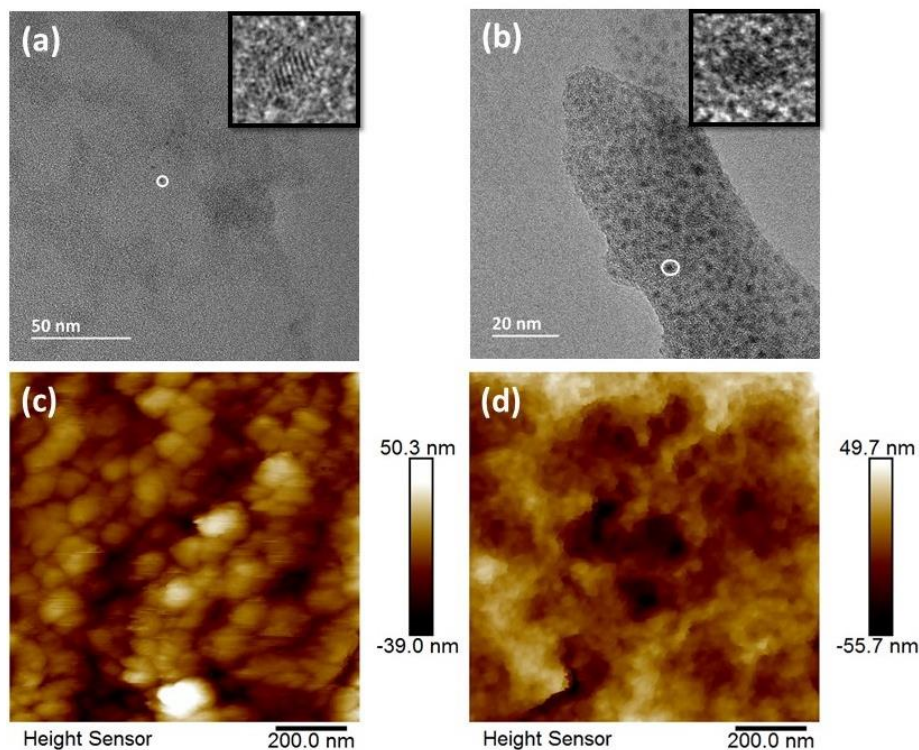


*Figure 36.* TEM and AFM micrographs of compound **1d** (a, c) and compound **6d** (b, d). Image modified from **paper IV**. Both the TEM and AFM micrographs confirm the formation of well-defined titania nanoparticles when the compounds are treated with water.

Hydrolysis studies were expanded to two complexes from **paper IV**, **1d**, and **6d**. Compound **1d** is modified with bridging phosphonate groups while **6d** has both bridging phosphonate groups and chelating  $\beta$ -diketonate groups. **1d**, and **6d** were submerged into water and the formed white precipitate were analyzed by HRTEM and AFM (Figure 36). As with **1a**, the microscopy studies revealed formation of homogenous, spherical particle aggregates of about 50 nm. HRTEM imaging of primary particles (insets in Figure 36a, b) revealed small crystalline particles. The lattice fringe distance were in both cases measured to 0.2 nm, which corresponds to the (2 0 0) plane of anatase.

Thus, none of the ligands or the combination of two ligands resulted in any apparent increase in hydrolytic stability. However, ligand-solvent

interactions are known to influence the morphology of the hydrolyzed products, which were investigated next.

Crystals of the bimetallic  $Ti_2Y$ -complex **1e** were also treated with water and imaged by HRTEM. From Figure 37 it can be seen that hydrolysis caused the formation of anatase nanoparticles of very narrow size distribution (ca. 3 nm average diameter).

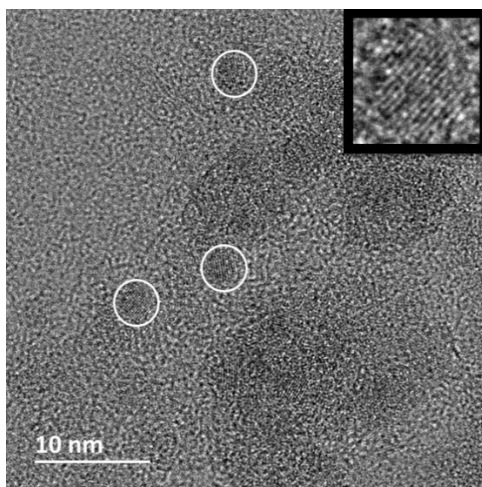


*Figure 37.* HRTEM micrograph of **1e** submerged in water. A few primary particles with crystalline cores (anatase) are indicated by white circles. The diameter of the particles are ca. 3 nm. Inset: increased magnification of an anatase nucleus. Image from **manuscript VII**.

### 3.2.2. Complex oxide structures from hydrolysis of precursors

Hydrolysis of carboxylate modified titanium alkoxides has resulted in diatom-like structures and it was reasonable to assume that also phosphonate modified could yield complex oxide structures. Hydrolysis of **7d** (its equilibrium forms in solution) under different conditions yielded quite different structures. In the first case, precursor solution (toluene) was quickly injected to a dilute CNF-suspension at ca. 90°C. CNF acted as a Pickering emulsifier at the organic-water interface (Bai et al., 2018; Varanasi et al., 2018). This yielded spherical titania of different sizes. Annealing resulted in

partial destruction of the spheres that revealed a very porous, hierarchical structure very similar to those obtained by Collins and co-workers (2004).

When the spherical toluene droplets enters the water the titanium alkoxide complexes at the surface instantaneously hydrolyzes, forming a semipermeable membrane. Water passes through the membrane into the sphere, causing hydrolysis of the titanium complexes to titania particles.

These particles make up channels through which water diffuses (Figure 38a and b). The hydrolysis of titanium(IV) methoxide to anatase was reported to occur topotactically upon contact with water. Simultaneous hydrolysis-condensation reactions of  $\text{Ti}(\text{OMe})_4$  precursor crystals lead to a contraction of the structure with formation of lamellar sheets with the emergence of anatase nuclei (Seisenbaeva et al., 2012). The same basic mechanism is probably responsible for the hierarchical hydrolysis structures observed in **paper IV**.

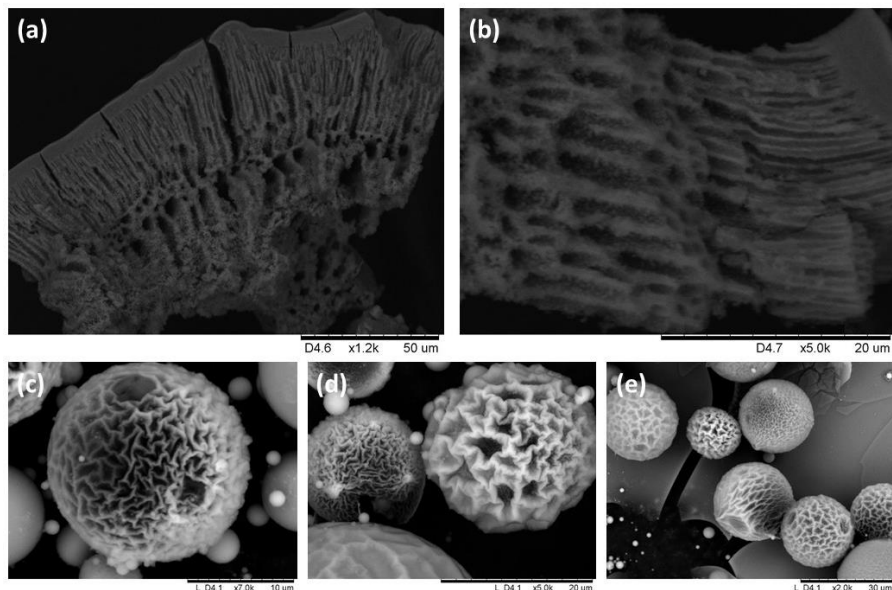


*Figure 38.* Hydrolyzed “complex 7d” under different conditions. (a) and (b) shows the structure obtained after hydrolysis in heated CNF-suspension and subsequent calcining. Figures (c), (d), and (e) show the structures obtained after hydrolysis in a water-acetone mixture at room temperature. Figure 38a is reproduced from **paper IV** with permission from the publisher.

### 3.2.3. Solution stability of selected modified titanium complexes

As mentioned above, for some applications (e.g. homogenous catalysts, precursors for hybrid materials, and single source precursors or metal oxides) the integrity of a coordination compound in solution is necessary. Traces of water in organic solvents can cause hydrolysis of water-sensitive compounds. Solvents containing free electron pairs (e.g. from N, O, and S) can shift the coordination equilibrium, thereby destroying the original complex. NMR spectrometry is a useful tool for investigating solution stability.  $^{31}\text{P}$  NMR was used for the phosphonate compounds in **paper IV**, and  $^{31}\text{P}$  NMR together with  $^1\text{H}$  DOSY NMR in **paper III**.  $^{31}\text{P}$  NMR spectra were recorded for compounds **1d**, **3d/4d**, **5d**, **6d**, and **7d**. Based on these spectra, it was concluded that the solid-state structure of **1d** and **5d** also were the major species in solution for solvent ( $\text{CDCl}_3$ ), Figure 39. For compounds **3d/4d**, **7d** (anhydrous  $\text{CDCl}_3$ ) and **6d** (anhydrous acetone- $d_6$ ) rather complex spectra were observed, suggesting formation of several different species in solution.

For complex mixtures of compounds DOSY NMR can be a valuable tool for separating different chemical species based on their diffusion constant.

Compound **1c** was investigated using  $^1\text{H}$  DOSY NMR. Its  $^{31}\text{P}$  NMR showed one dominant signal (representing ca. 97 area% of the integrated spectrum), suggesting integrity of the structure. The DOSY NMR (Figure 40) confirmed this. Signal assignments are available in **paper III**.  $^1\text{H}$  DOSY NMR was also employed for the RM of compound **2c**, which displayed a very complex  $^{31}\text{P}$  NMR spectrum. Based on the DOSY spectrum, there appears to be two major compounds in the RM, presumably titanium oxo-alkoxy compounds based on signal assignments (cf. **paper III**). Thermal stability of compound **5d** was followed by  $^{31}\text{P}$  NMR in  $\text{CDCl}_3$  (Figure 41).

The experiment started at  $5^\circ\text{C}$ , and was raised stepwise first by  $10^\circ\text{C}$  and then by  $5^\circ\text{C}$  until  $50^\circ\text{C}$ . The compound remains mostly stable with some minor degradation when approaching  $50^\circ\text{C}$ . Interestingly, as a final experiment a small amount of deionized water was added. The solution immediately became turbid. A new spectrum was then recorded and, as clearly seen, no phosphorus signals were detected. This clearly indicated hydrolysis of complex **5d** in contact with water.

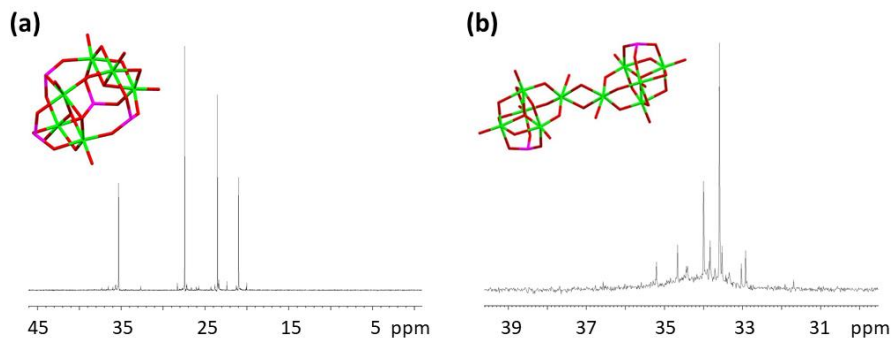


Figure 39.  $^{31}\text{P}$  NMR spectra of two titanium oxo-alkoxide phosphonates with different solution stability. The structure of compound **5d** (a) is predominantly retained in solution, while the spectrum of compound **7d** (b) contains more signals than expected that suggests dissociation in solution. Image modified from **paper IV**, all  $^{31}\text{P}$  NMR spectra of tBPA containing titanium alkoxide species are available in **papers III** and **IV**. Image modified from **paper IV**, reproduced with permission from the publisher.

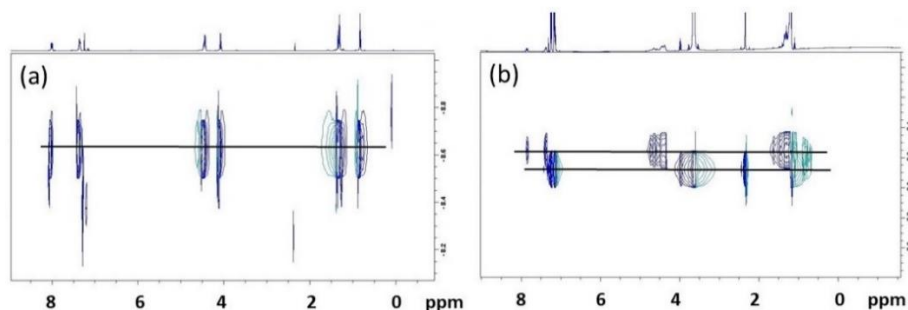


Figure 40. DOSY NMR spectra of (a) compound **1c** and (b) the reaction mixture of **2c** indicating the presence of one and two major species, respectively. The existence of two major species in (b) would have been difficult to sort out in an ordinary 1D spectrum. Image modified from **paper III**, reproduced with permission from the publisher.

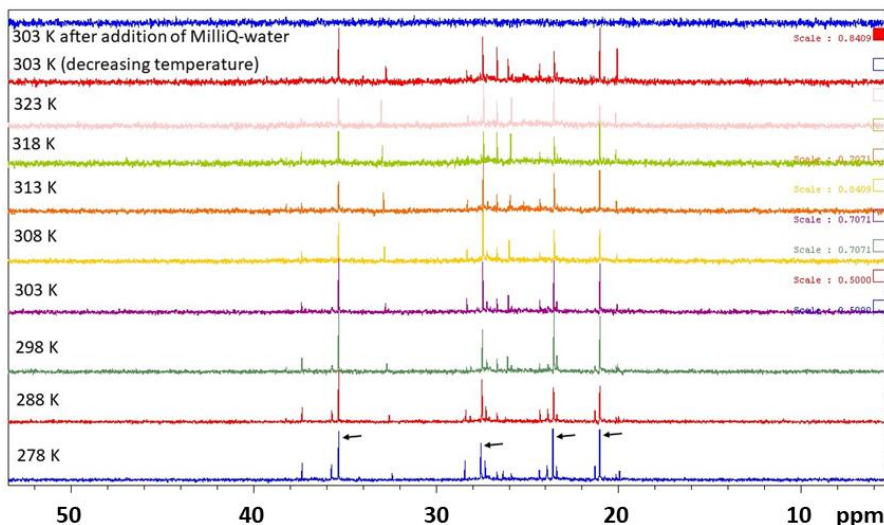


Figure 41.  $^{31}\text{P}$  NMR spectra over different temperatures for compound **5d**, ranging from 278 K (0°C) to 323 K (50°C) in  $\text{CDCl}_3$ . The four black arrows indicate signals for the four different P atoms in **5d**. After adding a small aliquot of  $\text{dH}_2\text{O}$  to the NMR tube, all signals vanish (with precipitate in the NMR tube) as evidence for hydrolytic instability of the compound. Reproduced from **paper IV** with permission from the publisher.

### 3.3. Photocatalytic properties of REE-modified titania

The effect on photocatalytic properties by modification of titania with Sm and Eu was investigated using trimethylphenol as model compound for degradation. The activity was compared to Degussa P25 titania as control. It can be seen from Figure 42 that when irradiated with visible light in the ranges 445-465 nm and 510-530 nm, all REE modified titania performed worse than the control. When using wide range visible light, performances were in most cases better for the modified titania compared to the P25 titania. However, the total conversions were still very low. It is hypothesized that the observed differences may depend on different positions of the REE-dopants on the surface of the titania nanoparticles. Different ionic radii may result in different chemical sites and also different kinds of catalytic centers, which may also be affected by annealing temperature. Photoluminescence

studies are underway to provide information about the chemical position of the REEs.

One of the mechanisms for promoted photocatalysis by REE doping is the inclusion of the REE *f*-orbitals that can act as electron traps, preventing electron-hole recombination (Zalas, 2014). Other works have suggested that above a certain amount, REE doping creates recombination centers, which instead decreases the activity (Weber et al., 2012). Rozman and co-workers (2019) studied photocatalytic activities of titania doped with Ce, La, and Gd.

They observed a decreased degradation for the modified titania, compared to the unmodified titania. They explained this by a decreased  $Ti^{3+}/Ti^{4+}$  ratio, resulting in a lower amount of surface hydroxyl groups.

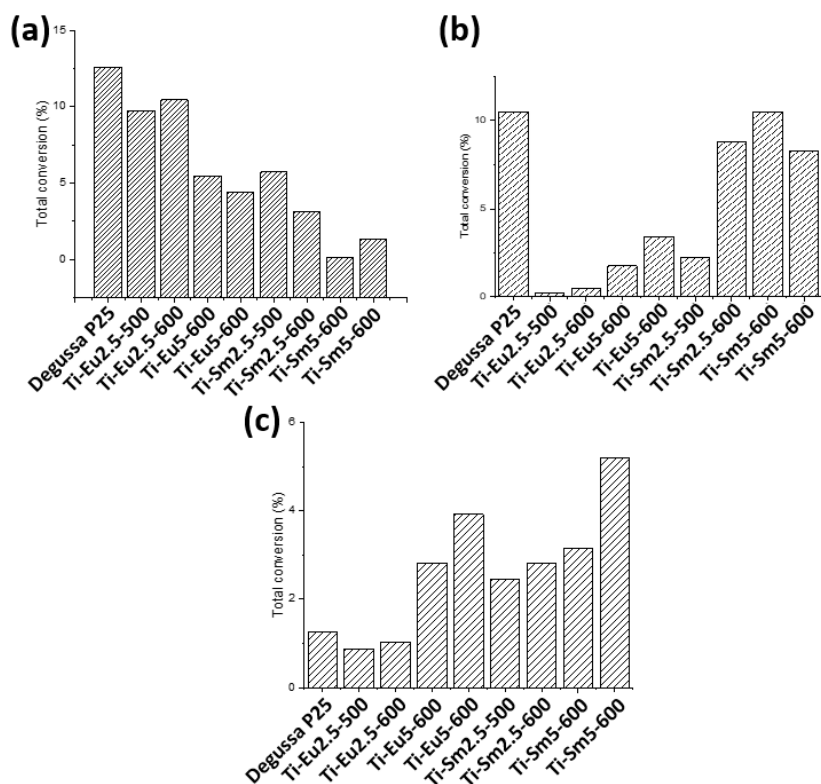


**Figure 42.** Photocatalytic degradation of trimethylphenol using titania modified with Eu and Sm under different wavelengths. (a), 445-465 nm LEDs, (b) 510-530 nm LEDs, and (c) wide range visible lamp. Figure from **manuscript VII**.

### 3.3.1. Photoluminescence

Photoluminescence (PL) spectra (cf. Figures 7 and Figure 8 in **manuscript VII**) were recorded for Ti-Eu2.5-500, Ti-Eu5-700, Ti-Sm2.5-500, and Ti-Sm5-700 and they revealed interesting differences. The Ti-Eu2.5-500 sample contains Eu ions both in the titania lattice and on the surface. The Ti-Eu5-700, on the other hand, did only display emissions corresponding to surface associated Eu. Apparently, the increased annealing temperature forced out the doped Eu with indications of a heterometallic surface phase.

The PL spectra of Ti-Sm2.5-500, and Ti-Sm5-700 both indicated the presence of two different substitutional positions for Sm, with one dominant position, and additionally indications of surface associated Sm. The position of the REE dopants will heavily influence the catalytic properties of the powders. Doping into the lattice will generate both new intermediate energy levels between the  $CB_{TiO_2}$  and the  $VB_{TiO_2}$ , and cause oxygen vacancies to balance the charge inequalities. Catalytic reactions take place on the particle surfaces and therefore changes in the surface chemistry can drastically effect catalytic properties. Migration of internal REEs out to the particle surface will increase surface defects and promote catalytic activity which may explain the observed higher degradation for powders with higher amounts of REEs and higher annealing temperatures under wide-range visible radiation. The control P25 titania will have less surface defects compared to the REE-modified because of the absence of dopants.

The overall degradation of TMB was very low and the REE-modified titania were not efficient photocatalysts. This study does, however, provide valuable information about position of  $Eu^{3+}$  and  $Sm^{3+}$  in titania, revealing both substitution and surface association. Despite the similarities in size of  $Eu^{3+}$  and  $Sm^{3+}$ , the latter apparently occupied two different coordination environments while  $Eu^{3+}$  only displayed one coordination environment. The observed increased activity under irradiation by wide-range visible light is probably a combination of volume doping of anatase, with red-shifted absorption spectrum and addition of energy levels between  $VB_{TiO_2}$  and  $CB_{TiO_2}$ , and an increased amount of surface defects.

Solvothermal (and sol-gel) methods, which presumably proceeds via bimetallic intermediates, appears to be good techniques to produce homogeneously REE-modified titania nanopowders.

### 3.4. Drug release from CNC\_TiO<sub>2</sub>\_TR and hydrolyzed complex **1a**

Many functional groups have good affinity towards metal oxides, including titania, making metal oxide nanoparticles interesting as drug carriers for controlled release. Nanocellulose wound dressings have demonstrated promising properties as improved healing and less tendency to adhere on the regenerated tissue compared to conventional wound-dressing.

Nanocellulose, however, does not have antibacterial properties and could also provide a good environment for microbial growth. Metal oxide nanoparticles slowly releasing antibacterial molecules embedded in nanocellulose could prevent microbial growth in the wound-dressing. Haemocompatibility of nanocellulose-titania hybrids are discussed in section 3.5.

#### 3.4.1. Drug release from hydrolyzed complex **1a**

During hydrolysis of metal oxo-alkoxide complexes some of the coordinating ligands will remain bound the formed nanoparticle surface. Thus, the hydrolysis of compound **1a** should result in triclosan-coated titania nanoparticles Drug release from hydrolyzed compound **1a** was investigated in **paper I**. Filter papers with MIC of triclosan from dissolved **1a**, a reference solution of triclosan, and a negative control was added to agar plates inoculated with *S. aureus*.

After 18 hours a clear difference in inhibitory zones were seen (Figure 43). The drug release from the hydrolyzed complex was significantly (by one-way ANOVA) slower compared to triclosan loaded on filter paper. The pure filter paper had, as expected, no visible effect on the growth of *S. aureus*.

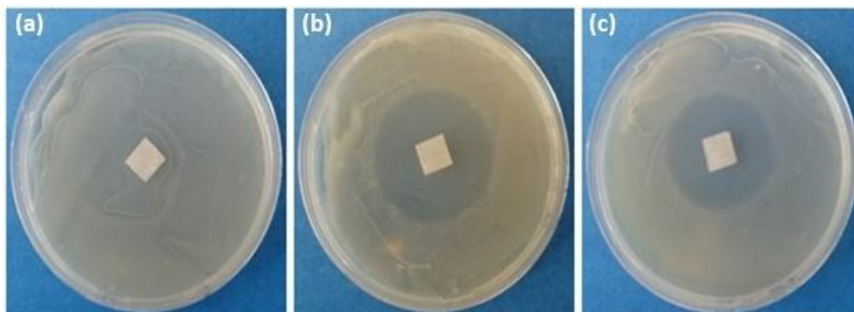
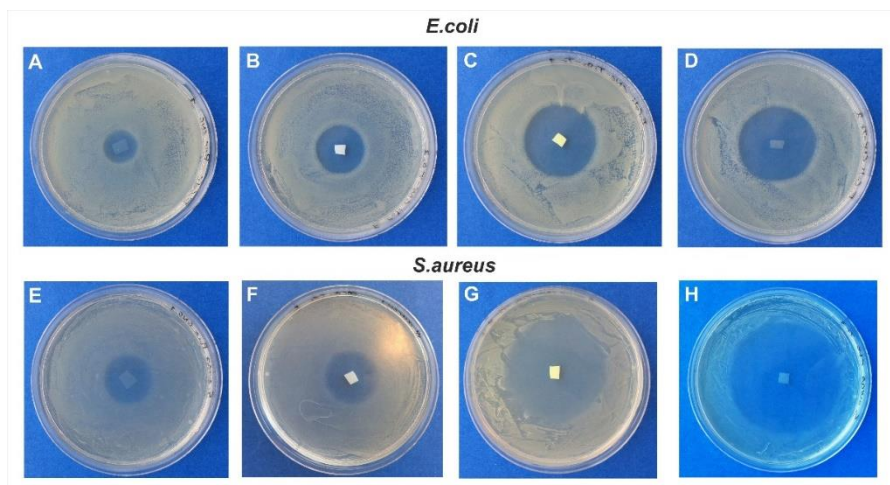


Figure 43. Inhibitory effect of triclosan released from filter paper (b), from hydrolyzed filter paper (c), and negative control (a) (N = 6). Reproduced from **paper I** with permission from the publisher.

### 3.4.2. Drug release from CNC\_TiO<sub>2</sub> composites

In **paper II** a drug delivery system based on nanotitania embedded in CNC as drug carrier was developed. They were loaded with triclosan and their activity tested against *E. coli* and *S. aureus*. As can be seen from Table 1 and Figure 44 inhibitory zones are larger for PCNC compared to CNC\_TiO<sub>2</sub> implying better retention when titania is present.

There are some inhibitory effects from the PCNC and PCNC-TiO<sub>2</sub> materials which do not contain triclosan. For the PCNC-TiO<sub>2</sub> material it was speculated that UV-light could cause formation of ROS that killed the bacteria. However, UV-irradiation (300 W lamp) of the PCNC-TiO<sub>2</sub> materials immediately before addition of bacteria did not result in any visible difference in inhibitory zone compared to the non-radiated PCNC-TiO<sub>2</sub> films. Further, the incubations with the materials were done in darkness with only a short time exposed to light during preparations. A likely explanation is an antibacterial effect of the 1,2,3,4–bytanetetra-carboxylic acid used to functionalize the pure CNC, as this compound has a documented antibacterial effect (Yazhini et al., 2015).



**Figure 44.** Inhibition zones of antibacterial activity against *E.coli*: PCNC (A), CNC\_TiO<sub>2</sub> (B), CNC\_TiO<sub>2</sub>\_TR (C), and CNC\_TR (D), and *S. aureus*: PCNC (E), CNC\_TiO<sub>2</sub> (F), CNC\_TiO<sub>2</sub>\_TR (G), and CNC\_TR (H) samples. Reproduced from **paper II** with permission from the publisher.

**Table 1.** Measured inhibitory zones on *E. coli* and *S. aureus* after incubation with the CNC\_TiO<sub>2</sub> composites and controls. SD = standard deviation. Modified from **paper II**. Reproduced with permission from the publisher.

Sample	Bacteria (strain)	MIC (mg/ml)[34]	Diameter of inhibition zone (mm ± SD)
PCNC		-	13 ± 4
CNC_TiO <sub>2</sub>	<i>E. coli</i>	-	19 ± 6
CNC_TR	CCUG24T	0.1	42 ± 3
CNC_TR_TiO <sub>2</sub>		0.1	38 ± 2
PCNC		-	16 ± 7
CNC_TiO <sub>2</sub>	<i>S. aureus</i>	-	26 ± 6
CNC_TR	CCUG1800T	0.1	62 ± 4
CNC_TR_TiO <sub>2</sub>		0.1	56 ± 2

### **3.5. Immunological studies of the nanocellulose-nanotitania hybrid materials**

The aim of this project was to investigate the haemocompatibility of nanocellulose-nanotitania films. First, human whole blood was incubated with the films and then concentration of platelets were determined.

The concentrations of TAT, C3a, sC5b-9, C1In-FXI, and C1In-FXII in the blood plasma were quantified by ELISA. These results are discussed separately below.

#### **3.5.1. Human whole blood chamber model**

Upon damage of blood vessels, exposed endothelium will activate platelets that circulates the blood. The platelets will adhere to the endothelium and to other platelets via linking by fibrin. This will eventually form a blood clot. Platelets will also become activated if blood is exposed to a foreign surface, such as a biomaterial, with subsequent coagulation and clot formation via the same mechanism. Thus, during coagulation the number of platelets in the blood decreases.

The platelet concentrations were measured for blood in contact with the different materials and compared to the CHS control and the initial samples (Figure 46). It was found that platelet reductions for CHS controls and CNF\_PEG were small compared to the initial sample. However, the three hybrid materials had significant ( $p < 0.05$ , by t-test) platelet reductions compared to both the control and CNF\_PEG. Still, the variation in response between donors for the three hybrid materials was larger than for the control and CNF\_PEG, as can be seen from the larger error bars. In addition, large clots were observed on the CNF\_PEG\_TiO<sub>2</sub> and CNF\_PEG\_Captigel after incubation (Figure 45). Interestingly, no clots were observed for CNF\_PEG\_TiBALDH. This may be a result of lactic acid from the TiBALDH precursor. It was previously demonstrated by Engström and co-workers (2006) that the presence of lactic acid, by decreasing pH, can inhibit coagulation.

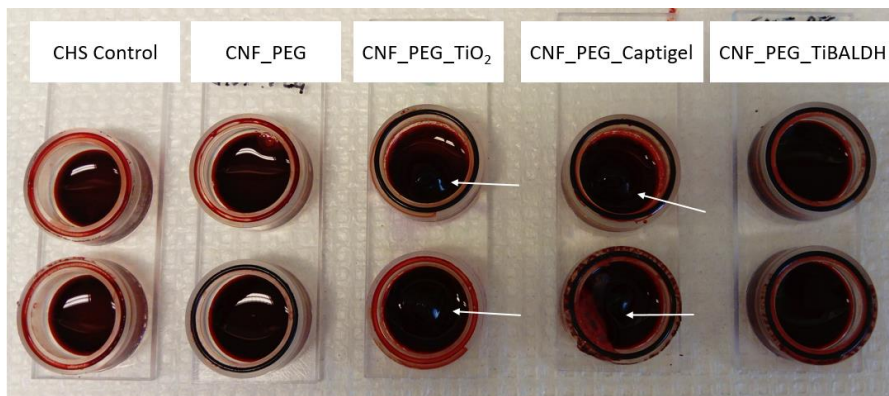


*Figure 45.* Blood chambers after incubation of the CHS control, control material and the three different hybrid materials. The white arrows indicate blood clots. Figure from **manuscript V**.

### 3.5.2. Thrombin-antithrombin ELISA

Thrombin is an enzyme that cleaves fibrinogen to fibrin, which function is to link platelets into a clot. The antithrombin complex acts as a regulator of coagulation and inactivates thrombin by binding to it, forming the thrombin-antithrombin (TAT) complex. High concentrations of TAT indicate strong activation of coagulation.

The generated thrombin-antithrombin levels were found to be variable between different blood donors as seen by the sometimes large error bars in Figure 46b. This can at least partly be explained by donors naturally having different concentrations of the TAT-components in their blood. Further, they can be “high” or “low” responders, meaning that some donors may respond more strongly than others on the same material. However, the CNF\_PEG\_TiO<sub>2</sub> and CNF\_PEG\_Captigel materials have statistically significant (by One-Way ANOVA) higher TAT-concentrations compared to all other treatments. This was also expected from the observation of large blood clots after incubation for these two materials.

### **3.5.3. C3a ELISA**

C3a is an activation product of the complement system. It induces both inflammatory responses, activates T-cells, and is important for initiation of healing processes. C3a concentrations were measured for the different treatments for the three first donors (Figure 47a). As the concentrations differed between the donors, concentrations were normalized to the initial sample for comparison. All treatments had somewhat elevated C3a concentrations after incubation relative to the initial sample. They did, however, not differ from to the CHS control. This suggests there were no strong promotion of complement activation by any of the materials.

The observed elevated C3a concentrations in all samples is likely an effect of the inevitable air bubble always present in incubation chamber. The cleavage of C3 into C3a also results in the formation of C3b, which easily attaches to surfaces (e.g. the incubation chamber and the test materials). C3b can also bind to neutrophils which may explain the observed decrease in neutrophil count in the blood plasma for many of the samples.

### **3.5.4. sC5b-9 ELISA**

sC5b-9 is also known as the membrane attack complex (MAC) which function is to damage cell membranes of pathogens, resulting in their death.

The MAC is formed upon activation of the complement system, and the sC5b-9 protein is thus indicator of complement activation (Nilsson-Ekdahl et al., 2016). As seen from Figure 47b, the sC5b-9 concentrations for CNF\_PEG, CNF\_PEG\_TiO<sub>2</sub>, and CNF\_PEG\_Captigel do not vary very much, indicating there is no particular inflammatory response by either the control material or the two hybrid materials. Very interestingly, the CNF\_PEG\_TiBALDH material shows sC5b-9 concentrations very close to the initial samples, significantly lower ( $p \ll 0.05$ , by t-test) compared to the other materials and CHS controls.

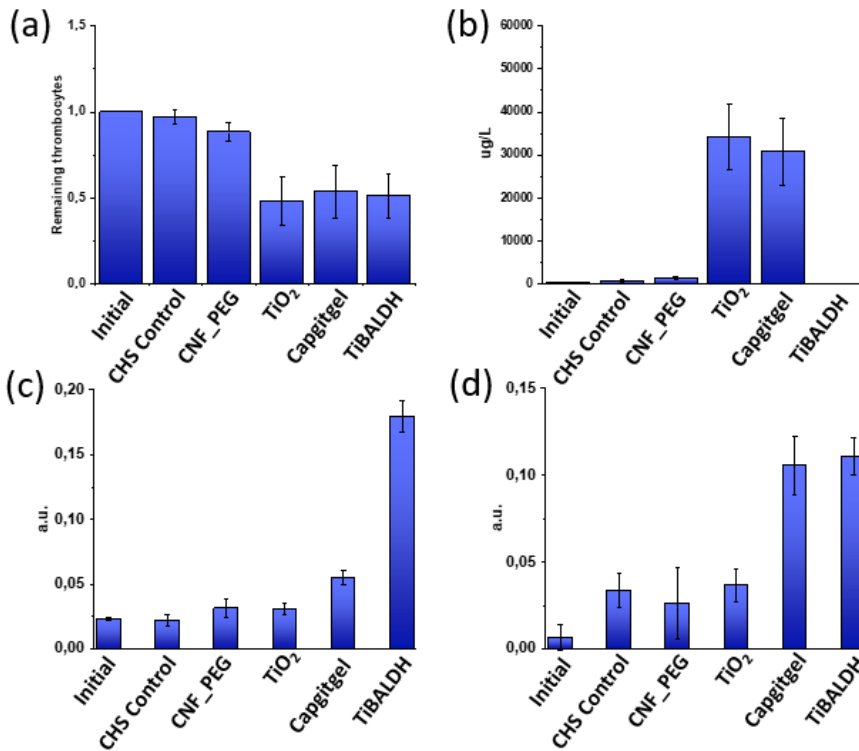


**Figure 46.** Concentrations of platelets, TAT, C1In-FXI, and C1In-FXII. (a) Average remaining platelets after incubation, compared to initial sample (n=5). (b) Average TAT-concentrations for the different materials after incubation compared to initial sample (n=5). (c) Amounts of C1In-FXI in the different treatments (n = 3), and (d) amounts of C1In-FXII in the different treatments (n = 3). Error bars are standard error of mean. CNF\_PEG\_TiO<sub>2</sub>, CNF\_PEG\_Captigel, and CNF\_PEG\_TiBALDH have been abbreviated to TiO<sub>2</sub>, Captigel, and TiBALDH, respectively, in the figure. Figure from **manuscript V**.

### 3.5.5. C1-inhibitor complex with FXI and FXII

Factor XII (FXII) is activated by foreign surfaces and will subsequently activate Factor XI (FXI), which eventually will lead to the activation of prothrombin into thrombin. Thrombin cleaves fibrinogen into fibrin, which together with platelets form blood clots. C1-inhibitor (C1In) as a regulator by binding to FXII and FXI, thereby inactivating them. Factor XII is

activated by contact activation, and the C1In-FXII and C1In-FXI complexes are indicators of contact activation of the coagulation cascade (Bäck et al., 2009; Nilsson-Ekdahl et al., 2016). In most cases, the concentrations of C1In-FXII and C1In-FXI were low (Figure 46). C1In tends to bind to fibrin in blood clots, thus reducing their numbers in the blood plasma. However, due to the presence of lactic acid that inhibits coagulation in the CNF\_PEG\_TiBALDH material, no clot is present to adsorb C1In-FXII and C1In-FXI and they remain in the plasma.

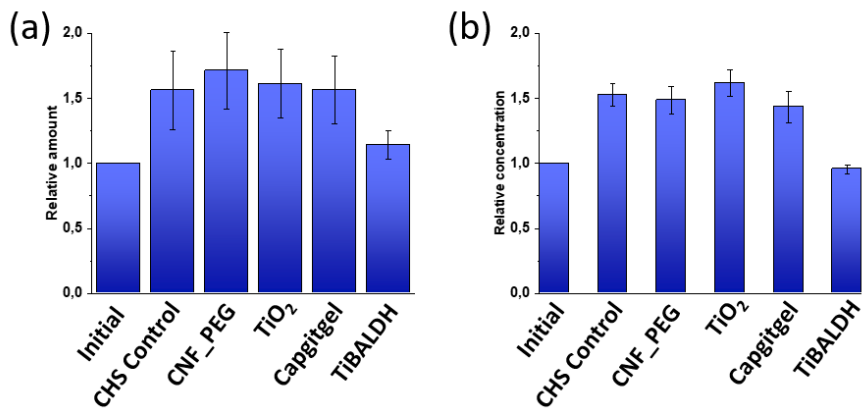


Figure 47. (a) Relative C3a concentrations after incubation compared to initial sample (n=3). (b) Relative concentrations of sC5b-9 (n=3). Error bars represent standard error of mean. CNF\_PEG\_TiO<sub>2</sub>, CNF\_PEG\_Captigel, and CNF\_PEG\_TiBALDH have been abbreviated to TiO<sub>2</sub>, Captigel, and TiBALDH, respectively, in the figure. Image from **manuscript V**.

### **3.6. What are the nanosafety risks associated with this work?**

With the rapid development of new nanomaterials their potential health and environmental impact must be considered. In this work, different titania based nanopowders were synthesized. Because of their high surface energy they easily aggregate to larger particles which should reduce their harm.

However, ligand-stabilized nanoparticles may enter waters and risk uptake by organisms. Larue and co-workers (2018) reported that mobility and bioavailability of TiO<sub>2</sub> NPs are much higher in sandy soils compared to soils with high contents of clay and organics. Inhalation during handling of nanopowders is a major risk. For the application of nanocellulose-nanotitania hybrid materials, potential release of titania aggregates from the films into blood vessels (with subsequent blood clots) appear to be the largest problem.

In some instances, such as the titania nanoshells, harmful chemicals were required for their production (in this case toluene). Thus, for biomaterials using hazardous chemicals during their production proper removal of these must be ensured, or, alternatively, substitution with less harmful chemicals for the process.

Research on nanomaterials is currently intense and rapid progress for applications in many different fields is made but safety research is falling behind. This may find analogy with the concerns raised by Rachel Carson in her influential book *Silent Spring*, covering the concerns and dangers from wide-spread applications of newly developed synthetic pesticides with poorly understood ecological effects. However, in case of the rapid development of nanomaterials the risks are generally well acknowledged although not properly understood. The lack of standardized protocols for safety evaluation of nanomaterials have been noted by Boyes and co-workers (2017). This is an important area of study and presents in itself a very interesting research field.

## 4. Conclusions and outlook

The work within this thesis was dedicated to development of new nanomaterials based on nanotitania and nanotitania-nanocellulose hybrid materials, starting from molecular precursors. Studies of the precursors, i.e. heteroleptic titanium oxo-alkoxide complexes, have contributed to the understanding of their solution stability, especially their susceptibility towards hydrolysis, and promising application as molecular precursors for titania with complex morphology. Several reports, from us and others, have investigated nanotitania-nanocellulose hybrid materials *in vitro* for drug delivery using bacterial cultures. Herein, the studies on these hybrid materials were continued to evaluate their biocompatibility towards human whole blood. Some of the hybrid materials strongly activated the coagulation system, presumably via the contact activation system, which was attributed to the inclusion of titania, a well-known initiator of blood clotting. Only moderate inflammatory responses were observed, which is important for activating tissue regeneration. The developed hybrid materials may find application as blood clotting patches with some healing promoting properties.

Titania nanopowders, modified with rare-earth elements, were synthesized. Interestingly, they showed inferior catalytic activity compared to Degussa P25 titania when radiated with visible light in two very narrow ranges. However, when irradiated with broad spectrum visible light, the rare-earth modified titania had a better catalytic activity compared to the commercial titania, still the overall degradation for all powders being low.

I would like to propose a few directions in which this thesis could be continued: (1) Further studies on the biocompatibility (cell viability) and biological responses (alterations in gene transcriptions) from the nanotitania-nanocellulose hybrids. (2) Synthesize titanium oxo-alkoxides with bifunctional ligands. Controlled hydrolysis of these compounds into complex morphologies could then enable further functionalization of their surfaces. (3) More detailed studies on the REE-modified titania nanopowders. The enhanced photocatalysis in the visible spectrum may be from a sensitizing effect of rare-earth oxides or different rare earth titanates. This would be interesting to investigate further using a combination of more powerful spectrometric and theoretical methods.

The promising potential of nanomaterials in medical therapy (including theranostics) is related to their high reactivity and interference with

biological systems on the molecular level. The same property is responsible for their potential harmful effects. The fact that the same nanomaterial can have different toxicities for different cell types surely complicates safety classifications. In several *in vitro* studies transcription profiles of cells were drastically changed when they were exposed to nanomaterials. Extensive evaluation of nanomaterials with biological applications will be required.

Certainly, nanomaterials are fascinating and will most likely become a central component in many future technologies. More and more experimental chemistry are nowadays supported by theoretical studies (such as density functional theory (DFT) and molecular dynamics (MD) simulations) providing better insight to reaction mechanisms and material properties. As more computational resources steadily becomes available and models becomes more sophisticated, theoretical studies may become increasingly important in designing new advanced nanomaterials. The currently rapid progress in machine learning and artificial intelligence could, if continued, become important tools for materials design and discovery (Boström 2016; Tegmark, 2014 & 2017; Ulissi et al., 2017; Xie et al., 2019).

As the final remark, bottom up synthesis using well defined molecular precursors and the directed self-assembly of nanoscale components to more complex materials are powerful methods to produce well-defined structures. During the coming years we will likely see a rapid progress using these methods to produce new, performant and attractive nanomaterials.

## 5. References

- Abbasi, P., Asadi, M., Liu, C., Sharifi-Asl, S., Sayahpour, B., Behranginia, A., Zapol, P., Shahbazian-Yassar, R., Curtiss, L.A., Salehi-Khojin, A. Tailoring the Edge Structure of Molybdenum Disulfide Toward Electrocatalytic Reduction of Carbon Dioxide. *ACS Nano* (2017) 11, 453-460.
- Abitbol, T., Rivkin, A., Cao, Y., Nevo, Y., Abraham, E., Ben-Shalom, T., Lapidot, S., Shoseyov, O. Nanocellulose, a Tiny Fiber with Huge Applications. *Current Opinion in Biotechnology* (2016) 39, 76-88.
- Andala, D.M., Shin, S.H., Lee, H.Y., Bishop, K.J.M., Templated Synthesis of Amphiphilic Nanoparticles at the Liquid-Liquid Interface. *ACS Nano* (2012) 6, 1044-1050.
- Andersson, M., Österlund, L., Ljungström, S., Palmqvist, A. Preparation of Nanosize Anatase and Rutile TiO<sub>2</sub> by Hydrothermal Treatment of Microemulsions and Their Activity for Photocatalytic Wet Oxidation of Phenol. *Journal of Physical Chemistry B* (2002) 106, 10674-10679.
- Arroyo, R., Cordoba, G., Padilla, J., Lara, V.H. Influence of Manganese Ions on the Anatase–Rutile Phase Transition of TiO<sub>2</sub> Prepared by the Sol–Gel Process. *Materials Letters* (2002) 54, 397-402.
- Artner, C., Kronister, S., Czakler, M., Schubert, U. Ion-Size-Dependent Formation of Mixed Titanium/Lanthanide Oxo Clusters. *European Journal of Inorganic Chemistry* (2014) 5596-5602.
- Asahi, R., Morikawa, T., Ohwaki, K., Aoki, K., Taga, Y. Visible-Light Photocatalysis in Nitrogen-Doped Titanium Oxides. *Science* (2001) 293, 269-271.
- Bai, L., Huan, S., Xiang, W., Rojas, O.J. Pickering Emulsions by Combining Cellulose Nanofibrils and Nanocrystals: Phase Behavior and Depletion Stabilization. *Green Chemistry* (2018) 20, 1571-1582.

- Barkley, JV., Cannadine, JC., Hannaford, I., Harding, MM., Steiner, A., Tallon, J., Whyman, R. Preparation and X-ray Crystallographic Characterisation of the Trititanate  $[\text{Ti}_3\text{O}(\mu\text{-OPr}^i)_3(\text{OPr}^i)_4\{\text{Me}_2\text{C}(\text{O})\text{CHNC}(\text{O})\text{CH}_2\text{C}(\text{O})\text{Me}_2\}]$ , a Reaction Product of  $[\text{Ti}(\text{OPr}^i)_4]$  and Propan-2-one. *Chemical Communications* (1997) 1653-1654.
- Beichel, F., Dubuc, J., Henry, M. General Principles Driving the Chemical Reactivity of Titanium(IV) Alkoxides. *New Journal of Chemistry* (2004) 28, 764-769.
- Bhardwaj, V., Kaushik, A. Biomedical Applications of Nanotechnology and Nanomaterials. *Micromachines* (2017) 8, 298.
- Bikondoa, O., Pang, CL., Ithnin, R., Muryn, CA., Onishi, H., Thornton, G. Direct Visualization of Defect-Mediated Dissociation of Water on  $\text{TiO}_2(110)$ . *Nature Materials* (2006) 5, 189-192.
- Boles, MA., Engel, M., Talapin, DV. Self-Assembly of Colloidal Nanocrystals: From Intricate Structures to Functional Materials. *Chemical Reviews* (2016) 116, 11220-11289.
- Boström, N. (2016). *Superintelligence. Paths, Dangers, Strategies*. Oxford: Oxford University Press.
- Boyes, WK., Thornton, BLM., Al-Abed, SR., Andersen, CP., Bouchard, DC., Burgess, RM., Hubal, EAC., Ho, KT., Hughes, MF., Kitchin, K., Reichman, JR., Rogers, KR., Ross, JA., Rygielwicz, PT., Scheckel, KG., Thai, SF., Zepp, RG., Zucker, RM. A Comprehensive Framework for Evaluating the Environmental Health and Safety Implications of Engineered Nanomaterials. *Critical Reviews in Toxicology* (2017) 47, 771-814.
- Bramwell, ST. & Gingras, MJP. Spin Ice State in Frustrated Magnetic Pyrochlore Materials. *Science* (2001) 294, 1495-1501.
- Bruce, DW., Walton, RI., O'Hare, D. Editors (2010). *Structure from Diffraction Methods*. West Sussex. John Wiley & Sons.
- Burns, A., Hayes, G., Li, W., Hirvonen, J., Demaree, JD., Shah, SI. Neodymium Ion Dopant Effects on the Phase Transformation in Sol-Gel Derived Titania Nanostructures. *Materials Science & Engineering B* (2004) 111, 150-155.
- Bäck, J., Lang, MH., Elgue, G., Kalbitz, M., Sanchez, J., Nilsson-Ekdahl, K., Nilsson, B. Distinctive Regulation of Contact Activation by Antithrombin and C1-Inhibitor on Activated Platelets and Material Surfaces. *Biomaterials* (2009) 30, 6573-6580.
- Cao, T., Li, Y., Wang, C., Zhang, Z., Zhang, M., Shao, C., Liu, Y.  $\text{Bi}_4\text{Ti}_3\text{O}_{12}$  Nanosheets/ $\text{TiO}_2$  Submicron Fibers Heterostructures: *in situ* Fabrication and High Visible Light Photocatalytic Activity. *Journal of Materials Chemistry* (2011) 21, 6922-6927.
- Cargnello, M., Gordon, TR., Murray, CB. Solution-Phase Synthesis of Titanium Dioxide Nanoparticles and Nanocrystals. *Chemical Reviews* (2014) 114, 9319-9345.

- Carson, R (2002). *Silent Spring*. HMH Books
- Chakraborty, M., Jain, S., Rani, V. Nanotechnology: Emerging Tool for Diagnostics and Therapeutics. *Applied Biochemistry and Biotechnology* (2011) 165, 1178-1187.
- Chatry, M., Henry, M., In, M., Sanchez, M., Livage, J. The Role of Complexing Ligands in the Formation of Non-Aggregated Nanoparticles of Zirconia. *Journal of Sol-Gel Science and Technology* (1994) 1, 233-240.
- Chen, JW., Shi, JW., Fu, ML. Nitrogen-Doped Anatase Titania Nanorods with Reactive {101} + {010} Facets Exposure Produced from Ultrathin Titania Nanosheets for High Photocatalytic Performance. *Catalysis Communications* (2016a) 76, 82-86.
- Chen, Y., Trzop E., Sokolow, JD., Coppens, P. Direct Observation of the Binding Mode of the Phosphonate Anchor to Nanosized Polyoxotitanate Clusters. *Chemistry A European Journal* (2013) 19, 16651-16655.
- Chen, Y., Jarzemska, KN., Trzop, E., Zhang, L., Coppens, P. How Does Substitutional Doping Affect Visible Light Absorption in a Series of Homodisperse Ti<sub>11</sub> Polyoxotitanate Nanoparticles? *Chemistry A European Journal* (2015) 21, 11538-11544.
- Chen, Y., Xu, M., Zhang, J., Ma, J., Gao, M., Zhang, Z., Xu, Y., Liu, S. Genome-Wide DNA Methylation Variations upon Exposure to Engineered Nanomaterials and Their Implications in Nanosafety Assessment. *Advanced Materials* (2016b) 29, 1604580.
- Cheng, K., Chhor, K., Kanaev, A. Solvent Effect on Nucleation-Growth of Titanium-Oxo-Alkoxy Nanoparticles. *Chemical Physics Letters* (2017) 672, 119-123.
- Choi, J., Park, H., Hoffmann, MR. Effects of Single Metal-Ion Doping on the Visible-Light Photoreactivity of TiO<sub>2</sub>. *The Journal of Physical Chemistry C* (2010) 114, 783-792.
- Collins, A., Carriazo, D., Davis, SA., Mann, S. Spontaneous Template-Free Assembly of Ordered Macroporous Titania. *Chemical Communications* (2004) 568-569.
- Colmenares, JC., Aramendía, MA., Marinas, A., Marinas, JM., Urbano, FJ. Synthesis, Characterization and Photocatalytic Activity of Different Metal-Doped Titania Systems. *Applied Catalysis A: General* (2006) 306, 120-127.
- Cooper, RJ. & Spitzer, N. Silver Nanoparticles at Sublethal Concentrations Disrupt Cytoskeleton and Neurite Dynamics in Cultured Adult Neural Stem Cells. *NeuroToxicology* (2015) 48, 231–238.
- Crosera, M., Prodi, A., Marcella, M., Pelin, M., Florio, C., Bellomo, F., Gianpiero, A., Apostoli, P., De Palma, G., Bovenzi, M., Campanini, M., Filon, FL. Titanium Dioxide Nanoparticle Penetration into the Skin and Effects on HaCaT Cells. *International Journal of Environmental Research and Public Health* (2015) 12, 9282-9297.

- Cruz, D., Arévalo, J.C., Torres, G., Margulis, R.G.B., Ornelas, C., Aguilar-Elguezabal, A. TiO<sub>2</sub> Doped with Sm<sup>3+</sup> by Sol-Gel: Synthesis, Characterization and Photocatalytic Activity of Diuron under Solar Light. *Catalysis Today* (2011) 166, 152-158.
- Czaja, W., Krystynowicz, A., Bielecki, S., Brown Jr., R.M. Microbial Cellulose – the Natural Power to Heal Wounds. *Biomaterials* (2006) 27, 145-151.
- Czakler, M., Artner, C., Schubert, U. Preparation of Carboxylato-Coordinated Titanium Alkoxides from Carboxylic Anhydrides: Alkoxido Group Transfer from Metal Atom to Carbonyl Group. *European Journal of Inorganic Chemistry* (2012) 3485-3489.
- Czakler, M., Artner, C., Schubert, U. Acetic Acid Mediated Synthesis of Phosphonate-Substituted Titanium Oxo Clusters. *European Journal of Inorganic Chemistry* (2014) 2038-2045.
- Czakler, M., Artner, C., Schubert, U. Titanium Oxo/Alkoxo Clusters with Both Phosphonate and Methacrylate Ligands. *Monatshefte für Chemie* (2015) 146, 1249-1256.
- Davidson, M.G., Jones, M.D., Lunn, M.D., Mahon, M.F. Synthesis and X-ray Structures of New Titanium(IV) Aryloxides and Their Exploitation for the Ring Opening Polymerization of  $\epsilon$ -Caprolactone. *Inorganic Chemistry* (2006) 45, 2282-2287.
- Deng, D., Hao, C., Sen, S., Xu, C., Král, P., Kotov, N.A. Template-Free Hierarchical Self-Assembly of Iron Diselenide Nanoparticles into Mesoscale Hedgehogs. *Journal of the American Chemical Society* (2017) 139, 16630-16639.
- Dhanalakshmi, J., Ahila, M., Selvakumari, J.C., Padiyan, D.P. Impact of Structural, Morphological and Electrical Properties of Gd<sub>x</sub>Ti<sub>1-x</sub>O<sub>2</sub> Nanocomposites on the Photocatalytic Degradation of Rhodamine B Dye. *Journal of Materials Science: Materials in Electronics* (2017) 28, 16384-16396.
- Díez, I., Eronen, P., Österberg, M., Linder, M.B., Ikkala, O., Ras, R.H.A. Functionalization of Nanofibrillated Cellulose with Silver Nanoclusters: Fluorescence and Antibacterial Activity. *Macromolecular Bioscience* (2011) 11, 1185-1191.
- Ding, S., Huang, F., Mou, X., Wu, J., Lu, X. Mesoporous Hollow TiO<sub>2</sub> Microspheres with Enhanced Photoluminescence Prepared by a Smart Amino Acid Template. *Journal of Materials Chemistry* (2011) 21, 4888-4892.
- Dwyer, D.B., Cooke, D.J., Hidalgo, M.F., Li, B., Stanton, J., Omenya, F., Bernier, W.E., Jones Jr, W.E. Fluorine Doping of Nanostructured TiO<sub>2</sub> Using Microwave Irradiation and Polyvinylidene Fluoride. *Journal of Fluorine Chemistry* (2019) 227, 109375.
- Egerton, R.F. (2016). *Physical Principles of Electron Microscopy. An Introduction to TEM, SEM, and AEM*. 2<sup>nd</sup> ed. Springer.

- Nilsson, KN., Huang, S., Nilsson, B., Teramura, Y. Complements Inhibition in Biomaterial- and Biosurface-Induced Thromboinflammation. *Seminars in Immunology* (2016) 28, 268-277.
- Ekstrand-Hammerström, B., Hong, J., Davoodpour, P., Sandholm, K., Ekdahl, KN., Bucht, A., Nilsson, B. TiO<sub>2</sub> Nanoparticles Tested in a Novel Screening Whole Human Blood Model of Toxicity Trigger Adverse Activation of the Kallikrein System at Low Concentrations. *Biomaterials* (2015) 51, 58-68.
- Engström, M., Schott, U., Nordström, CH., Romner, B., Reinstrup, P. Increased Lactate Levels Impair the Coagulation System - A Potential Contributing Factor to Progressive Hemorrhage After Traumatic Brain Injury. *Journal of Neurosurgical Anesthesiology* (2006) 18, 200-204.
- Eslava, S., Goodwill, BPR., McPartlin, M., Wright, DS. Extending the Family of Titanium Heterometallic-Oxo-Alkoxy Cages. *Inorganic Chemistry* (2011) 50, 5655-5662.
- Eslava, S., Hengesbach, F., McPartlin, M., Wright, DS. Heterometallic Cobalt(II)-Titanium(IV) Oxo Cages; Key Building Blocks for Hybrid Materials. *Chemical Communications* (2010) 46, 4701-4703.
- Eslava S., McPartlin, M., Thomson, RI., Rawson, JM., Wright, DS. Single-Source Materials for Metal-Doped Titanium Oxide: Syntheses, Structures, and Properties of a Series of Heterometallic Transition-Metal Titanium Oxo Cages. *Inorganic Chemistry* (2010) 49, 11532-11540.
- Essington, ME. (2015). *Soil and Water Chemistry: an Integrative Approach*. 2<sup>nd</sup> ed. CRC Press.
- Evdokimova, OL., Svensson, FG., Agafonov, AV., Håkansson, S., Seisenbaeva, GA., Kessler, VG. Hybrid Drug Delivery Patches Based on Spherical Cellulose Nanocrystals and Colloid Titania-Synthesis and Antibacterial Properties. *Nanomaterials* (2018) 8, 228.
- Fadeel, B. Hide and Seek: Nanomaterial Interactions With the Immune System. *Frontiers in Immunology* (2019) 9, 133.
- Fang, W., Khrouz, L., Zhou, Y., Shen, B., Dong, C., Xing, M., Mishra, S., Daniele, S., Zhang, J. Reduced {001}-TiO<sub>2-x</sub> Photocatalysts: Noble-Metal-Free CO<sub>2</sub> Photoreduction for Selective CH<sub>4</sub> Evolution. *Physical Chemistry Chemical Physics* (2017) 19, 13875-13881.
- Farmer, JM., Boatner, LA., Chakoumakos, BC., Du, MH., Lance, MJ., Rawn, CJ., Bryan, JC. Structural and Crystal Chemical Properties of Rare-Earth Titanate Pyrochlores. *Journal of Alloy and Compounds* (2014) 605, 63-70.
- Flemming, S. (2005). *Analyseteknik: Instrument och Metoder*. Lund: Studentlitteratur.
- Fujishima, A., Honda, K. Electrochemical Photolysis of Water at a Semiconductor Electrode. *Nature* (1972) 238, 37-38.

- Galkina, OL., Öneby, K., Huang, P., Ivanov, VK., Agafonov, AV., Seisenbaeva, GA., Kessler, VG. Antibacterial and Photochemical Properties of Cellulose Nanofiber–Titania Nanocomposites Loaded with Two Different Types of Antibiotic Medicines. *Journal of Materials Chemistry B* (2015) 3, 7125-7134.
- Galland, S., Andersson, RL., Salajkova, M., Ström, V., Olsson, RT., Berglund, LA. Cellulose Nanofibers Decorated with Magnetic Nanoparticles – Synthesis, Structure and Use in Magnetized High Toughness Membranes for a Prototype Loudspeaker. *Journal of Materials Chemistry C* (2013) 1, 7963-7972.
- Gao, Y., Wahi, R., Kan, AT., Falkner, JC., Colvin, VL., Tomson, MB. Adsorption of Cadmium on Anatase Nanoparticles - Effect of Crystal Size and pH. *Langmuir* (2004) 20, 9585-9593.
- Gliga, AR., Endoff, K., Caputo, F., Källman, T., Blom, H., Karlsson, HL., Ghibelli, L., Traversa, E., Ceccatelli, S., Fadeel, B. Cerium Oxide Nanoparticles Inhibit Differentiation of Neural Stem Cells. *Scientific Reports* (2017) 7, 9284.
- Glotzer, SC., Solomon, MJ., Kotov, NA. Self-Assembly: From Nanoscale to Microscale Colloids. *AIChE Journal* (2004) 50, 2978-2985.
- Goutailler, G., Guillard, C., Daniele, S., Hubert-Pfalzgraf, LG. Low Temperature and Aqueous Sol-Gel Deposit of Photocatalytic Active Nanoparticulate TiO<sub>2</sub>. *Journal of Materials Chemistry* (2003) 13, 342–346.
- Greenwood, NN. & Earnshaw, A. (1997). *Chemistry of the Elements*. 2<sup>nd</sup> ed. Butterworth-Heinemann.
- Gribb, AA. & Banfield, JF. Particle Size Effects on Transformation Kinetics and Phase Stability in Nanocrystalline TiO<sub>2</sub>. *American Mineralogist* (1997) 82, 717–728.
- Hakkarainen, T., Koivuniemi, R., Kosonen, M., Escobedo-Lucea, C., Sanz-Garcia, A., Vuola, J., Valtonen, J., Tammela, P., Mäkitie, A., Luukko, K., Yliperttula, M., Kavola, H. Nanofibrillar Cellulose Wound Dressing in Skin Graft Donor Site Treatment. *Journal of Controlled Release* (2016) 244, 292-301.
- Hammond, C. (2001). *The Basics of Crystallography and Diffraction*. (2<sup>nd</sup> ed). Oxford: Oxford University Press.
- Haugstad, G. (2012). *Atomic Force Microscopy: Understanding Basic Modes and Advanced Applications*. New Jersey: John Wiley & Sons.
- Hayami, R., Sagawa, T., Tsukada, S., Yamamoto, K., Gunji, T. Synthesis, Characterization and Properties of Titanium Phosphonate Clusters. *Polyhedron* (2018) 147, 1-8.
- Hench, LL. & West, JK. The Sol-Gel Process. *Chemical Reviews* (1990) 90, 33-72.

- Herrera, MA., Mathew, AP., Oksman, K. Barrier and Mechanical Properties of Plasticized and Cross-Linked Nanocellulose Coatings for Paper Packaging Applications. *Cellulose* (2017) 24, 3969-3980.
- Hubert-Pfalzgraf, LG. Metal Alkoxides and  $\beta$ -diketonates as Precursors for Oxide and Non-Oxide Thin Films. *Applied Organometallic Chemistry* (1992) 6, 627-643.
- Hui, CY., Liu, M., Li, Y., Brennan, JD. A Paper Sensor Printed with Multifunctional Bio/Nano Materials. *Angewandte Chemie International Edition* (2018) 57, 4549-4553.
- Ignatchenko, A., Nealon, DG., Dushane, R., Humphries, K. Interaction of Water with Titania and Zirconia Surfaces. *Journal of Molecular Catalysis A: Chemical* (2006) 256, 57-74.
- Jalilehvand, F. (2000). Structure of Hydrated Ions and Cyanide Complexes by X-ray Absorption Spectroscopy. PhD Thesis. KTH. Stockholm.
- Katagiri, K., Inami, H., Ishikawa, Y., Koumoto, K. Enzyme-Assisted Synthesis of Titania under Ambient Conditions. *Journal of the American Ceramic Society* (2009) 92, 181-184.
- Kelkar, SS. & Reineke, TM. Theranostics: Combining Imaging and Therapy. *Bioconjugate Chemistry* (2011) 22, 1879-1903.
- Kessler, VG. Molecular Structure Design and Synthetic Approaches to the Heterometallic Alkoxide Complexes (Soft Chemistry Approach to Inorganic Materials by the Eyes of a Crystallographer). *Chemical Communications* (2003) 1213-1222.
- Kessler, VG. The Chemistry Behind the Sol-Gel Synthesis of Complex Oxide Nanoparticles for Bio-Imaging Applications. *Journal of Sol-Gel Science and Technology* (2009) 51, 264-271.
- Kessler, VG. Aqueous Route to TiO<sub>2</sub>-Based Nanomaterials Using pH-neutral Carboxylate Precursors. *Journal of Sol-Gel Science and Technology* (2013) 68, 464-470.
- Kessler, VG., Seisenbaeva, GA., Unell, M., Håkansson, S. Chemically Triggered Biodelivery Using Metal-Organic Sol-Gel Synthesis. *Angewandte Chemie International Edition* (2008) 47, 8506-8509.
- Kessler, VG., Spijksma, GI., Seisenbaeva, GA., Håkansson, S., Blank, DHA., Bouwmeester, HJM. New Insight in the Role of Modifying Ligands in the Sol-Gel Processing of Metal Alkoxide Precursors: A Possibility to Approach New Classes of Materials. *Journal of Sol-Gel Science and Technology* (2006) 40, 163-179.
- Khanal, LR., Sundararajan, JA., Qiang, Y. Advanced Nanomaterials for Nuclear Energy and Nanotechnology. *Energy Technology* (2019) 8, 1901070.
- Klemm, D., Heublein, B., Fink, HP., Bohn, A. Cellulose: Fascinating Biopolymer and Sustainable Raw Material. *Angewandte Chemie International Edition* (2005) 44, 3358-3393.

- Kozma, K., Wang, M., Molina, P.I., Martin, N.P., Feng, Z., Nyman, M. The Role of Titanium-Oxo Clusters in the Sulfate Process for TiO<sub>2</sub> Production. *Dalton Transactions* (2019) 48, 11086.
- Kranjc, E. & Drobne, D. Nanomaterials in Plants: A Review of Hazard and Applications in the Agri-Food Sector. *Nanomaterials* (2019) 9, 1094.
- Laure, C., Baratange, C., Vantelon, D., Khodja, H., Surblé, S., Elger, A., Carrière, M. Influence of Soil Type on TiO<sub>2</sub> Nanoparticle Fate in an Agro-Ecosystem. *Science of the Total Environment* (2018) 630, 609-617.
- Lawrence, G.A. (2010). *Introduction to Coordination Chemistry*. John Wiley & Sons.
- Le, Q.C., Ropers, M.H., Terrisse, H., Humbert, B. Interactions Between Phospholipids and Titanium Dioxide Particles. *Colloids and Surfaces B: Biointerfaces* (2014) 123, 150-157.
- Legaria-Polido, E., Topel, S.D., Kessler, V.G., Seisenbaeva, G.A. Molecular Insights into the Selective Action of a Magnetically Removable Complexone-Grafted Adsorbent. *Dalton Transactions* (2015) 44, 1273-1282.
- Lennerstad, H., Jogr us, C. (2013). *Serier och Transformer*. (3<sup>rd</sup> ed). Lund: Studentlitteratur.
- Leroux, G., Neumann, M., Meunier, C.F., Michiels, C., Wang, L., Su, B.L. Alginate@TiO<sub>2</sub> Hybrid Microcapsules as a Reservoir of Beta INS-1E Cells with Controlled Insulin Delivery. *Journal of Materials Science* (2020) 55, 7857-7869.
- Li, N., Subramanian, G.S., Matthews, P.D., Xiao, J., Chellappan, V., Rosser, T.E., Reisner, E., Luo, H.K., Wright, D.S. Energy Transfer and Photoluminescence Properties of Lanthanide-Containing Polyoxotitanate Cages Coordinated by Salicylate Ligands. *Dalton Transactions* (2018) 47, 5679-5686.
- Lin, L.Y., Yeh, M.H., Chen, C.Y., Vittal, R., Wu, C.G., Ho, K.C. Surface Modification of TiO<sub>2</sub> Nanotube Arrays with Y<sub>2</sub>O<sub>3</sub> Barrier Layer: Controlling Charge Recombination Dynamics in Dye-Sensitized Solar Cells. *Journal of Materials Chemistry A* (2014) 2, 8281-8287.
- Lionel, N., Rozes, L., Sanchez, C. Integrative Approaches to Hybrid Multifunctional Materials: From Multidisciplinary Research to Applied Technologies. *Advanced Materials* (2010) 22, 3208-3214.
- Livage, J., Sanchez, C., Henry, M., Doeuff, S. The Chemistry of the Sol-Gel Process. *Solid State Ionics* (1989) 33, 633-638.
- Lomoschitz, M., Peterlik, H., Zorn, K., Baumann, S.O., Schubert, U. Titanium Alkoxo Oximates, with Surfactant-Like Properties of the Oximate Ligands, as Precursors for Porous TiO<sub>2</sub> and Mixed Oxide Sol-Gel Films. *Journal of Materials Chemistry* (2010) 20, 5527-5532.

- Loryuenyong, V., Angamnuaysiri, K., Sukcharoenpong, J., Suwannasri, A. Sol–Gel Derived Mesoporous Titania Nanoparticles: Effects of Calcination Temperature and Alcoholic Solvent on the Photocatalytic Behavior. *Ceramics International* (2012) 38, 2233-2237.
- Lovatel, RH., Neves, RM., Oliveira, GR., Mauler, RS., Crespo, JS., Carli, LN., Giovanela, M. Disinfection of Biologically Treated Industrial Wastewater Using Montmorillonite/Alginate/Nanosilver Hybrids. *Journal of Water Processing Engineering* (2015) 7, 273-279.
- Lu, H., Wright, DS., Pike, SD. The Use of Mixed-Metal Single Source Precursors for the Synthesis of Complex Metal Oxides. *Chemical Communications* (2020) 56, 854-871.
- Machon, D., Daniel, M., Bouvier, P., Daniele, S., LeFloch, S., Melinon, P., Pischedda V. Interface Energy Impact on Phase Transitions: The Case of TiO<sub>2</sub> Nanoparticles. *The Journal of Physical Chemistry C* (2011) 115, 22286–22291.
- Machon, D., Daniel, M., Pischedda, V., Daniele, S., Bouvier, P., LeFloch, S. Pressure-Induced Polyamorphism in TiO<sub>2</sub> Nanoparticles. *Physical Review B* (2010) 82, 140102.
- Maeda, K. Rhodium-Doped Barium Titanate Perovskite as a Stable p-Type Semiconductor Photocatalyst for Hydrogen Evolution under Visible Light. *ACS Applied Materials & Interfaces* (2014) 6, 2167-2173.
- Mahata, S., Mondal, B., Mahata, SS., Usha, K., Mandal, N., Mukherjee, K. Chemical Modification of Titanium Isopropoxide for Producing Stable Dispersion of Titania Nano-Particles. *Materials Chemistry and Physics* (2015) 151, 267-274.
- Maity, P., Mohammed, OF., Katsiev, K., Idriss, H. Study of the Bulk Charge Carrier Dynamics in Anatase and Rutile TiO<sub>2</sub> Single Crystals by Femtosecond Time-Resolved Spectroscopy. *The Journal of Physical Chemistry C* (2018) 122, 8925-8932.
- McMurry, J. (2007). *Organic Chemistry a Biological Approach*. Thomson Brooks/Cole.
- Meyer, G., Gloger, T., Beekhuizen, J. Halides of Titanium in Lower Oxidation States. *Zeitschrift für Anorganische und Allgemeine Chemie* (2009) 635, 1497-1509.
- Miller, M., Robinson, WE., Oliveira, AR., Heidary, N., Kornienko, N., Warnan, J., Pereira, IAC., Reisner, E. Interfacing Formate Dehydrogenase with Metal Oxides for the Reversible Electrocatalysis and Solar-Driven Reduction of Carbon Dioxide. *Angewandte Chemie International Edition* (2019) 58, 4601-4605.
- Molina, PI., Kozma, K., Santala, M., Falaise, C., Nyman, M. Aqueous Bismuth Titanium–Oxo Sulfate Cluster Speciation and Crystallization. *Angewandte Chemie International Edition* (2017) 56, 16277–16281.

- Mrázek, J., Surýnek, M., Bakardjieva, S., Bursik, J., Kasík, I. Synthesis and Crystallization Mechanism of Europium-Titanate  $\text{Eu}_2\text{Ti}_2\text{O}_7$ . *Journal of Crystal Growth* (2014) 391, 25-32.
- Mrázek, J., Surýnek, M., Bakardjieva, S., Bursik, J., Probstova, J., Kasík, I. Luminescence Properties of Nanocrystalline Europium Titanate  $\text{Eu}_2\text{Ti}_2\text{O}_7$ . *Journal of Alloys and Compounds* (2015) 645, 57-63.
- Nakamoto, K. (2008). *Infrared and Raman Spectra of Inorganic and Coordination Compounds, Part A*. 6<sup>th</sup> ed. Wiley.
- Nakata, K., Fujishima, A.  $\text{TiO}_2$  Photocatalysis: Design and Applications. *Journal of Photochemistry and Photobiology C: Photochemistry Reviews* (2012) 13, 169–189.
- Nattestad, A., Mozer, AJ., Fischer, MKR., Cheng, YB., Mishra, A., Bäuerle, P., Bach, U. Highly Efficient Photocathodes for Dye-Sensitized Tandem Solar Cells. *Nature Materials* (2010) 9, 31-35.
- Nel, A., Xia, T., Mädler, L., Li, N. Toxic Potential of Materials at the Nanolevel. *Science* (2006) 311, 622-627.
- Nguyen, VN., Doan, MT., Nguyen, MV. Photoelectrochemical Water Splitting Properties of  $\text{CdS}/\text{TiO}_2$  Nanofibers-Based Photoanode. *Journal of Materials Science: Materials in Electronics* (2019) 30, 926-932.
- Oun, AA., Shankar, S., Rhim, JW. Multifunctional Nanocellulose/Metal and Metal Oxide Nanoparticle Hybrid Nanomaterials. *Critical Reviews in Food Science and Nutrition* (2020) 60, 435-460.
- Parola, S., Papiernik, R., Hubert-Pfalzgraf, LG., Jagner, S., Håkansson, M. The Quest for Mixed-Metal Oxide Precursors Based on Bismuth: Synthesis and Molecular Structure of  $\text{BiTi}_2(\mu_3\text{-O})(\mu\text{-OPri})_4(\text{OPri})_5$  and  $[\text{Bi}_2(\mu\text{-OPri})_2(\text{OPri})_2(\text{acac})_2]_\infty$  (acac = acetylacetonate). *Journal of the Chemical Society Dalton Transactions* (1997) 4631-4635.
- Patel, DK., Dutta, SD., Lim, KT. Nanocellulose-Based Polymer Hybrids and Their Emerging Applications in Biomedical Engineering and Water Purification. *RSC Advances* (2019) 9, 19143-19162.
- Pellegrin, Y., Odobel, F. Sacrificial Electron Donor Reagents for Solar Fuel Production. *Comptes Rendus Chimie* (2017) 20, 283-295.
- Peng, Y., Lu, B., Wu, F., Zhang, F., Lu, JE., Kang, X., Ping, Y., Chen, S. Point of Anchor: Impacts on Interfacial Charge Transfer of Metal Oxide Nanoparticles. *Journal of the American Chemical Society* (2018) 140, 15290-15299.

- Pogorilyi, RP., Pylypchuk, I., Melnyk, IV., Zub, YL., Seisenbaeva, GA., Kessler, VG. Sol-Gel Derived Adsorbents with Enzymatic and Complexonate Functions for Complex Water Remediation. *Nanomaterials* (2017) 7, 298.
- Qian, L., Du, ZL., Yang, SY., Jin, ZS. Raman Study of Titania Nanotube by Soft Chemical Process. *Journal of Molecular Structure* (2005) 749, 103-107.
- R Core Team (2019). R: A Language and Environment for Statistical Computing. R Foundation for Statistical Computing, Vienna, Austria. URL <https://www.R-project.org/>
- Rahal, R., Daniele, S., Hubert-Pfalzgraf, LG., Guyot-Ferréol, V., Tranchant, JF., Synthesis of *para*-Amino Benzoic Acid-TiO<sub>2</sub> Hybrid Nanostructures of Controlled Functionality by an Aqueous One-Step Process. *European Journal of Inorganic Chemistry* (2008) 980-987.
- Rao, CNR. & Kanishka, B. (2015). *Essentials of Inorganic Materials Synthesis*. (1<sup>st</sup> ed). New Jersey: John Wiley and Sons.
- Reszczyńska, J., Grzyb, T., Sobczak, JW., Lisowski, W., Gazda, M., Ohtani, B., Zaleska A. Visible light activity of rare earth metal doped (Er<sup>3+</sup>, Yb<sup>3+</sup> or Er<sup>3+</sup>/Yb<sup>3+</sup>) titania photocatalysts. *Applied Catalysis B: Environmental* (2015) 163, 40-49.
- Robel, I., Subramanian, V., Kuno, M., Kamat, PV. Quantum Dot Solar Cells. Harvesting Light Energy with CdSe Nanocrystals Molecularly Linked to Mesoscopic TiO<sub>2</sub> films. *Journal of the American Chemical Society* (2006) 128, 2385-2393.
- Rodríguez-Campuzano, AG., Hernández-Kelly, LC., Ortega, A. Acute Exposure to SiO<sub>2</sub> Nanoparticles Affects Protein Synthesis in Bergmann Glia Cells. *Neurotoxicity Research* (2020) 37, 366–379.
- Rozes, L., Sanchez, C. Titanium Oxo-Clusters: Precursors for a Lego-Like Construction of Nanostructured Hybrid Materials. *Chemical Society Reviews* (2011) 40, 1006-1030.
- Rozman, N., Tobaldi, DM., Cvelbar, U., Puliyalil, H., Labrincha, JA., Legat, A., Skapin, AS. Hydrothermal Synthesis of Rare-Earth Modified Titania: Influence on Phase Composition, Optical Properties, and Photocatalytic Activity. *Materials* (2019) 12, 713.
- Prasad, R., Bhattacharyya, A., Nguyen, QD. Nanotechnology in Sustainable Agriculture: Recent Developments, Challenges, and Perspectives. *Frontiers in Microbiology* (2017) 8, 1014.
- Sayes, CM., Wahi, R., Kurian, PA., Liu, Y., West, JL., Ausman, KD., Warheit, DB., Colvin, VL. Correlating Nanoscale Titania Structure with Toxicity: A Cytotoxicity and Inflammatory Response Study with Human Dermal Fibroblasts and Human Lung Epithelial Cells. *Toxicological Sciences* (2006) 92, 174-185.
- Schubert, U. Chemical Modification of Titanium Alkoxides for Sol–Gel Processing. *Journal of Materials Chemistry* (2005) 15, 3701-3715.

- Schütz, C., Sort, J., Bacsik, Z., Oliynyk, V., Pellicer, E., Fall, A., Wågberg, L., Berglund, L., Bergström L., Salazar-Alvarez, G. Hard and Transparent Films Formed by Nanocellulose-TiO<sub>2</sub> Nanoparticle Hybrids. *PLOS One* (2012) 7, 45828.
- Seisenbaeva, GA., Daniel, G., Nedelec, JM., Gun'ko, YK., Kessler, VG. High Surface Area Ordered Mesoporous Nano-Titania by a Rapid Surfactant-Free Approach. *Journal of Materials Chemistry* (2012) 22, 20374-20380.
- Seisenbaeva, GA. Daniel, G., Nedelec, JM., Kessler, VG. Solution Equilibrium Behind the Room-Temperature Synthesis of Nanocrystalline Titanium Dioxide. *Nanoscale* (2013) 5, 3330-3336.
- Seisenbaeva, GA., Fromell, K., Vinogradov, VV., Terekhov, AN., Pakhomov, AV., Nilsson, B., Nilsson Ekdahl, K., Vinogradov, VV., Kessler, VG. Dispersion of TiO<sub>2</sub> Nanoparticles Improves Burn Wound Healing and Tissue Regeneration Through Specific Interaction with Blood Serum Proteins. *Scientific Reports* (2017) 7, 15448.
- Seisenbaeva, GA., Ilina, E., Håkansson, S., Kessler, VG. A New Concept for Titanium Oxo-Alkoxo-Carboxylates' Encapsulated Biocompatible Time Temperature Food Indicators Based on Arising, not Fading Color. *Journal of Sol-Gel Science and Technology* (2010a) 55, 1-8.
- Seisenbaeva, GA., Melnyk, IV., Hedin, N., Chen, Y., Eriksson, P., Trzop, E., Zub, YL., Kessler, VG. Molecular Insight Into the Mode-of-Action of Phosphonate Monolayers as Active Functions of Hybrid Metal Oxide Adsorbents. Case Study in Sequestration of Rare Earth Elements. *RSC Advances* (2015) 5, 24575-24585.
- Seisenbaeva, GA., Moloney, MP., Tekoriute, R., Hardy-Dessources, A., Nedelec, JM., Gun'ko, YK., Kessler, VG. Biomimetic Synthesis of Hierarchically Porous Nanostructured Metal Oxide Microparticles - Potential Scaffolds for Drug Delivery and Catalysis. *Langmuir* (2010b) 26, 9809-9817.
- Shannon, RD. Revised effective ionic radii and systematic studies on interatomic distances in halides and chalcogenides. *Acta Crystallographica Section A* (1976) 32, 751-767.
- Shimizu, M., Saito, T., Fukuzumi, H., Isogai, A. Hydrophobic, Ductile, and Transparent Nanocellulose Films with Quaternary Alkylammonium Carboxylates on Nanofibril Surfaces. *Biomacromolecules* (2014) 15, 4320-4325.
- Shulaker, MM., Hills G., Park, RS., Howe, RT., Saraswat, K., Wong, HSP., Mitra, S. Three-Dimensional Integration of Nanotechnologies for Computing and Data Storage on a Single Chip. *Nature* (2017) 547, 74-78.
- Sibu, CP., Kumar, SR., Mukundan, P., Warriar, KGK. Structural Modifications and Associated Properties of Lanthanum Oxide Doped Sol-Gel Nanosized Titanium Oxide. *Chemistry of Materials* (2002) 14, 2876-2881.

- Skoog, DA., Holler, FJ., Crouch, SR. (2007). *Principles of Instrumental Analysis*. (6<sup>th</sup> ed). Brooks/Cole.
- Sobota, P., Drag-Jarzabek, A., John, L., Utko, J., Jerzykiewicz, LB., Duczma, M. Cyclopentadienyl/Alkoxo Ligand Exchange in Group 4 Metallocenes: A Convenient Route to Heterometallic Species. *Inorganic Chemistry* (2009) 48, 6584-6593.
- Stengl, V., Bakardjieva, S., Bludska, J. Se and Te-Modified Titania for Photocatalytic Applications. *Journal of Materials Science* (2011) 46, 3523-3536.
- Steunou N., Ribot, F., Boubekour, K., Maquet, J., Sanchez, C. Ketones as an Oxolation Source for the Synthesis of Titanium-Oxo-Organoclusters. *New Journal of Chemistry* (1999) 23, 1079-1086.
- Tegmark, M. (2014) *Our Mathematical Universe*. Vintage.
- Tegmark, M. (2017). *Life 3.0. Being Human in the Age of Artificial Intelligence*. Penguin Books.
- Toloman, D., Popa, A., Stefan, M., Pana, O., Silipas, TD., Macavei, S., Barbu-Tudoran, L. Impact of Gd Ions from the Lattice of TiO<sub>2</sub> Nanoparticles on the Formation of Reactive Oxygen Species During the Degradation of RhB Under Visible Light Irradiation. *Materials Science in Semiconductor Processing* (2017) 71, 61-68.
- Tong, Z., Jiang, Y., Yang, D., Shi, J., Zhang, S., Liu, C., Jiang, Z. Biomimetic and Bioinspired Synthesis of Titania and Titania-Based Materials. *RSC Advances* (2014) 4, 12388-12403.
- Turova, NYA., Turevskaia, EP., Kessler, VG., Yanovskaya, MI. Oxoalkoxides – True Precursors of Complex Oxides. *Journal of Sol-Gel Science and Technology* (1994) 2, 17-23.
- Turova, NY., Turevskaia, EP., Kessler, VG., Yanovskaya, MI. (2002). *The Chemistry of Metal Alkoxides*. Kluwer Academic Press.
- Ulissi, ZW., Tang, MT., Xiao, J., Liu, X., Torelli, DA., Karamad, M., Cummins, K., Hahn, C., Lewis, NS., Jaramillo, TF., Chan, K., Norskov, JK. Machine-Learning Methods Enable Exhaustive Searches for Active Bimetallic Facets and Reveal Active Site Motifs for CO<sub>2</sub> Reduction. *ACS Catalysis* (2017) 7, 6600-6608.
- Varanasi, S., Henzel, L., Mendoza, L., Prathapan, R., Batchelor, W., Tabor, R., Garnier, G. Pickering Emulsions Electrostatically Stabilized by Cellulose Nanocrystals. *Frontiers in Chemistry* (2018) 6, 409.
- Volova, TG., Schumilova, AA., Shidlovskiy, IP., Nikolaeva, ED., Sukovatiy, AG., Vasiliev, AD., Shishatskaya, EI. Antibacterial Properties of Films of Cellulose Composites with Silver Nanoparticles and Antibiotics. *Polymer Testing* (2018) 65, 54-68.

- Wang, J., Bowie, D., Zhang, X., Filipe, C., Pelton, R., Brennan, JD. Morphology and Entrapped Enzyme Performance in Inkjet-Printed Sol – Gel Coatings on Paper. *Chemistry of Materials* (2014) 26, 1941-1947.
- Wang, J., Liu, CY., Senftle, TP., Zhu, J., Zhang, G., Guo, X., Song, C. Variation in the In<sub>2</sub>O<sub>3</sub> Crystal Phase Alters Catalytic Performance toward the Reverse Water Gas Shift Reaction. *ACS Catalysis* (2020) 10, 3264-3273.
- Weber, AS., Grady, AM., Koodali, RT. Lanthanide Modified Semiconductor Photocatalysts. *Catalysis Science & Technology* (2012) 2, 683-693.
- Werndrup, P., Kessler, VG. Interaction of Co(acac)<sub>2</sub> and Ta(OMe)<sub>5</sub>: Isolation and Single Crystal Study of the Products. M<sup>II</sup><sub>2</sub>M<sup>V</sup><sub>2</sub>(acac)<sub>2</sub>(OMe)<sub>12</sub>, M<sup>II</sup> = Co, Ni, Zn or Mg and M<sup>V</sup> = Ta or Nb: A New Class of Heterometallic Heteroleptic Alkoxide Complexes. *Journal of the Chemical Society Dalton Transactions* (2001) 574-579.
- Williams, DB. & Carter, CB. (2009). *Transmission Electron Microscopy. A Textbook for Materials Science*. (2<sup>nd</sup> ed). New York: Springer-Verlag.
- Williams, DH. & Fleming, I. (1995). *Spectroscopic Methods in Organic Chemistry*. (5<sup>th</sup> ed). McGraw-Hill.
- Willkomm, J., Orchard, KL., Reynal, A., Pastor, E., Durrant, JR., Reisner, E. Dye-Sensitized Semiconductors Modified with Molecular Catalysts for Light-Driven H<sub>2</sub> Production. *Chemical Society Reviews* (2016) 45, 9-23.
- Woolerton, TW., Sheard, S., Reisner, E., Pierce, E., Eagsdale, SW., Armstrong, FA. Efficient and Clean Photoreduction of CO<sub>2</sub> to CO by Enzyme-Modified TiO<sub>2</sub> Nanoparticles Using Visible Light. *Journal of the American Chemical Society* (2010) 132, 2132-2133.
- Wu, M., He, Q., Shao, Q., Zuo, Y., Wang, F., Ni, H. Preparation and Characterization of Monodispersed Microflocules of TiO<sub>2</sub> Nanoparticles with Immobilized Multienzymes. *ACS Applied Materials & Interfaces* (2011) 3, 3300-3307.
- Xie, T., France-Lanord, A., Wang, Y., Shao-Horn, Y., Grossman, JC. Graph Dynamical Networks for Unsupervised Learning of Atomic Scale Dynamics in Materials. *Nature Communications* (2019) 10, 2667.
- Xun, H., Ma, X., Chen, J., Yang, Z., Liu, B., Gao, X., Li, G., Yu, J. Wang, L., Pang, J. Zinc Oxide Nanoparticle Exposure Triggers Different Gene Expression Patterns in Maize Shoots and Roots. *Environmental Pollution* (2017) 229, 479-488.
- Yanagisawa, K., Ovenstone J. Crystallization of Anatase from Amorphous Titania Using the Hydrothermal Technique: Effects of Starting Material and Temperature. *Journal of Physical Chemistry B* (1999) 103, 7781–7787.

- Yang, HG., Sun, CH., Qiao, SZ., Zou, J., Liu, G., Smith, SC., Cheng, HM., Lu, GQ. Anatase TiO<sub>2</sub> Single Crystals with a Large Percentage of Reactive Facets. *Nature* (2008) 453, 638-642.
- Yang, F., Zhang, HR., Li, L., Reaney, IM., Sinclair, DC. High Ionic Conductivity with Low Degradation in A-Site Strontium-Doped Nonstoichiometric Sodium Bismuth Titanate Perovskite. *Chemistry of Materials* (2016) 28, 5269-5273.
- Yazhini, KB., Prabu, HG., Nandhini, JR. Synthesis and Coating of ZnO-BTCA Composite on Cotton for Antibacterial Activity. *Journal of Environmental and Applied Bioresearch* (2015) 3, 150-154.
- Youn, W., Ko, EH., Kim, MH., Park, M., Hong, D., Seisenbaeva, GA., Kessler, VG., Choi, IS. Cytoprotective Encapsulation of Individual Jurkat T-Cells within Durable TiO<sub>2</sub> Shells for T-Cell Therapy. *Angewandte Chemie International Edition* (2017) 56, 10702-10706.
- Yurtsever, HA., Ciftcioglu, M. The Effect of Rare Earth Element Doping on the Microstructural Evolution of Sol-Gel Titania Powders. *Journal of Alloys and Compounds* (2017) 695, 1336-1353.
- Zhang, H. & Banfield, JF. Size Dependence of the Kinetic Rate Constant for Phase Transformation in TiO<sub>2</sub> Nanoparticles. *Chemistry of Materials* (2005) 17, 3421-3425.
- Zhang, R., Elzatahry, AA., Al-Deyab, SS., Zhao, D. Mesoporous Titania: From Synthesis to Application. *Nano Today* (2012) 7, 344-366.
- Zhao, YR., Zhen, H., Chen, LQ., Chen, HJ., Kong, XJ., Long, LS., Zheng, LS. The Effect on the Luminescent Properties in Lanthanide-Titanium Oxo Clusters. *Inorganic Chemistry* (2019) 58, 10078-100083.
- Zhou, WY., Cao, QY., Liu, YJ., Yu., XY., Luo, Y. Enhancement of TiO<sub>2</sub> Photocatalytic Activity by Gd<sup>3+</sup> Doping. *Advances in Applied Ceramics* (2007) 106, 222-225.
- Zhang, G., Li, W., Liu, C., Jia, J., Tung, CH., Wang, Y. Titanium-Oxide Host Clusters with Exchangeable Guests. *Journal of the American Chemical Society* (2018) 140, 66-69.
- Zhang, G., Liu, C., Long, DL., Cronin, L., Tung, CH., Wang, Y. Water-Soluble Pentagonal-Prismatic Titanium-Oxo Clusters. *Journal of the American Chemical Society* (2016) 138, 11097-11100.
- Zou, X., Hovmöller, S., Oleynikov, P. (2011). *Electron Crystallography: Electron Microscopy and Electron Diffraction*. Oxford: Oxford University Press.



## Popular science summary

Nanomaterials are emerging as an important technology for both advanced applications, such as medicine and electronic devices, and everyday products, such as cosmetics, clothing, and different material coatings. However, nanotechnology is still in its infancy; synthetic strategies for more precise control of materials need to be developed. Safety concerns require attention due to the high risk of interference with cellular components and biological pathways on the molecular scale.

Titanium (IV) dioxide (titania) is one of the most commonly manufactured nanomaterials among the metal oxides. Titania finds use as photocatalyst, pigment in white paint, hydrophobic window coatings and, previously, additive in cosmetics and food. Studies within the thesis have investigated, on one hand, synthesis of pure titania materials and also rare-earth modified nanopowders from molecular precursors for improved photocatalysis. On the other hand, organic-inorganic hybrid materials based on nanotitania and nanocellulose, and self-assembled structures based on surface-modified titania were synthesized for potential medical applications such as drug delivery, wound-dressings, and blood clotting patches. An initial safety assessment of the hybrid materials based on haemocompatibility studies with human whole blood was undertaken with preliminarily promising results for use as blood clotting patches. Production of the nanomaterials and hybrid materials was found to be highly sensitive to small changes in their protocols. This presents a challenge for production of useful volumes, but offers also an opportunity to tune material's properties with very small changes, a possibility generally not observed in macroscale materials.

## Populärvetenskaplig sammanfattning

Nanomaterial blir allt vanligare i högteknologiska och vardagliga sammanhang och finner applikationer inom avancerade tillämpningar så som medicin och elektronik, samt i vardagliga föremål som kosmetika, kläder och ytbeläggningar. Nanoteknologin befinner sig fortfarande i sin linda och syntetiska metoder för framställning med precis kontroll behöver utvecklas.

På grund av den lilla storleken interagerar nanomaterial lätt med cellulära komponenter och molekylära signalvägar, vilket har lett till oro över skadliga effekter för både djur och växter. Titan(IV)dioxid ( $\text{TiO}_2$ ) är antagligen det vanligaste nanomaterialet baserade på metalloxider.  $\text{TiO}_2$  används i stor skala som vitt pigment i färg, fotokatalysator, för hydrofobiska glasytor och tidigare som tillsatts i livsmedel och kosmetika. Delarbeten inom den här avhandlingen har undersökt syntes av ren  $\text{TiO}_2$  och  $\text{TiO}_2$  modifierad med sällsynta jordartsmetaller för förbättrad fotokatalys.

Andra delarbeten har fokuserat på utvecklingen av organiska-oorganiska hybridmaterial baserade på titandioxidnanopartiklar och nanocellulosa, samt självsamordnade ihåliga sfärer baserade på ytfunktionaliserade titandioxidnanopartiklar för potentiella applikationer inom kontrollerad läkemedelsdistribution, förbättrad sårläkning och blodstoppande material. Biokompatibiliteten för nanotitania-nanocellulosa hybridmaterial mot humanblod har undersökts som ett bidrag till ökad förståelse av säkerheten av dessa material. Resultat visar att dessa material kan vara möjliga framtida material för såromläggning och för att stoppa blödningar. Syntes av nanomaterial från molekylära prekursorer har visat sig kunna vara väldigt känsliga mot små förändringar i framställningsmetoden. Detta kan vara en utmaning för storskalig produktion av vissa nanomaterial men erbjuder samtidigt en möjlighet att med små modifieringar erhålla stora skillnader i morfologi och egenskaper.

## Acknowledgements

The almost five years since I started at SLU have passed very quickly, it feels like last week I arrived to Ultuna. I remember first seeing the advertisement for this project in late spring/early summer 2015 and I was very interested, but at that point I had yet not finished my Master's degree. A few months later, by chance, I noticed that the position was out again and gave it a shoot – and was lucky. Like all PhD projects it has been challenging every now and then (rather frequently actually), but it has been amazingly fun most of the time. During this period I have met a lot of nice people and probably made some friends for life.

This is certainly the trickiest part of the thesis to write and, most likely, the first and only part that most people actually will read. Therefore, names will not be in bold so that some reading effort will be required.

First of all I would like to express my sincere gratitude to my main supervisor, Vadim Kessler, who gave me this opportunity. I really appreciate the kind support and encouragement I have got through the years. I am very impressed by your broad and deep knowledge, both in chemistry and other fields, and it has been great to be part of your research group.

I am also very grateful to Gulaim Seisenbaeva who has provided good support and particularly for kindly sharing her instrumental and laboratory expertise. You have always only been an office away when in need for advice.

I also want to thank my co-supervisor Karin Fromell at Rudbeck, UU, for guiding me through the complexity of blood coagulation and immunological pathways and providing good feedback on the immunology section.

Also thanks to my former immunology lecturer (at LNU), and now co-supervisor, Kristina Nilsson-Ekdahl at Rudbeck, UU, for the opportunity to

carry out the very interesting work in manuscript V and providing valuable input on the project.

I like to thank my co-supervisor Tomas Edvinsson, UU; you show deep knowledge and have funny humor, it would have been nice spending more time learning from you.

I do like to thank my final co-supervisor, Nicholas Kotov, for his valuable contributions to the work of manuscript VI. You have very interesting research projects going on, unfortunately time prohibited further collaborations.

I am very grateful to the first two people I got to know in Uppsala; my former office buddies and group members Elizabeth Polido-Legaria and Martin Palmqvist. You both contributed to a very fun and nice office and lab environment and we had several fun conference visits together. I guess you both had major influence on me joining the “vegan side”.

Ievgen Pylypchuk, former office buddy and good friend, thanks for joining me to the gym and for all interesting and hilarious conversations in the office, as well as many useful discussions regarding research.

Olga Evdokimova, former colleague and co-author, your stay here was quite short but very fun. Miss going to the gym sessions at Friskis together.

Ani Vardanyan, current office buddy and newest group member, thanks for many nice and funny conversations, and valuable advices. Björn Greijer, current office buddy, thanks for providing a much needed down-to-earth attitude in the office. Members of the now long ceased “lunch-bunch”: Pernilla Elander, Alyona Minina, and Kerstin Dalman (also including Martin and Elizabeth) for great lunch company and fun discussions.

I have had the nice opportunity to supervise a number of motivated and talented students over the years: it has been very fun to see you all grow and become more independent in the lab during your stay here. I like to thank Pauline Bourzeix, Philipp Simon, Emiel van Wetter, Emile Maucotel, and Timo de Donder for their good work and contributions. Also a special thanks to Philipp for assistance with proof reading!

In addition wish to thank the following people: Hanna Eriksson-Röhnisch for many nice discussions and valuable advices, also big thanks for your help with proof reading the references! Johnny Östman for providing a never-ending flow of unique discussion topics during lunch and fika. Elin Alexandersson for joining me to the gym at least once each semester and many nice conversations. Mathilde Brunel for many nice conversations and for patience when I try to speak French. Yan Xue for many nice and funny

discussion during lunch and fika. Christina Nord, I am impressed by your brewing skills, never dared to taste but I have heard the rumors... Solja Pietiäinen for nice conversations and those 5 kg of bran you gave me. Anja Herneke, for many good conversations and for representing the PhD student council in the Equal Opportunity committee. Klara Nilsson for always bringing a positive attitude and good conversations. Frida Wende for keeping the order in the corridor, now when you have left things are spiraling away... Lena Lundqvist, you finally had enough of us other and left... good luck on your new job. I really appreciated your sense of humor. Eva Bajnoczi, fellow lab teacher in many chemistry courses and many nice lunch discussions. Anders Sandström for making sure I never ran out of teaching opportunities and many interesting conversations regarding teaching. Corine Sandström for kindly answering NMR questions and for agreeing to chair my defense. Jan Eriksson for teaching me how to operate the HPLC-MS and for many, various, interesting discussion. Ingmar Persson for introducing me to the exciting field of EXAFS and for kindly answering my random chemistry questions every now and then. Peter Agback for enthusiastically teaching me how to operate the NMR spectrometers. Gustav Nestor for kindly sharing your experience in grant application. Sebastian Håkansson for sharing your expertise in microbial cultivations. Tobias Bölscher, former office buddy, for introducing me to the PhD Student Council and to the floorball group. Daniel Lundberg for convincing me to join the annual teachers vs. students hockey game, "Ultuna Winter Classics", (I'll never do that again!). Gunnar Almqvist for providing valuable advices and perspectives. Nils Mikkelsen for computer support.

Some of you I don't know so well, but you have nevertheless provided to the good working environment: Mathias Johansson, Anders Broberg, Daniel Johansson, Saeid Karkehabadi, Ali Moazzami, Tatiana Agback, Maud Langton, Henrik Hansson, and Suresh Gohil.

I have spent quite a lot of time at the Rudbeck laboratory, Uppsala University, and several people there provided both good working environment, valuable advices, and fun conversations: Vivek Anad Manivel, Anna Adler, Amanda Åman, Ulrika Johansson, Bo Nilsson, and Jaan Hong.

I am grateful for the contributions of all members of ULS PhD Student Council during my time as member and latter as chairperson, these meetings really provided great perspectives and insights.

Collaborators who contributed to the papers: Geoffrey Daniel (SLU), Cheuk-Wai Tai (SU), Zhen Qiu (UU).

Mattias Larsson, SLU Alnarp, for providing my with an interesting project for my degree work in Biology.

The IT department for repairing my computer after the horrific “coffee-in-the-computer-incident” at MaxIV.

Vetenskapsrådet for funding this project.

Furthermore, I'd like to express my gratitude towards my previous supervisors and teachers at Linnaeus University (in Kalmar) from my undergraduate studies for their support and encouragement: Anna Blücher, Christian Schiebe, Kjell Edman, Björn Karlsson, Boel Lindegård, Ian Nicholls, and Gustaf Olsson, and, in particular, to my former degree project supervisors Rikard Unelius and Maria Bergström.

Finally, I would like to thank my mother, father, sister and brother for their superb support. I could not had made it through all these years in school without it – thanks!

ACTA UNIVERSITATIS AGRICULTURAE SUECIAE

DOCTORAL THESIS NO. 2020:56

This thesis focuses on the syntheses and characterization of nanomaterials based on nanotitania and nanotitania-nanocellulose from molecular precursors. Materials for photocatalysis, encapsulation, drug delivery, and wound-dressing have been developed and evaluated. Heteroleptic titanium oxo-alkoxide complexes (molecular precursors for titania nanoparticles) have been synthesized and extensively investigated in both solid-state and in solution.

**Fredric G. Svensson** received his graduate education at the Department of Molecular Sciences, SLU, Uppsala. He received his B.Sc. degrees in Chemistry and Biology from Linnaeus University and SLU, respectively, and his M.Sc. degree in Chemistry from Linnaeus University.

Acta Universitatis Agriculturae Sueciae presents doctoral theses from the Swedish University of Agricultural Sciences (SLU).

SLU generates knowledge for the sustainable use of biological natural resources. Research, education, extension, as well as environmental monitoring and assessment are used to achieve this goal.

Online publication of thesis summary: <http://pub.epsilon.slu.se/>

ISSN 1652-6880

ISBN (print version) 978-91-7760-630-7

ISBN (electronic version) 978-91-7760-631-4